EXPERIMENTAL AND NUMERICAL INVESTIGATION OF VORTEX FORMATION AT MULTIPLE HORIZONTAL INTAKES

A THESIS SUBMITTED TO
THE GRADUATE SCHOOL OF NATURAL AND APPLIED SCIENCES
OF
MIDDLE EAST TECHNICAL UNIVERSITY

BY

TUĞÇE YILDIRIM

IN PARTIAL FULFILLMENT OF THE REQUIREMENTS
FOR
THE DEGREE OF DOCTOR OF PHILOSOPHY
IN
CIVIL ENGINEERING

AUGUST 2020

Approval of the thesis:

EXPERIMENTAL AND NUMERICAL INVESTIGATION OF VORTEX FORMATION AT MULTIPLE HORIZONTAL INTAKES

submitted by **TUĞÇE YILDIRIM** in partial fulfillment of the requirements for the degree of **Doctor of Philosophy in Civil Engineering Department, Middle East Technical University** by,

Prof. Dr. Halil Kalıpçılar
Dean, Graduate School of **Natural and Applied Sciences** _____

Prof. Dr. Ahmet Türer
Head of Department, **Civil Engineering** _____

Prof. Dr. Mustafa Göğüş
Supervisor, **Civil Engineering, METU** _____

Prof. Dr. Mete Köken
Co-supervisor, **Civil Engineering, METU** _____

Examining Committee Members:

Prof. Dr. Ayşe Burcu Altan Sakarya
Civil Engineering, METU _____

Prof. Dr. Mustafa Göğüş
Civil Engineering, METU _____

Prof. Dr. Dilek Funda Kurtuluş
Aerospace Engineering, METU _____

Prof. Dr. Şahnaz Tiğrek
Civil Engineering, Batman University _____

Assist. Prof. Dr. Aslı Numanoğlu Genç
Civil Engineering, TED University _____

Date: **31.08.2020**

I hereby declare that all information in this document has been obtained and presented in accordance with academic rules and ethical conduct. I also declare that, as required by these rules and conduct, I have fully cited and referenced all material and results that are not original to this work.

Name, Last Name: TUĞÇE YILDIRIM

Signature :

ABSTRACT

EXPERIMENTAL AND NUMERICAL INVESTIGATION OF VORTEX FORMATION AT MULTIPLE HORIZONTAL INTAKES

Yıldırım, Tuğçe
Ph.D., Department of Civil Engineering
Supervisor : Prof. Dr. Mustafa Göğüş
Co-Supervisor : Prof. Dr. Mete Köken

August 2020, 92 pages

Although most of the equations given in the literature for critical submergence are for symmetrical single intakes; in practice approach flow conditions are not mainly symmetrical. In this study, formation of the vortices in asymmetrical approach flow conditions was investigated for a multiple water intake structure composed of a reservoir and several pipe systems. Different scenarios were tested when some of the intake units were in operation whereas some others were not. The geometrical and hydraulic conditions of the system such as the distance between the sidewalls of the intake and the flow discharge were altered and the critical submergence required for the formation of the vortex for each test is determined. The variation of dimensionless critical submergence with related dimensionless parameters is presented and empirical equations were derived for single, double and triple intake structures. The results of the experiments were compared with each other and with those presented in the literature. This investigation has done both experimentally and numerically where software namely FLOW-3D was used in the three dimensional numerical simulations. Numerical and experimental results were compared. It was shown that it is not easy

to capture air entrainment and free surface dynamics by numerically.

Keywords: Horizontal Intakes, Critical Submergence, Vortex, CFD, FLOW-3D

ÖZ

ÇOKLU YATAY SU ALMA YAPILARINDA VORTEKS OLUŞUMUNUN DENEYSEL VE SAYISAL OLARAK İNCELENMESİ

Yıldırım, Tuğçe
Doktora, İnşaat Mühendisliği Bölümü
Tez Yöneticisi : Prof. Dr. Mustafa Göğüş
Ortak Tez Yöneticisi : Prof. Dr. Mete Köken

Ağustos 2020 , 92 sayfa

Her ne kadar literatürde kritik batıklık derinliği için verilen denklemlerin çoğu simetrik tekil su alma yapıları için olsa da pratikteki yaklaşım akım koşulları çoğunlukla asimetriktir. Bu çalışmada, bir rezervuar-boru sisteminden oluşan su alma yapısında, asimetrik yaklaşımlı akım koşullarında vortekslerin oluşumu incelenmiştir. Bazı su alma uniteleri açıkken diğerlerinin kapalı olduğu şeklinde değişik senaryolar test edilmiştir. Boru çapı, su alma yapısı yan duvarları ara mesafesi ve akımın debisi gibi sistemin geometrik ve hidrolik şartları değiştirilerek bu durumların her birisi için yapılan deneylerde vortekslerin oluşacağı kritik batıklık derinlikleri tesbit edilmiştir. Tek, ikili ve üçlü su alma yapıları için boyutsuz kritik batıklığın değişimi ilgili boyutsuz parametreler ile sunulmuştur ve ampirik denklemler elde edilmiştir. Deney sonuçları birbirleri ile ve sunulan literatürdeki denklemler ile karşılaştırılmıştır. Deneysel ve numerik olarak yapılan çalışmada üç boyutlu sayısal modelleme için FLOW-3D kullanılmıştır. Deney sonuçları ile numerik hesaplamanın karşılaştırması yapılmıştır. Numerik olarak hava girişinin ve serbest yüzey dinamiklerini yakalamanın kolay olmadığı anlaşılmıştır.

Anahtar Kelimeler: Su Alma Yapısı, Kritik Batıklık, Vorteks, HAD, FLOW-3D

To the Sun bringing light into my life...

ACKNOWLEDGMENTS

Firstly and foremost, I would like to thank you to my advisor Prof. Dr. Mustafa Göğüş for his patience and support during this study. I am especially grateful to Prof. Dr. Doğan Altınbilk for his support and encouragement. Also, I would like to express my gratitude to Prof. Dr. Şahnaz Tiğrek and Prof. Dr. Dilek Funda Kurtuluş for their time and contribution during all those thesis monitoring committees and every part of the thesis work. I would like to acknowledge the guidance I received from my co-advisor Prof. Dr. Mete Köken for the numerical study part of this thesis.

I would like to thank the technical staff of Middle East Technical University, Hydromechanics Laboratory for their assistance in times of need, and also my colleagues who have created such a pleasant environment in the Hydromechanics Laboratory.

I am grateful for the support that I have received from my friends and family. I want to especially thank Gizem Okyay for accompanying all of the existential crisis we have during our PhD studies, and also for her support and friendship even from miles away. I would also thank Sülen Kitapçıgil, Zeynep Çekinmez Bayram, Beren Yılmaz Ersan and Meriç Selamoğlu Yılmaz for their companion and friendship during every time of this period. I would particularly like to thank my parents who have always encouraged and assisted me in everything that I do. I want to pay tribute to my mother since she always encouraged and supported me for my education.

Finally, I want to express my deepest gratitude to my husband Güneş Başar for his patience and understanding, this thesis would not have been possible without his support and encouragement.

TABLE OF CONTENTS

ABSTRACT v

ÖZ vii

ACKNOWLEDGMENTS x

TABLE OF CONTENTS xi

LIST OF TABLES xiv

LIST OF FIGURES xvi

LIST OF SYMBOLS AND ABBREVIATIONS xx

CHAPTERS

1 INTRODUCTION 1

2 LITERATURE REVIEW 3

2.1 General Information 3

2.2 Experimental Research for Defining Critical Submergence . . 7

2.2.1 Experimental Studies on Horizontal Intakes 7

2.2.2 Experimental Studies on Vertical Intakes 11

2.3 Numerical Studies 12

3 DIMENSIONAL ANALYSIS 15

3.1 Dimensional Analysis of Critical Submergence 15

3.2 Effect of Froude Number 17

3.3 Effect of Reynolds Number 17
3.4 Effect of Weber Number 18
3.5 Effect of Kolf Number 18
3.6 Dimensionless Relationship For Critical Submergence 18
4 EXPERIMENTAL STUDY 19
4.1 Experimental Setup and Procedure 19
4.2 Experimental Study on Single Intakes 33
4.3 Experimental Study on Double Intakes 39
4.4 Experimental Study on Triple Intakes 46
4.5 Comparison Between the Proposed Equation of Present Study and Related Formulas in The Literature 53
5 NUMERICAL SIMULATION 57
5.1 Numerical Simulation with ANSYS FLUENT 58
5.2 Numerical Simulation with FLOW-3D 61
5.2.1 Large Eddy Simulation (LES) 61
5.3 Geometrical Modeling and Computational Mesh 62
5.4 Numerical Model Development 65
5.5 Boundary Conditions 65
5.6 Initial Conditions 65
5.7 Simulation Cases 67
5.8 Analysing FLOW-3D Simulations 68
6 CONCLUSION 73
REFERENCES 75

APPENDICES

A EXPERIMENTAL RESULTS OF THE STUDY FOR SINGLE INTAKES 79

B EXPERIMENTAL RESULTS OF THE STUDY FOR DOUBLE INTAKES 83

C EXPERIMENTAL RESULTS OF THE STUDY FOR TRIPLE INTAKES 89

CURRICULUM VITAE 91

LIST OF TABLES

TABLES

Table 4.1 Ranges of the Parameters Tested for Single Intake Case 33

Table 4.2 Ranges of the Parameters Tested for Double Intake Case 40

Table 4.3 Ranges of the Parameters Tested for Triple Intake Case 46

Table 5.1 List of Simulations 68

Table A.1 Results for $b_1 = 40\ cm\ and\ b_2 = 20\ cm, \psi = 1.132$ 79

Table A.2 Results for $b_1 = 40\ cm\ and\ b_2 = 80\ cm, \psi = 2.264$ 79

Table A.3 Results for $b_1 = 60\ cm\ and\ b_2 = 20\ cm, \psi = 1.006$ 80

Table A.4 Results for $b_1 = 60\ cm\ and\ b_2 = 100\ cm, \psi = 3.623$ 80

Table A.5 Results for $b_1 = 60\ cm\ and\ b_2 = 140\ cm, \psi = 3.235$ 80

Table A.6 Results for $b_1 = 100\ cm\ and\ b_2 = 20\ cm, \psi = 0.906$ 80

Table A.7 Results for $b_1 = 100\ cm\ and\ b_2 = 160\ cm, \psi = 6.132$ 81

Table A.8 Results for $b_1 = 120\ cm\ and\ b_2 = 20\ cm, \psi = 0.881$ 81

Table A.9 Results for $b_1 = 120\ cm\ and\ b_2 = 160\ cm, \psi = 7.925$ 81

Table A.10 Results for $b_1 = 147\ cm\ and\ b_2 = 183\ cm, \psi = 10.003$ 81

Table B.1 Results for $b_1 = 70\ cm\ and\ b_2 = 80\ cm, \psi = 4.953$ 83

Table B.2 Results for $b_1 = 70\ cm\ and\ b_2 = 90\ cm, \psi = 4.696$ 83

Table B.3 Results for $b_1 = 70\ cm\ and\ b_2 = 100\ cm, \psi = 4.491$ 83

Table B.4 Results for $b_1 = 70\ cm\ and\ b_2 = 110\ cm, \psi = 4.322$ 84

Table B.5 Results for $b_1 = 70\ cm\ and\ b_2 = 120\ cm, \psi = 4.182$ 84

Table B.6 Results for $b_1 = 80\ cm\ and\ b_2 = 90\ cm, \psi = 5.702$ 84

Table B.7 Results for $b_1 = 80\ cm\ and\ b_2 = 100\ cm, \psi = 5.434$ 85

Table B.8 Results for $b_1 = 80\ cm\ and\ b_2 = 110\ cm, \psi = 5.214$ 85

Table B.9 Results for $b_1 = 80\ cm\ and\ b_2 = 120\ cm, \psi = 5.031$ 85

Table B.10 Results for $b_1 = 90\ cm\ and\ b_2 = 100\ cm, \psi = 6.453$ 86

Table B.11 Results for $b_1 = 90\ cm\ and\ b_2 = 110\ cm, \psi = 6.175$ 86

Table B.12 Results for $b_1 = 90\ cm\ and\ b_2 = 120\ cm, \psi = 5.943$ 86

Table B.13 Results for $b_1 = 100\ cm\ and\ b_2 = 110\ cm, \psi = 7.204$ 87

Table B.14 Results for $b_1 = 100\ cm\ and\ b_2 = 120\ cm, \psi = 6.918$ 87

Table B.15 Results for $b_1 = 110\ cm\ and\ b_2 = 120\ cm, \psi = 7.956$ 87

Table C.1 Results for $b_1 = 120\ cm\ and\ b_2 = 140\ cm, \psi = 8.410$ 89

Table C.2 Results for $b_1 = 120\ cm\ and\ b_2 = 160\ cm, \psi = 7.925$ 89

Table C.3 Results for $b_1 = 140\ cm\ and\ b_2 = 160\ cm, \psi = 9.906$ 90

Table C.4 Results for $b_1 = 140\ cm\ and\ b_2 = 170\ cm, \psi = 9.634$ 90

Table C.5 Results for $b_1 = 147\ cm\ and\ b_2 = 183\ cm, \psi = 10.003$ 90

LIST OF FIGURES

FIGURES

Figure 2.1 Vortex Classification According to Alden Research Laboratory [1] . 5

Figure 2.2 Classification of Intake Types [1] 6

Figure 3.1 Sketch of the Model 16

Figure 4.1 General Layout of the Experimental Model (Top-view), Dimensions are in cm 21

Figure 4.2 General Layout of the Experimental Model (Side-view), Dimensions are in cm 22

Figure 4.3 View of the Experimental Model from Downstream 23

Figure 4.4 Close View of the Hydraulic Intakes 23

Figure 4.5 Buffle Blocks at the entrance of the reservoir 24

Figure 4.6 Electronic Flowmeters Attached to Downstream of Each Intake . . 25

Figure 4.7 An Example Vortex with Scale 26

Figure 4.8 Close View of the Vortex Mouth 27

Figure 4.9 Top View of Vortex 28

Figure 4.10 Single Intake Setups 29

Figure 4.11 Double Intake Setups 30

Figure 4.12 Cont. Double Intake Setups 31

Figure 4.13 Triple Intake Setups 32

Figure 4.14 Dimensionless Critical Submergence vs Froude Number 34

Figure 4.15 Dimensionless Critical Submergence vs Reynolds Number 34

Figure 4.16 Dimensionless Critical Submergence vs Weber Number 35

Figure 4.17 Comparison of Measured S_c/D_i Data With Calculated S_c/D_i Data From Equation 4.3 36

Figure 4.18 Comparison Between the Measured Values of S_c/D_i and the Ones Calculated by Equation 4.4 37

Figure 4.19 Variation of S_c/D_i with ψ as a Function of Fr 38

Figure 4.20 Comparison of Measured S_c/D_i Data With Calculated S_c/D_i Data from Equation 4.2 38

Figure 4.21 Comparison Between the Measured Values of S_c/D_i and the Ones Calculated by Equation 4.6 39

Figure 4.22 Dimensionless Critical Submergence vs Froude Number 40

Figure 4.23 Dimensionless Critical Submergence vs Reynolds Number 41

Figure 4.24 Dimensionless Critical Submergence vs Weber Number 41

Figure 4.25 Comparison of Measured S_c/D_i Data With Calculated S_c/D_i Data From Equation 4.9 42

Figure 4.26 Comparison Between the Measured Values of S_c/D_i and the Ones Calculated by Equation 4.10 43

Figure 4.27 Variation of S_c/D_i with ψ as a function of Fr 44

Figure 4.28 Comparison of Measured S_c/D_i Data With Calculated S_c/D_i Data From Equation 4.11 45

Figure 4.29 Comparison Between the Measured Values of S_c/D_i and the Ones Calculated by Equation 4.12 46

Figure 4.30 Dimensionless Critical Submergence vs Froude Number 47

Figure 4.31 Dimensionless Critical Submergence vs Reynolds Number 48

Figure 4.32 Dimensionless Critical Submergence vs Weber Number 48

Figure 4.33 Comparison of Measured S_c/D_i Data With Calculated S_c/D_i Data From v Equation 4.15 49

Figure 4.34 Comparison Between the Measured Values of S_c/D_i and the Ones Calculated by Equation 4.16 50

Figure 4.35 Variation of S_c/D_i with ψ as a function of Fr 51

Figure 4.36 Comparison of Measured S_c/D_i Data With Calculated S_c/D_i Data From Equation 4.17 52

Figure 4.37 Comparison Between the Measured Values of S_c/D_i and the Ones Calculated by Equation Equation 4.18 53

Figure 4.38 Comparison of the Simplified S_c/D_i Equations of Present Study for Single Intake, Double Intake and Triple Intake Structures 54

Figure 4.39 Comparison of the Simplified S_c/D_i Equation of Present Study for Single Intake Structure with the Related Ones Presented in Literature . . . 55

Figure 5.1 Mesh Planes for Fluent Simulation 58

Figure 5.2 General View of Constructed Mesh 59

Figure 5.3 Close View of Meshes Behind Intake 60

Figure 5.4 Free Surface as Result of the Simulation Represented by Volume Fraction 60

Figure 5.5 Free Surface Behind the Intake and Bubble formation 61

Figure 5.6 General View of Computational Mesh in FLOW-3D 64

Figure 5.7 Close View of the Mesh in Intake Area 64

Figure 5.8 View of Boundary Conditions from Inlet 66

Figure 5.9 View of Boundary Conditions from Outlet 66

Figure 5.10 Initial Condition of the Reservoir 67

Figure 5.11 Free Surface and View of Reservoir Conditions 70

Figure 5.12 Free Surface Behind Intake 70

Figure 5.13 Velocity Vectors Coloured by Magnitude of Velocity 71

Figure 5.14 Streamlines Coloured by Magnitude of Velocity 71

LIST OF SYMBOLS AND ABBREVIATIONS

a	Intake Gate Height
b	Horizontal distance from the center of the intake to a side wall of the reservoir
b_1	Horizontal distance from the center of the intake to the right-side plexiglass wall
b_2	Horizontal distance from the center of the intake to the left-side plexiglass wall
c	Vertical distance between the lowest point of the intake pipe and reservoir bottom
$\frac{b_1}{D_i}$	Aspect ratio of right side wall clearance to intake centerline
$\frac{b_2}{D_i}$	Aspect ratio of left side wall clearance to intake centerline
$\frac{c}{D_i}$	Aspect ratio of bottom clearance to intake wall
D, D_i	Intake Diameter
Fr	Froude Number
g	Gravitational Acceleration
K_o	Kolf Number
Re	Reynolds Number
S_c	Critical Submergence with respect to centerline of the intake pipe
S_{ce}	Critical Submergence with respect to the top point of the intake pipe
$\frac{S_c}{D_i}$	Dimensionless Critical Submergence
V_i	Intake Velocity
We	Weber Number

CFD	Computational Fluid Dynamics
DNS	Direct Numerical Simulation
LES	Large Eddy Simulation
METU	Middle East Technical University
VOF	Volume of Fluids
Γ	Circulation
ρ	Fluid Density
μ	Dynamic Viscosity
ψ	Representation of geometrical parameter for asymmetrical approach flow conditions
σ	Surface Tension

CHAPTER 1

INTRODUCTION

Water is used for many years to produce energy, irrigate crops, and satisfy the drinking water needs of the population by means of water structures. The evolution of the human being increased dependence on water for energy production and irrigation, so the effective design of water structures gain importance. These types of structures should be optimized to work at the most effective way to produce the maximum energy, to deliver the desired amount of water with minimizing losses, costs, etc. Horizontal intake structures have been used to divert water from rivers for domestic and industrial use, withdraw water from reservoirs for irrigation, satisfy the drinking water needs of society, producing energy from hydropower, and even in cooling systems of nuclear power plants.

Vortex formation in hydropower intakes and pump intakes of nuclear power plant cooling facilities creates various problems as decreasing efficiency, increasing vibrations as well as a complete failure. Sediment and debris entrance also can occur in the presence of a vortex in a reservoir so it is important to analyse the vortex formation to prevent these problems. Although there are many sources of vortex formation, the most frequent is the asymmetry of the intake and the eccentricity of approach flow conditions [1], and in most cases, due to the irregularities in an earth formation, it is not possible to build a symmetrical intake approach. Also if an ideal symmetrical case for a hydropower scheme exists, there would be asymmetrical intake conditions due to operational constraints. It is not possible to begin energy production simultaneously in the case of multiple turbine installations. The disturbance and turbulence in the flow increase circulation and creates vortices. It is impossible to eliminate these vortices, there will always be vortices even in uniform flow but it is important to re-

duce their intensities to prevent air entrainment [2]. For a proper design of hydraulic intakes, the air entraining vortex should be avoided. An approach could be decreasing their strength by vortex preventing devices so that air can not entrain [3]. It is crucial to determine the critical submergence which is defined as the height from intake centerline to the surface of the water at the moment an air core vortex occurs.

There are distinct options such as experimental investigations, analytical approaches and with the emerging technology in computational technology, Computational Fluid Dynamics (CFD) analysis may help us to interrogate vortex phenomena. Among these options, hydraulic model studies have advantages as they help to understand the flow phenomena in the whole structure for every specific case, where it stays sceptical about scale effects in turbulence, viscosity, and surface tension, additionally it is expensive to construct. CFD gives a cheaper solution by giving detailed flow characteristics, it is easy to change the geometry and a general approach can be made with trying different geometries and conditions with ease but it requires further validation. CFD takes less time to construct a model where it is longer for experimental studies but in the analysis phase a set of experiments takes less time with respect to a CFD analyse done in a PC with a standard configuration.

In this study, experimental analysis of single and multiple intakes with asymmetrical approach conditions is analysed and CFD validation is aimed to do to give a design approach. A 1/29.9 scaled physical laboratory model of a planned Dam project's reservoir with three inlets is used for experimental studies and the same geometry is analysed with two commercial CFD codes namely ANSYS Fluent and FLOW-3D. Air core vortex is aimed at observations and simulations, critical submergence is obtained and its relationship with Reynolds, Weber, and Froude numbers was examined. The results were compared with the well known equations in literature.

CHAPTER 2

LITERATURE REVIEW

2.1 General Information

Vortex phenomena is a complex behaviour of fluids in nature with the effect of turbulence. It is important to predict vortex location and occurrence in hydraulic intakes to prevent structures from vibration, cavitation, loss of efficiency and failure in extreme cases. The transition from free surface flow to pressurized flow in intakes makes the problem much more difficult. There are many experimental and analytical studies regarding free surface vortex, and with the development of the computational technology also numerical studies are in rise recently.

The velocity increases as getting closer to the vortex core where the local hydrostatic pressure decreases accordingly, so this drop in the pressure leads to a dimple or an air core vortex depending on the strength of the circulation [1].The basic classification of vortices is made visually.

Vortices could be divided into two according to occurrence location, as a free surface vortex that starts from the water surface and a subsurface vortex that starts from either bottom or wall of the structure [4]. There is a classification based on Alden Research Laboratory studies [5] [6] to differentiate between types of vortices visually. There are six types of free surface vortex as could be seen in Figure 2.1 classified according to their strength, which type 5 and 6 are the concern of this study. From 1 to 6 vortex strength is increasing, where there is an air bubble entrance in type 5 and air entrainment due to air core formation in type 6. Recently Sarkardeh et al. [7] made a new categorization for vortex types as type A, B and C which among them A is the most strong and should be avoided as it is the vortex type that air bubble or core is

formed and the air is trapped and conveyed from water surface to the pipe structure.

Intakes are also classified structurally according to two criteria; first the direction or orientation of the intake and second the location of the intake either in the wall or on the floor as could be seen in Figure 2.2 retrieved from Knauss [1].

Usually studied vortices are intermittent, unstable and in chaotic fashion, either they are not steady and their cores do not move periodic or even quasi periodic so it is hard to understand the interaction between the vortices of different observations done at distinct time intervals [2]. The study of Tokyay and Constantinescu [2] shows that the existence of highly unstable, wall attached vortices move within the study area and their strength, core size and structure changes as they move and they also interact with other main vortices or the turbulence around them. So it is good to use CFD models as a design tool to review and solve problems at existing pump intakes or test the new ones and they can partially replace expensive scaled-model studies [2].

There are only a few studies on dual pipe intakes in the literature. Ansar et al. [8] used three-dimensional (3D) numerical simulations of the inviscid flow of pump approach in single and dual vertical upward pump intakes and compared the results with the laboratory experiments.

There are also studies regarding the position of the intake structure, Khanarmuei et al. [9] state that horizontal intakes have smaller critical submergences with respect to others because of the smaller circulation in the water surface and weakest vortices occur in that type of intakes. They performed experiments on three different withdrawal directions as 0°, 45° and 90° in single and dual intakes.
Critical submergence is defined as the height difference between the water surface and intake centerline at the instance where the air reaches to the intake (type 5 and 6 vortex). It is important to know the critical submergence for operational conditions. There are several studies in order to observe the critical submergence and they led to several equations in literature. There is not an exact difference in these equations as either for a circular cross section or rectangular, for symmetrical intake or asymmetrical, for one intake or multiple intakes or for large reservoirs or small intakes. There are general equations that can be used to estimate critical submergence.

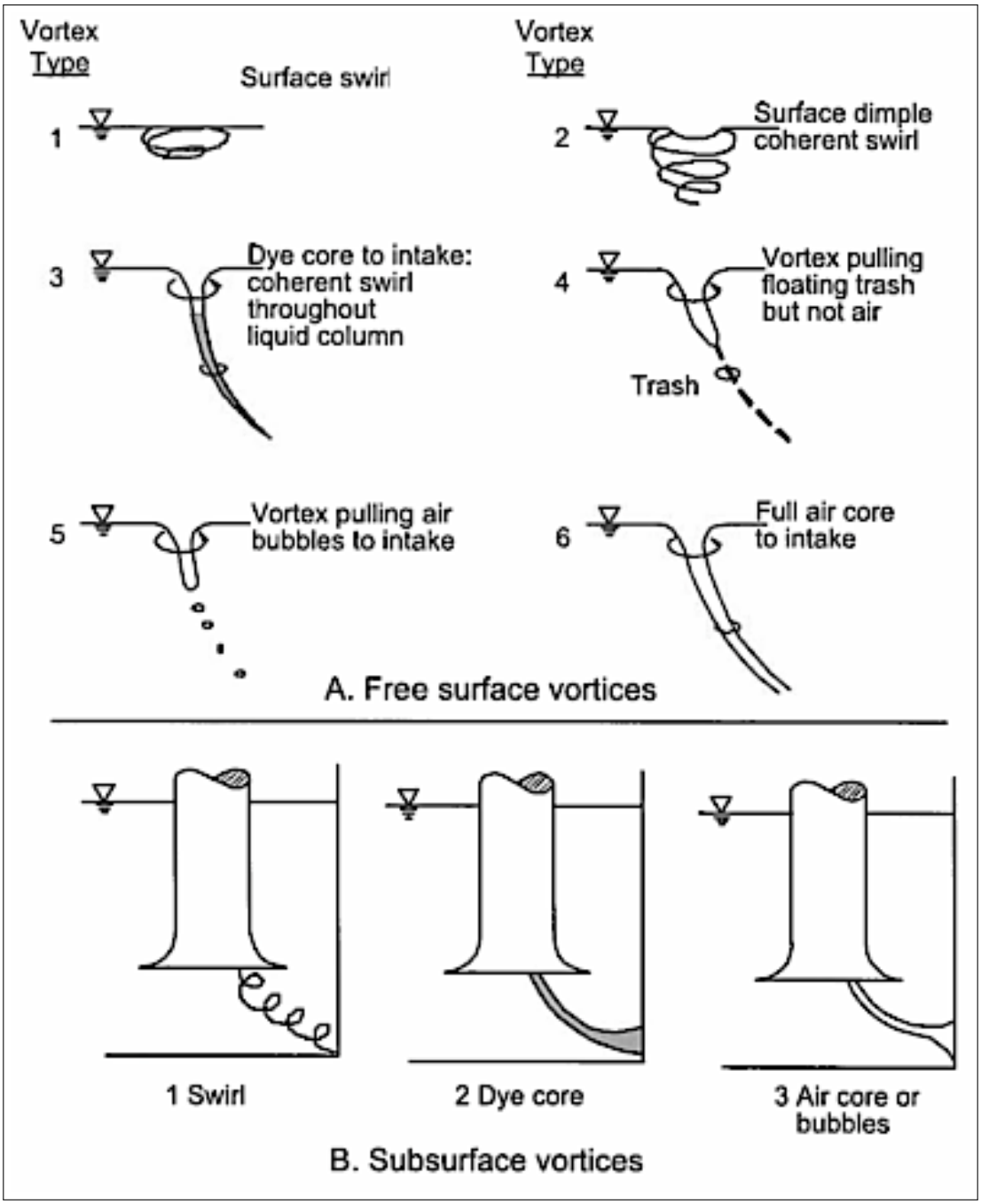

Figure 2.1: Vortex Classification According to Alden Research Laboratory [1]

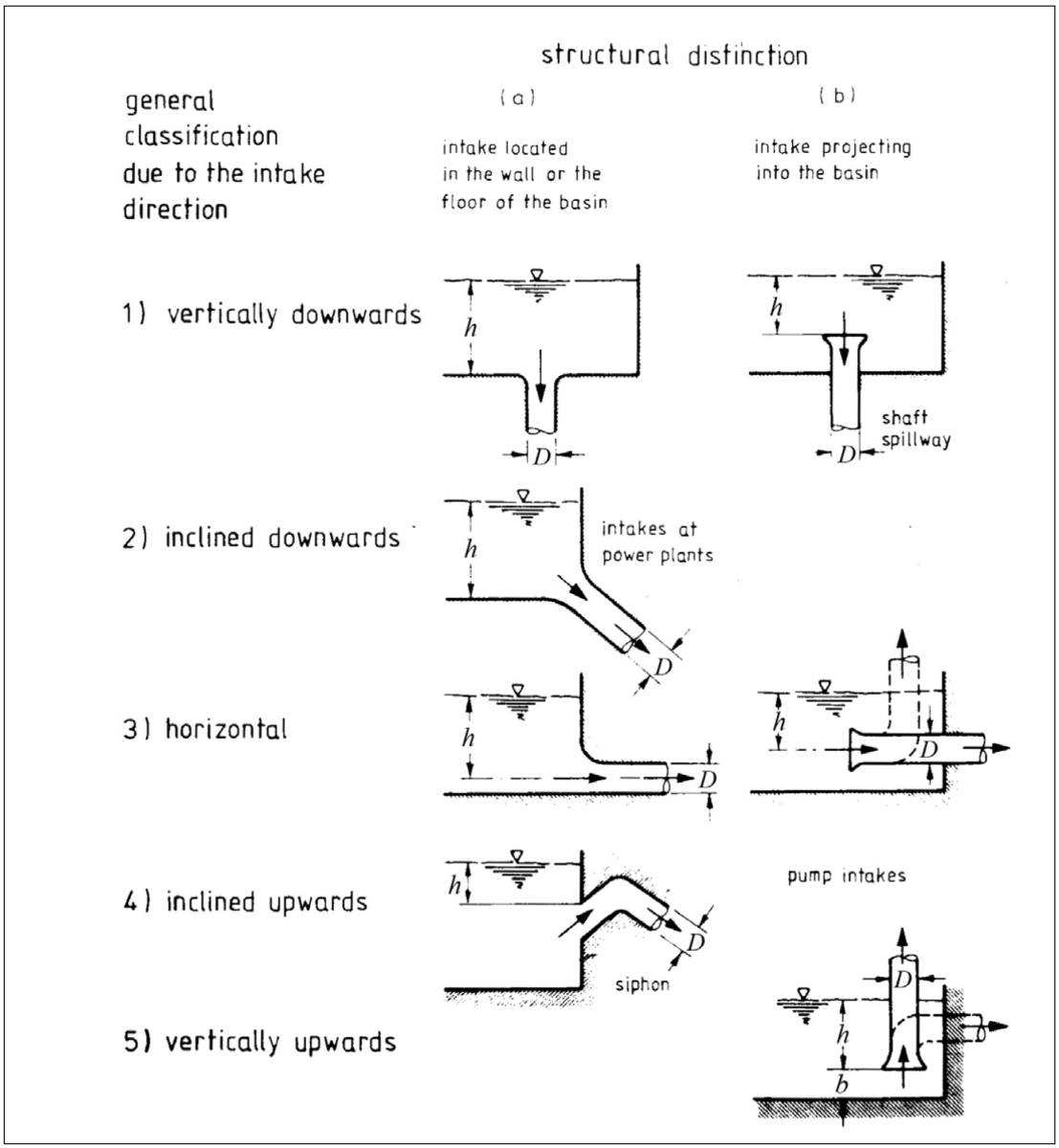

Figure 2.2: Classification of Intake Types [1]

2.2 Experimental Research for Defining Critical Submergence

Anwar [10] made experiments in a cylindrical vortex chamber with a vertical bottom intake and take tangential velocity measurements in different water levels outside of the intake radius and compared them with an analysis based on laminar flow. He used glycerol as fluid and measured the distribution of circulation at various levels and concluded that tangential velocity thus circulation is dependent on radius only. He also offered an equation based on circulation, however it is unclear how to adapt it to field conditions.

Daggett and Keulegn [11] investigated the effect of surface tension, viscosity and inertial circulation on free surface vortex. Their study shows that the surface tension has minimal effect on vortices when Weber number is greater than 10^4, but the viscosity and inertial circulation has an influence. They used different fluids and mixtures in order to count the effect of viscosity and surface tension in a vertical circular intake with a constant diameter of 0.1 m in their studies.

2.2.1 Experimental Studies on Horizontal Intakes

Gordon (1970, cited in [1, p. 62]) made experiments in horizontal intakes, leading weak but unstable vortices and defined the relationship between critical submergence, S_c, and intake Froude Number, Fr, as:

$$\frac{S_c}{D_i} = 1.7Fr \qquad for\ symmetrical\ approach. \tag{2.1}$$

$$\frac{S_c}{D_i} = 2.3Fr \qquad for\ asymmetrical\ approach. \tag{2.2}$$

where $Fr = V_i/\sqrt{gD_i}$; V_i = average intake velocity and D_i = intake diameter. That contributes to a conclusion there is a linear relationship between relative critical submergence, S_c/D_i and Froude Number, Fr.

Knauss [1] proposed the following equation for critical submergence, according to the own data of experiments on horizontal intakes and minimum submergences of well operating prototypes given by Gordon (1970), Penino and Hecker (1979) and

Hecker (1981) .

$$\frac{S_c}{D_i} = 0.5 + 2Fr \tag{2.3}$$

Also Amphlett (1976, cited in [1, p. 62]) used a horizontal intake in his experiments and he regulated the flow with 30° plates and studied for a more organized circulation with stable and steady vortices. In that case the relation is dependent on square root of Fr.

$$\frac{S_c}{D_i} = 3.3\sqrt{Fr} - 0.5 \tag{2.4}$$

for $c/D_i = 0.5$, and

$$\frac{S_c}{D_i} = 3.95\sqrt{Fr} - 0.5 \tag{2.5}$$

for $c/D_i = 4$, where c is the vertical distance between the lowest point of the intake pipe and reservoir bottom.

Prosser (1977, cited in [1, p. 61]) suggested very basic relation for critical submergence in rectangular intakes as:

$$\frac{S_c}{D_i} = 2.5 \tag{2.6}$$

This relation is recommended for small to medium size intakes.

Reddy and Pickford (1972, cited in [1], [12]) offered two equations in case if any vortex suppression device presents or not. They used Gordon's data and other data in the literature as well and set a minimum limit to the submergence depth that it should always be greater than the Froude number. The data they analyzed include both horizontal and vertically inverted intakes, suggesting that the approach flow field is the same in vertical inverted and horizontal intakes, so the required submergence will be the same. However this will not be the case in reality, the approach flow conditions are different for vertical and horizontal intakes. Equation 2.7 is the upper limit for critical submergence by Reddy and Pickford (1972, cited in [1], [12]) and should be used when no vortex suppressing devices present.

$$\frac{S_c}{D_i} = 1 + Fr \tag{2.7}$$

Equation 2.8 is the minimum limit and also should be used when vortex suppressing

devices present.

$$\frac{S_c}{D_i} = Fr \tag{2.8}$$

Paterson and Noble (1982, cited in [4]) suggested the critical submergence as:

$$\frac{S_c}{D_i} = 1.5 + 2.5Fr \tag{2.9}$$

Hydraulic Institute Standards ([5], [6]) have become a guide for pump intake design and aims to increase pump performance by proper design of the intakes and filling the gap between industry and academy. The main consideration to achieve the most of the hydraulic efficiency is to prevent the pump from swirls, unsteady flow, non-uniform flow and entrained air which could be basically condensed as, idealizing flow conditions in a vortex free environment. This should also be achieved for all operating conditions with optimization. The 1998 edition of this standard [5] uses design diameter as inlet bell outside diameter and submergence 'S_c' as a function of Froude Number 'Fr' and 'D_i' while the newer and older version [6] uses design rate of flow for the basis of the intake design. Also suggests the following formula for critical depth, which is the same equation suggested by Hecker [1] :

$$\frac{S_c}{D_i} = 1 + 2.3Fr \tag{2.10}$$

Orientation, wall clearance value according to intake diameter and position of intakes are also recommended in order to ensure desired flow conditions. For non-symmetric approach which is most of the time the case for hydraulic intakes of reservoirs Hydraulic Institute Standards suggests model tests. Both of them has acceptance criteria for physical model tests as:

- Allowing up to type 3 vortex for surface vortices and type 2 for subsurface vortices
- Average swirl angle less than 5 degrees and swirl angles less than 7 degrees but the occurrence of maximum 10% of time

The newer version also accepts these criteria and suggests model tests for those conditions, also it adds CFD.

Möller [13] investigated the air entrainment ratio over vortex formation in his work. He made experiments in a steel reservoir of 50 m^3 with a horizontal intake. He measured the entrained air in order to predict the relationship between entrained air and vortex.

In Flygt's [14] design recommendations for pump intakes for dry installed pumps it is recommended that critical submergence should be determined as given in Equation 2.11 and also not be less then $1.75D_i$

$$\frac{S_c}{D_i} = 1.7Fr \tag{2.11}$$

Khanarmuei et al. [9] have studied both horizontal and vertical intakes and they gave different equations for all 3 withdrawal directions which are applicable to dual intakes. Their study is based on a model setup composed of two circular pipes next to each other, and the aforementioned equations are given as:

$$\frac{S_c}{D_i} = 4.44Fr^{0.859} \qquad for\ 90°(vertical) \tag{2.12}$$

$$\frac{S_c}{D_i} = 4.2Fr^{0.869} \qquad for\ 45° \tag{2.13}$$

$$\frac{S_c}{D_i} = 4.21Fr^{1.351} \qquad for\ 0°(horizontal) \tag{2.14}$$

Baykara [15] conducted experiments with six different pipe diameters to investigate vortex formation under symmetrical approach flow conditions with different side wall distances and presented empirical equations for critical submergence. The most simplified equation of S_{ce}/D_i as a function of Fr was given as

$$\frac{S_c}{D_i} = 1.278Fr^{0.558} \tag{2.15}$$

Gökmener [16] conducted a series of experiments to investigate vortex formation for symmetrical and asymmetrical approach flow conditions using the same experimental setup used in this study considering that critical submergence is measured from the free surface to the top point of the intake pipe, S_{ce}. He proposed the following

empirical equations for S_{ce}/D_i as a function of Fr:

For symmetrical approach flow conditions;

For single water intake case:

$$\frac{S_{ce}}{D_i} = 1.520Fr^{0.785} \tag{2.16}$$

For double water intake case:

$$\frac{S_{ce}}{D_i} = 1.579Fr^{0.339} \tag{2.17}$$

For triple water intake case:

$$\frac{S_{ce}}{D_i} = 1.824Fr^{0.624} \tag{2.18}$$

For asymmetrical approach flow conditions;

For single water intake case:

$$\frac{S_{ce}}{D_i} = 1.441Fr^{0.827} \tag{2.19}$$

For double water intake case:

$$\frac{S_{ce}}{D_i} = 1.479Fr^{0.602} \tag{2.20}$$

For triple water intake case:

$$\frac{S_{ce}}{D_i} = 1.806Fr^{0.529} \tag{2.21}$$

2.2.2 Experimental Studies on Vertical Intakes

Vertical Intakes are more common on pump structures, while horizontal intakes or angled intakes are more common on hydropower structures. They were widely investigated throughout the history.

Jain et al. (1978, cited in [1, p. 62]) made experiments on vertically downwards intakes with 30° plates presented surrounding the intake in order to stabilize the flow. They proposed an equation for critical submergence as:

$$\frac{S_c}{D_i} = 4.5\sqrt{Fr} \tag{2.22}$$

Berge (1966, cited in [1, p. 62]) studied on vertically upwards intakes and obtained the following equation:

$$\frac{S_c}{D_i} = 3.3\sqrt{Fr} + 0.25 \tag{2.23}$$

Chang (1979, cited in [1, p. 62]) studied on vertically upward intakes and obtained an equation linearly dependent on Froude Number as:

$$\frac{S_c}{D_i} = 1.35Fr \tag{2.24}$$

Werth and Frizzell [17] made experiments to prevent low intensity vortex (type 3), on vertically downward flowing intakes that are suitable to Hydraulic Institutes's [5] standards. They proposed an equation based on Fr number as:

$$\frac{S_c}{D_i} = 2.1 + \frac{4}{3}Fr^{\frac{2}{3}} \tag{2.25}$$

Yıldırım and Kocabas [18] applied potential flow theory in order to predict critical submergence for vertical intakes.

2.3 Numerical Studies

Along with the development of experimental searches in vortex formation, numerical studies are also present and started with vertical examples cylindrical tanks or pipes as forced vortex or plughole vortex. Plughole vortex can be seen in nature when draining of water.

There are numerous researches for determining critical submergence that leads to various relationships as stated above. Quite variations along the range of critical submergence and the broadness in that range gives arise the question that could we predict the critical submergence more precisely.

Ansar et al. [8] used the numerical method developed by Sotiropoulos and Patel (1992) and Constantinescu and Patel (1997) both cited in Ansar et al. [8]. After

comparing the numerical simulation results with experimental results they suggested using the numerical solution to identify approach flow character and as a guide to the physical model by reducing the scenarios.

Tokyay and Constantinescu [3] tried two different Turbulent models namely DNS/LES and RANS with a code developed by Mahesh and with the commercial FLUENT software respectively. They investigated the vortices on a vertical pump sump and compared the numerical model with the experimental study of Patel. As a result, LES is more accurate than DNS when compared with data collected by PIV measurements.

Panzadis and Blömeling [19] used a combined analytical-numerical method to predict the critical submergence in vertical upward pump sumps. First, they interpolated the critical submergence by the air core length of two different simulation results. However, since this method underestimates the critical submergence compared to the experimental results and further studies show that in order to improve the ANSYS CFX results it requires a significantly higher computational effort. Then they determined the flow field around the intake with help of the ANSYS CFX. Combining CFD results of circulation and suction parameter with the analytical vortex model of Burgers and Rott's critical submergences were predicted.

Later Pandazis and Babcsany [20] took PIV measurements in vertical upward pump sumps to compare with the experimental study and CFD results and also investigated the effect of vortex breakers. They also applied the combined method of Panzadis and Blömeling [19] and they reported that the tangential velocity distribution calculated from the combined method is in a good agreement with PIV measurements.

In the study of Nöid [21] a scale model of the Akkats hydropower plant dam located in Sweden has been built. CFD was used for solving the Unsteady Reynolds Average Navier-Stokes equations (URANS) in addition to scale testing with ANSYS Fluent software using RNG k-ϵ turbulence model. No vortex is formed in any cases at the horizontal intake and the simulation blows up after some time.

Wu et al. [22] simulated three cases for a vertical pump sump with a commercial software namely STAR-CCM+, and they also took PIV measurements for one case. Their simulation model was based on the experiments of Rajendran et al. [23]. They

reported that a well defined free surface vortex could not be presented in simulations despite deformations on the free surface.

CHAPTER 3

DIMENSIONAL ANALYSIS

3.1 Dimensional Analysis of Critical Submergence

Dimensional analysis has been used to make sure that the results obtained in experiments shall successfully represent the real flow field and to determine the key parameters that govern a physical study. The scaled model should be simplified with the help of dimensional analysis in order to distinguish the physical model from geometrical measurements. The general dimensions of the physical model used in this study are shown in Figure 3.1 and with the help of dimensional analysis the results of this study could be carried on a prototype scale. In this study critical submergence is defined as the height of the water from the centerline of the intake pipe to the water surface when an air core vortex is present and it is a function of the independent quantities, which can be classified as flow, fluid and geometric parameters, as given in Equation 3.1:

$$S_c = f_1(\rho, \mu, \sigma, g, V_i, \Gamma, b_1, b_2, c, D_i) \tag{3.1}$$

The fluid properties are: density (ρ), dynamic viscosity (μ) and surface tension (σ).

Flow properties are: average velocity in intake (V_i) , average circulation exposed to flow (Γ) and gravitational acceleration, (g).

Geometric properties are: horizontal distance from the center of the intake to the right- side plexiglass wall (b_1), horizontal distance from the center of the intake to the left- side plexiglass wall (b_2), vertical distance between the lowest point of the intake pipe and reservoir bottom (c) and diameter of intake (D_i).

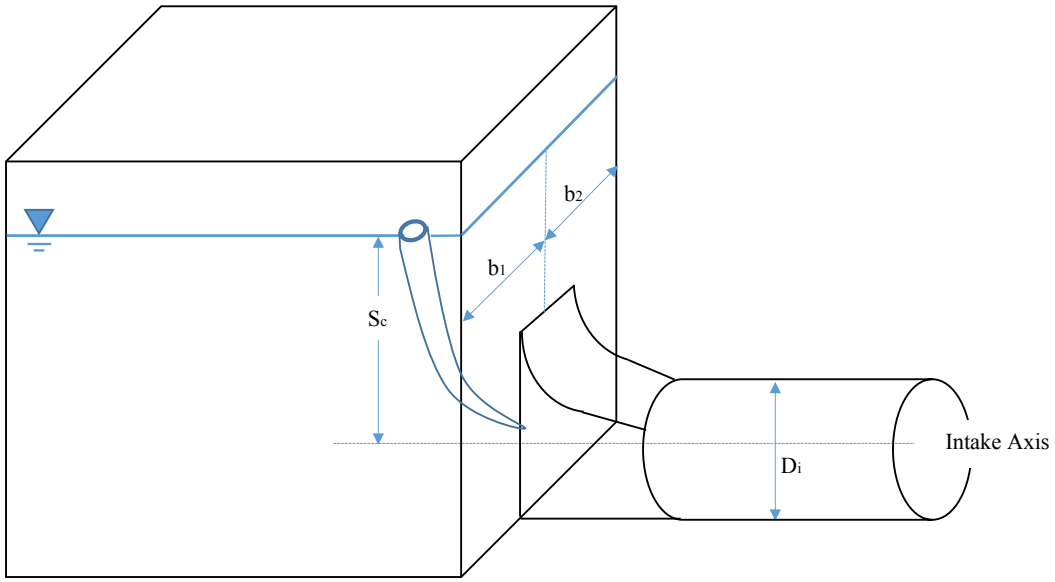

Figure 3.1: Sketch of the Model

From the application of Buckingham's π theorem to Equation 3.1 the following dimensionless parameters given in Equation 3.2 were obtained.

$$\frac{S_c}{D_i} = f_2(\frac{b_1}{D_i}, \frac{b_2}{D_i}, \frac{c}{D_i}, Fr, Re, We, K_o) \tag{3.2}$$

where;

$\frac{b_1}{D_i}$ = Aspect ratio of right side wall clearance to intake centerline

$\frac{b_2}{D_i}$ = Aspect ratio of left side wall clearance to intake centerline

$\frac{c}{D_i}$ = Aspect ratio of bottom clearance to intake wall

$Re = \frac{V_i D_i \rho}{\mu}$ = Intake Reynolds Number

$Fr = \frac{V_i}{\sqrt{g D_i}}$ = Intake Froude Number

$We = \frac{\rho V_i^2 D_i}{\sigma}$ = Intake Weber Number

$K_o = \frac{\Gamma}{V_i D_i}$ = Intake Kolf Number

Bottom clearance for the physical model used in this study is zero, so this ratio could be omitted, leading to the below equation for the dimensionless critical submergence:

$$\frac{S_c}{D_i} = f_3[\frac{(b_1 + b_2)}{D_i}.(\frac{b_1}{b_2}), Fr, Re, We, K_o] \tag{3.3}$$

Equation 3.3 could be used for asymmetrical flow conditions which is the case in this study. The term $((b_1 + b_2)/D_i.(b_1/b_2))$ is a new dimensionless number defining the asymmetrical approach geometry and it is represented by ψ throughout the study. So the Equation 3.4 is obtained as:

$$\frac{S_c}{D_i} = f_4[\psi, Re, Fr, We, K_o] \tag{3.4}$$

In model studies to have a complete similarity between the model and prototype all of the corresponding dimensionless parameters given in the governing equation of the problem must be the same. Since this situation is not practically satisfied, otherwise length scale of unity is required for the model, the most important dimensionless parameters are assumed to be equal to each other, which is the Fr, in practice. Therefore, the importance of the related dimensionless parameters given in Equation 3.3 are discussed below briefly.

3.2 Effect of Froude Number

Froude similarity is used in most cases in hydraulic problems. It is applicable when the main force in the system is due to gravity, like open channel flows, weirs, free surface flows and reservoir flows. Most of the studies in literature give the relationship between critical submergence and Froude number [1],[4],[5], [6], [9], and [14]. Froude similarity is used for air entraining vortex studies however in order to be sure to mitigate the surface tension and viscosity effects, the minimum value of Reynolds and Weber number criteria should be satisfied.

3.3 Effect of Reynolds Number

Reynolds similarity is suitable for the problems that viscosity and inertia forces are dominant. It is used in pipe flows, where the viscosity is dominant. In vortex prob-

lems, Reynolds Number and viscosity effect could be eliminated when Re$> 10^4$ according to Daggett & Keulegan (1974, cited in [1]). Hydraulic Institute [5] and [6] and Jain et al. (1978, cited in [1]) suggested a minimum values of 6×10^4 and 5×10^4 for Reynolds Number, respectively.

3.4 Effect of Weber Number

Weber similarity is used when the surface tension is the significant force in the system. Yıldırım and Jain [24] concluded that Weber number is important only in low circulation where a weak dimple occurs at the free surface. The minimum magnitude of Weber number should be greater than 240 according to Hydraulic Institute ([5], [6]) in order to eliminate the surface tension effect in modeling of vortex formation. Jain et al. (1978, cited in [1]) suggested a minimum value of 120 for Weber Number.

3.5 Effect of Kolf Number

Kolf number is a dimensionless parameter that shows the effect of circulation of the flow. Since an unnatural circulation is not created by an external response in this study, the circulation parameter, Γ, could be omitted, so the related dimensionless number which is Kolf Number, K_o, can be removed from Equation 3.4.

3.6 Dimensionless Relationship For Critical Submergence

As a result the dimensionless relationship between relative critical submergence, S_c/D_i, and the independent dimensionless parameters; geometrical parameter for asymmetrical approach flow conditions, ψ, Froude Number, Fr, Reynolds Number, Re, and Weber Number, We, is obtained as in Equation 3.5. The relationship given in Equation 3.5 is investigated using a systematic experiment program.

$$\frac{S_c}{D_i} = f[\psi, Fr, Re, We] \tag{3.5}$$

CHAPTER 4

EXPERIMENTAL STUDY

4.1 Experimental Setup and Procedure

In the present study, a series of experiments were conducted in the Hydromechanics Laboratory of METU. Figure4.1 and Figure 4.2 show the top and side views of the experimental model constructed in order to observe the intake behaviour of a planned Dam project with Froude similarity with a scale of $1/29.99$, the scale which is chosen according to the commercially available pipe diameters. The reservoir was constructed with concrete and plexiglass where three of the walls and basement of the reservoir, as well the half of the front wall is concrete. The front wall is defined as the wall that intakes are mounted and the lower half is constructed with concrete where the upper half of it is constructed with plexiglass in order to visualize the air entraining vortex. Also the intakes were constructed from plexiglass in half and steel on the other half as details can be seen in Figure 4.3 and 4.4. This design of using transparent plexiglass lets in the experiments to visually observe air bubble and air core formation of the vortex furthermore to track the captured air's journey inside the intake pipe. In the closed circuit system, the water is filled to reservoir from the supply tank with help of gravity and the same water is pumped to the supply tank after circulating in the reservoir and intake pipes. In the entrance of the reservoir after the back wall a perforated wall system constructed from hollow bricks as shown in Figure 4.5, it is used in order to regulate the flow of water entering to the reservoir. The perforated wall has a purpose to obtain more uniform flow and reduce disturbances in the flow hence sustain calmer reservoir conditions for experiments. The experimental system consists of a supply tank, a reservoir, vanes and four intakes which three of them are used in this study. All of the three intakes were starting with a square cross-section in

44 cm length and then turns to a circular pipe with 26.5 cm diameter.

For the experimental procedure, water is filled to the reservoir from the supply tank up to maximum water level and intake vanes were opened then waited until the steady reservoir level is sustained, then type 5 and 6 vortex formation is observed in the reservoir for approximately 1 cm increments starting from the highest level. The level of water in the reservoir is lowered if no vortex is observed for half an hour. Discharge of intake is arranged by the valves downstream of the intakes and it is measured with help of an electromagnetic discharge-meter attached to each pipe in upstream as can be seen in Figure 4.6, the exact discharge when the vortex is observed has been noted with the critical depth. A range of 60 l/s to 120 l/s is examined in the study for single, double and triple intakes. Critical depths were obtained with a ruler attached to the plexiglass walls behind the intake structure with an accuracy of $\pm 1mm$, also piezometer readings were taken for calibration. The intake structure and the wall behind it were made of plexiglass in order to enable visual observation of the air bubble and air core formation of vortex and also to track the captured air's journey inside the intake pipe. Intake structure is also made of plexiglass at some extend, then it turns to a metal pipe with a diameter of 26.5 cm. For the asymmetry of approach channel, intakes were arranged with two plexiglass attachments, that were used not to disturb the visual observation and obtain a smooth free surface and they arranged for every different opening. An example of vortex captured is presented in Figure 4.7, vortices captured were always in the same fashion in terms of scale and time of observation, only the vortex location changed from left to right at a point close to the walls. A close view of their mouth could be seen as in Figure 4.8, varying between 3.5 cm to 4 cm in diameter, and the time of occurrence is between 3-4 seconds. The top view of the vortex formation behind could be seen in Figure 4.9. Froude, Weber and Reynolds numbers at the intake were calculated for the instance vortex type of 5 or 6.

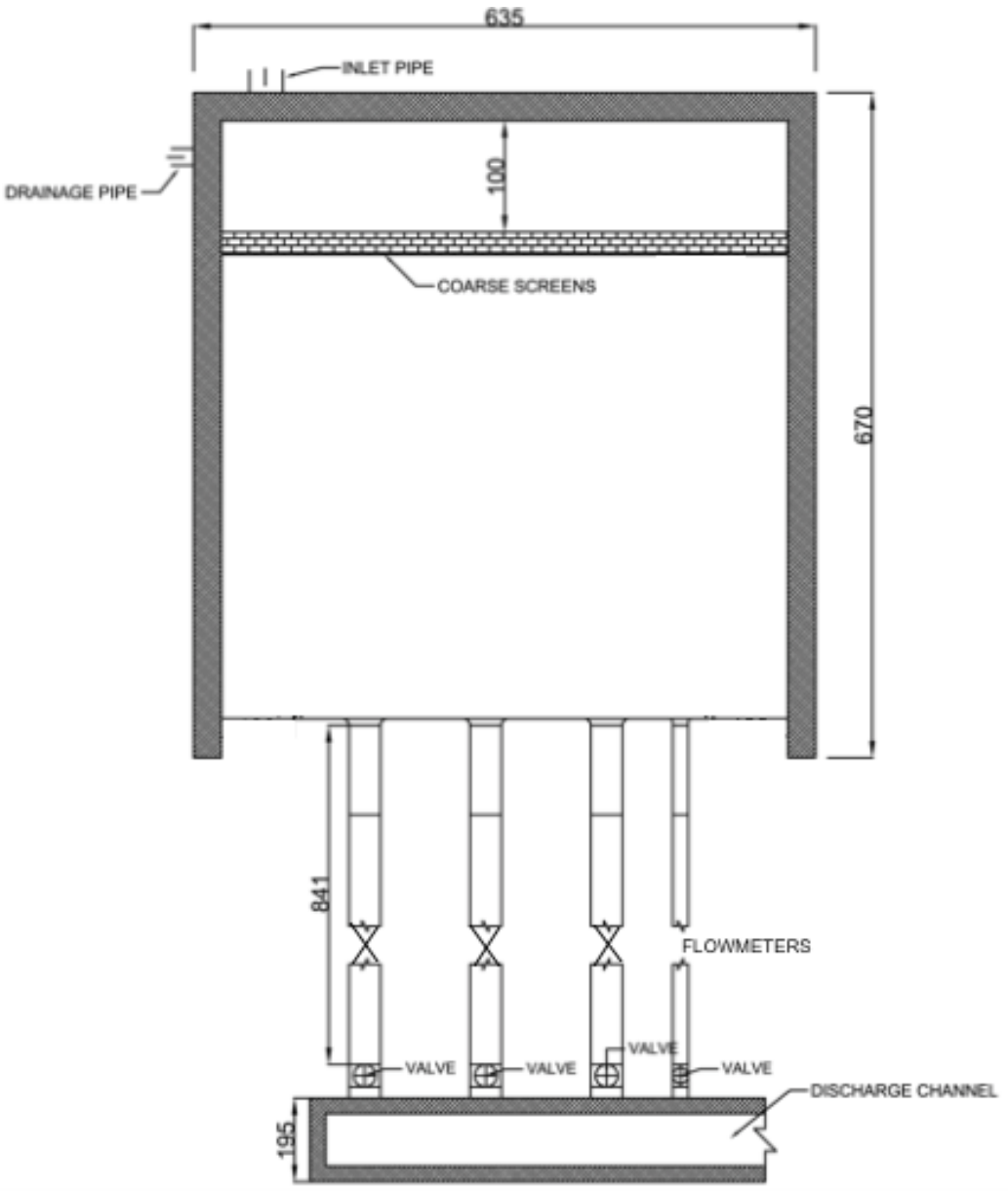

Figure 4.1: General Layout of the Experimental Model (Top-view), Dimensions are in cm

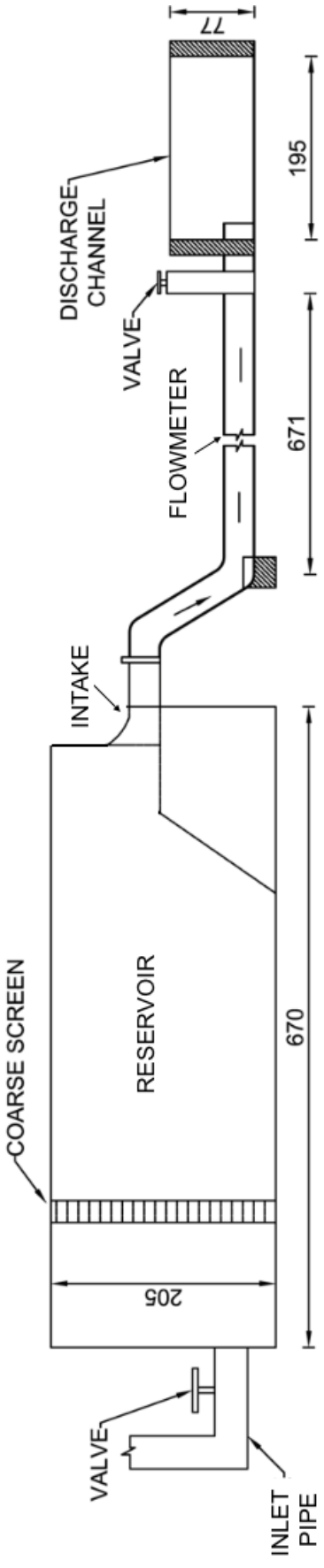

Figure 4.2: General Layout of the Experimental Model (Side-view), Dimensions are in cm

Figure 4.3: View of the Experimental Model from Downstream

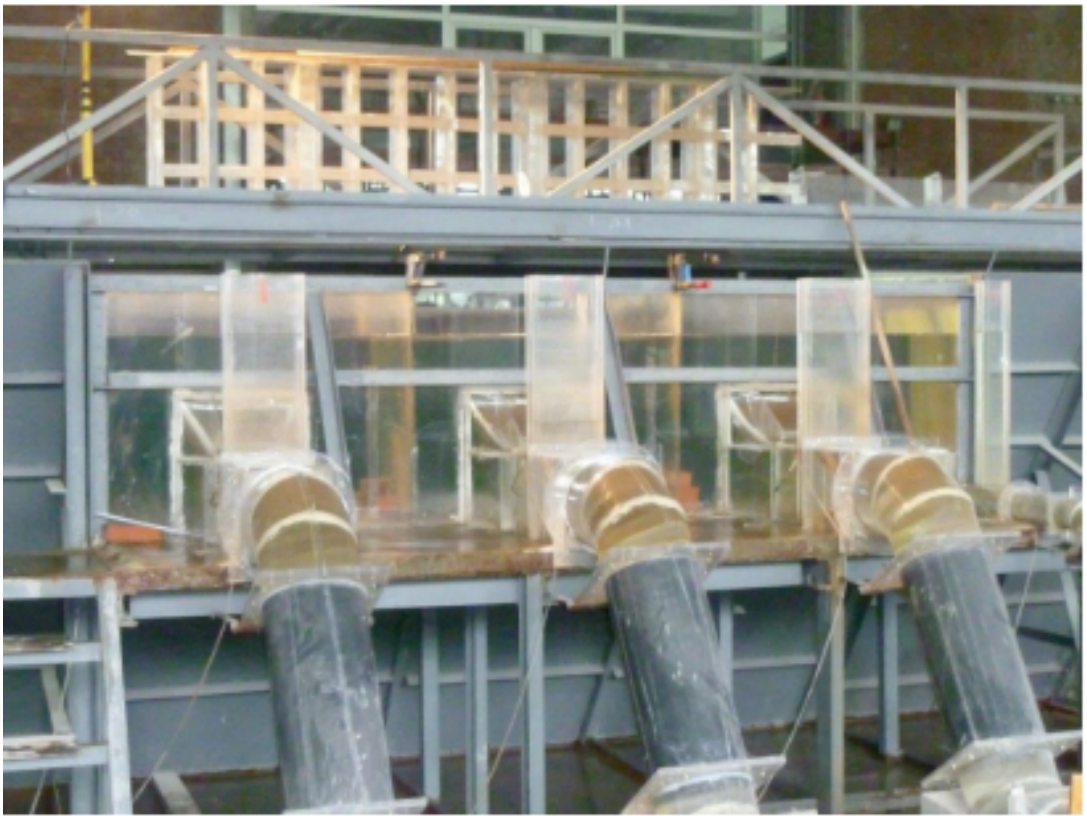

Figure 4.4: Close View of the Hydraulic Intakes

Figure 4.5: Buffle Blocks at the entrance of the reservoir

Figure 4.6: Electronic Flowmeters Attached to Downstream of Each Intake

There was a totall of 30 different setups made in the experimental study which 10 of them were with single intake, 15 of them were with double intakes and 5 of them were with triple intakes. First of all the number of intake which would be in operation was decided. After that for that selected intake type; single, double or triple, different openings were arranged around that intake with plexiglass walls in such a way that asymmetrical flow conditions would prevail in front of the intake. Every different case with their openings are shown in Figures 4.10 - 4.13.

Figure 4.7: An Example Vortex with Scale

Figure 4.8: Close View of the Vortex Mouth

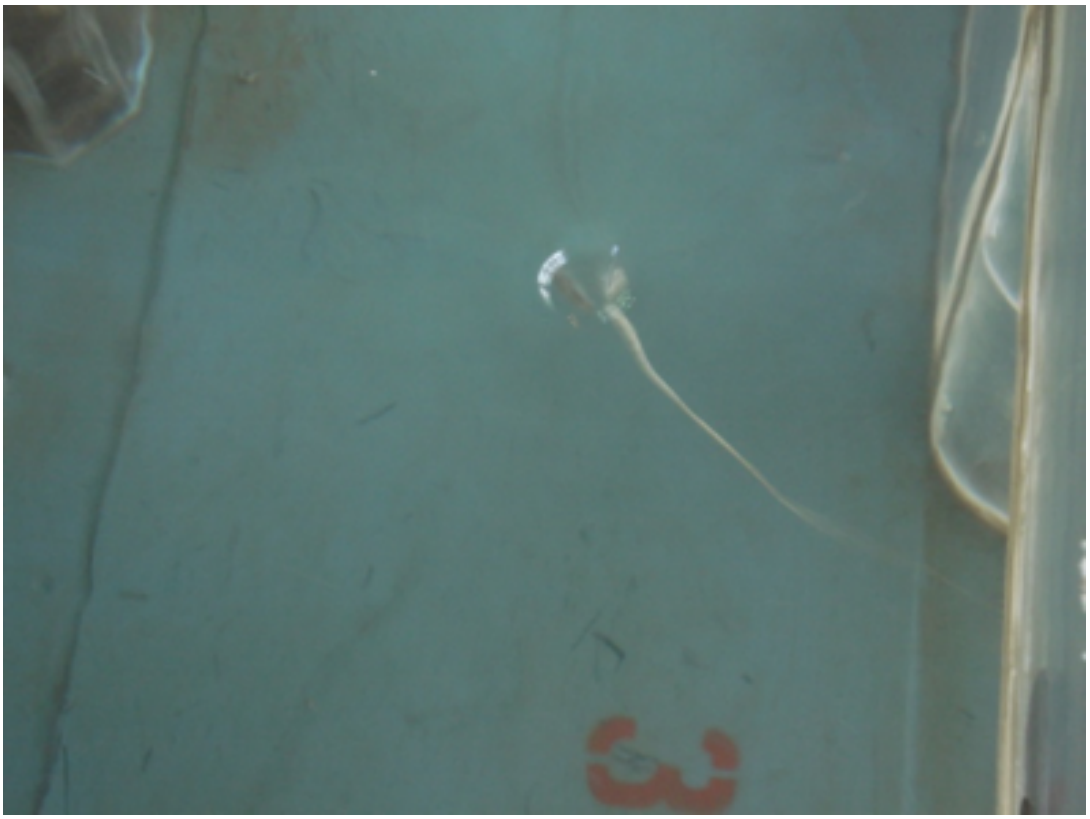

Figure 4.9: Top View of Vortex

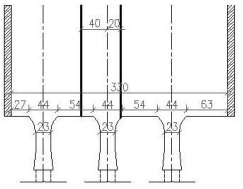

40 cm left, 20 cm right
SCALE:1/50

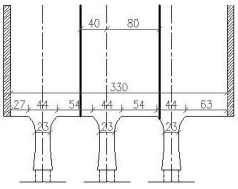

40 cm left, 80 cm right
SCALE:1/50

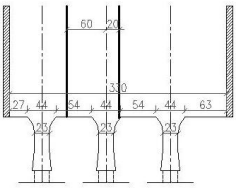

60 cm left, 20 cm right
SCALE:1/50

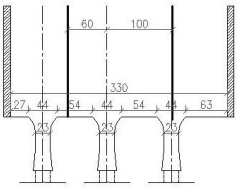

60 cm left, 100 cm right
SCALE:1/50

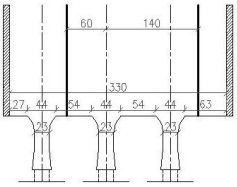

60 cm left, 140 cm right
SCALE:1/50

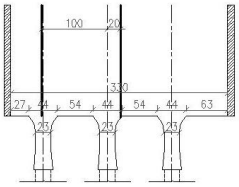

100 cm left, 20 cm right
SCALE:1/50

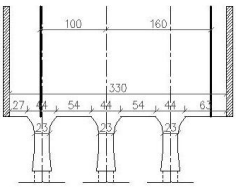

100 cm left, 160 cm right
SCALE:1/50

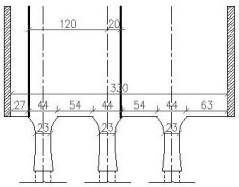

120 cm left, 20 cm right
SCALE:1/50

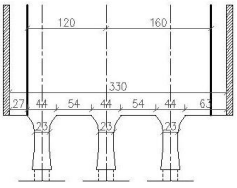

120 cm left, 160 cm right
SCALE:1/50

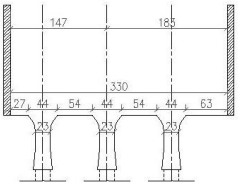

147 cm left, 183 cm right
SCALE:1/50

Figure 4.10: Single Intake Setups

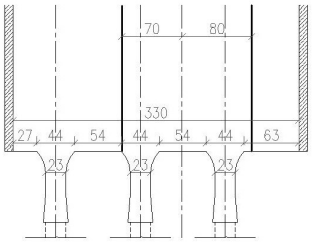

70 cm left, 80 cm right
SCALE:1/50

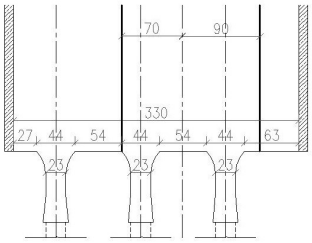

70 cm left, 90 cm right
SCALE:1/50

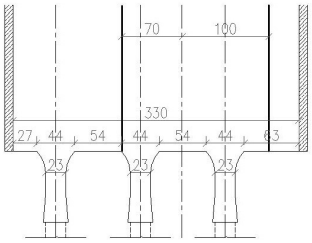

70 cm left, 100 cm right
SCALE:1/50

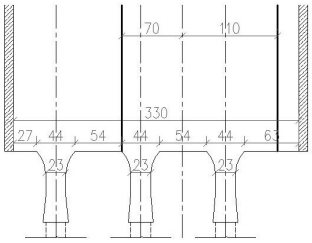

70 cm left, 110 cm right
SCALE:1/50

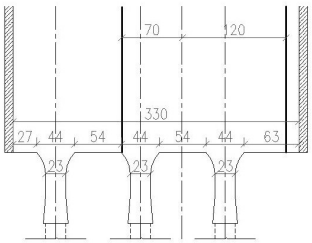

70 cm left, 120 cm right
SCALE:1/50

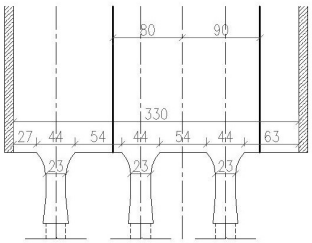

80 cm left, 90 cm right
SCALE:1/50

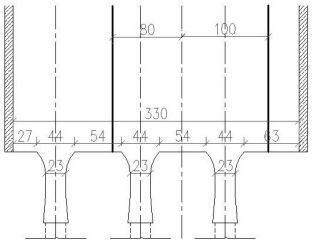

80 cm left, 100 cm right
SCALE:1/50

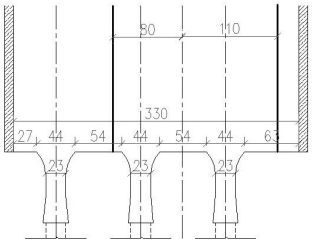

80 cm left, 110 cm right
SCALE:1/50

Figure 4.11: Double Intake Setups

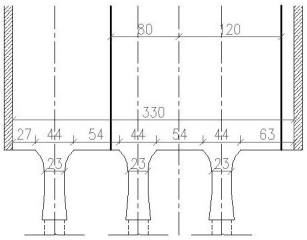

80 cm left, 120 cm right
SCALE:1/50

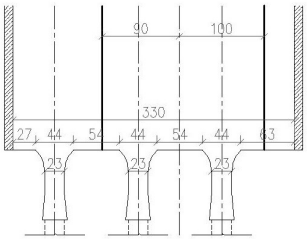

90 cm left, 100 cm right
SCALE:1/50

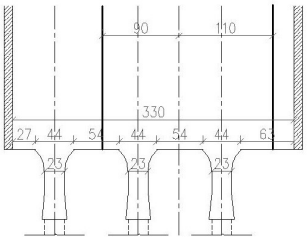

90 cm left, 110 cm right
SCALE:1/50

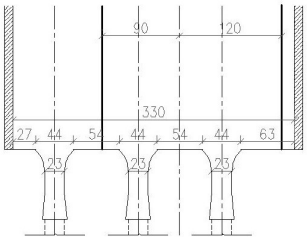

90 cm left, 120 cm right
SCALE:1/50

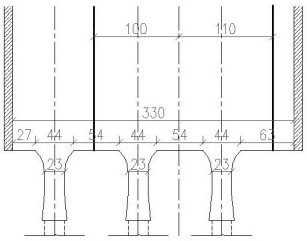

100 cm left, 110 cm right
SCALE:1/50

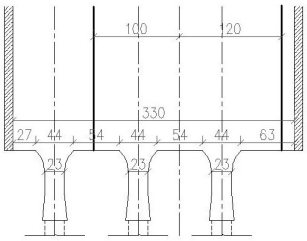

100 cm left, 120 cm right
SCALE:1/50

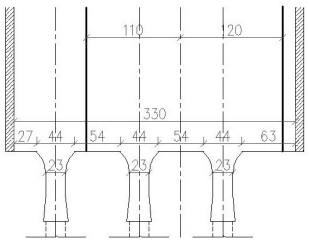

110 cm left, 120 cm right
SCALE:1/50

Figure 4.12: Cont. Double Intake Setups

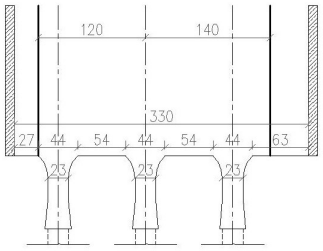

120 cm left, 140 cm right
SCALE:1/50

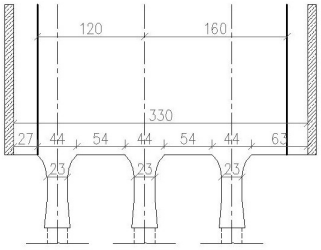

120 cm left, 160 cm right
SCALE:1/50

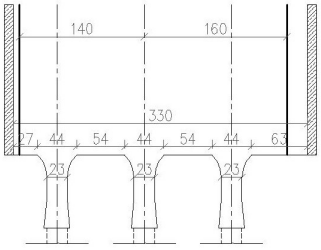

140 cm left, 160 cm right
SCALE:1/50

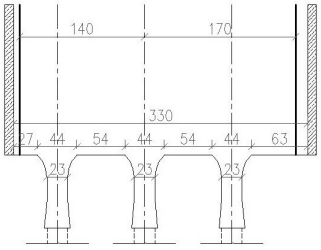

140 cm left, 170 cm right
SCALE:1/50

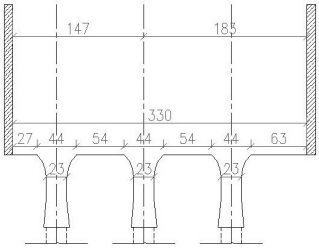

147 cm left, 183 cm right
SCALE:1/50

Figure 4.13: Triple Intake Setups

4.2 Experimental Study on Single Intakes

There were 10 different setups with 42 experiments in single intake study. The middle intake pipe is used in the study, different openings were arranged with plexiglass walls. The ranges of the parameters investigated as a result of the study are shown in Table 4.1, where intermediate values are presented in Appendix A.

Table 4.1: Ranges of the Parameters Tested for Single Intake Case

V_i(m/s)	Fr	Re	We	S_c/D_i	ψ
1.08	0.67	286545.63	4248.42	1.73	0.88
$\sim$	$\sim$	$\sim$	$\sim$	$\sim$	$\sim$
2.30	1.43	609259.44	19206.37	2.54	7.92

The relationship between dimensionless critical submergence and Froude number, Reynolds number and Weber number for single intakes are shown in Figures 4.14 - 4.16, respectively. These figures show that for a given ψ, S_c/D_i increases with increasing Fr, Re and We, respectively. Since the curves of S_c/D_i versus Fr, Re and We for a given ψ intersect each other at various points as seen in those aforementioned figures, it is not easy to say something about the effect of ψ on S_c/D_i for a given Fr, Re or We. From the figures and also from Table 4.1 it is also clearly seen that the ranges of Re and We tested in this study are larger than those limit values given in Section 3.3 and 3.4 to neglect the effect of Re and We on the values of S_c/D_i. In the following sections, only the Froude number and ψ are to be considered as the predominant parameters for S_c/D_i. Therefore, regression analysis will be applied to the available data as to be discussed below.

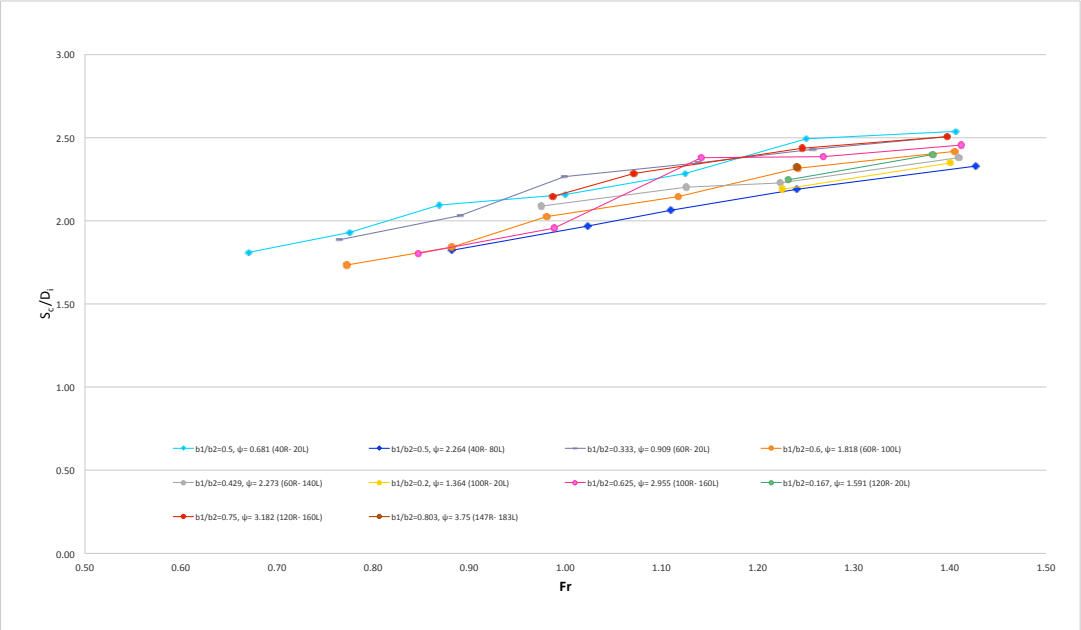

Figure 4.14: Dimensionless Critical Submergence vs Froude Number

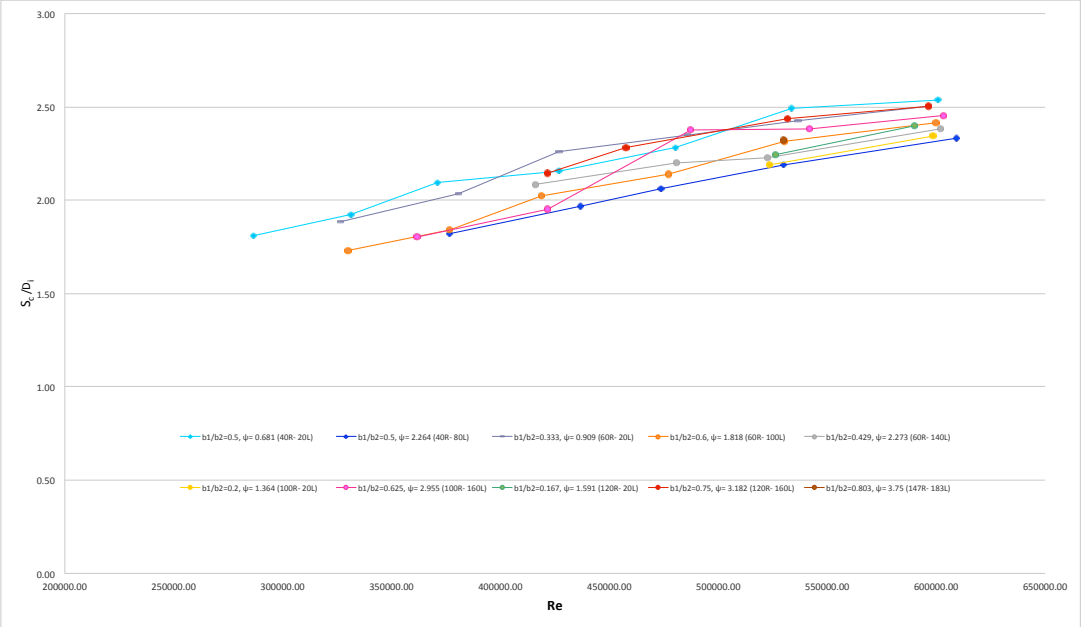

Figure 4.15: Dimensionless Critical Submergence vs Reynolds Number

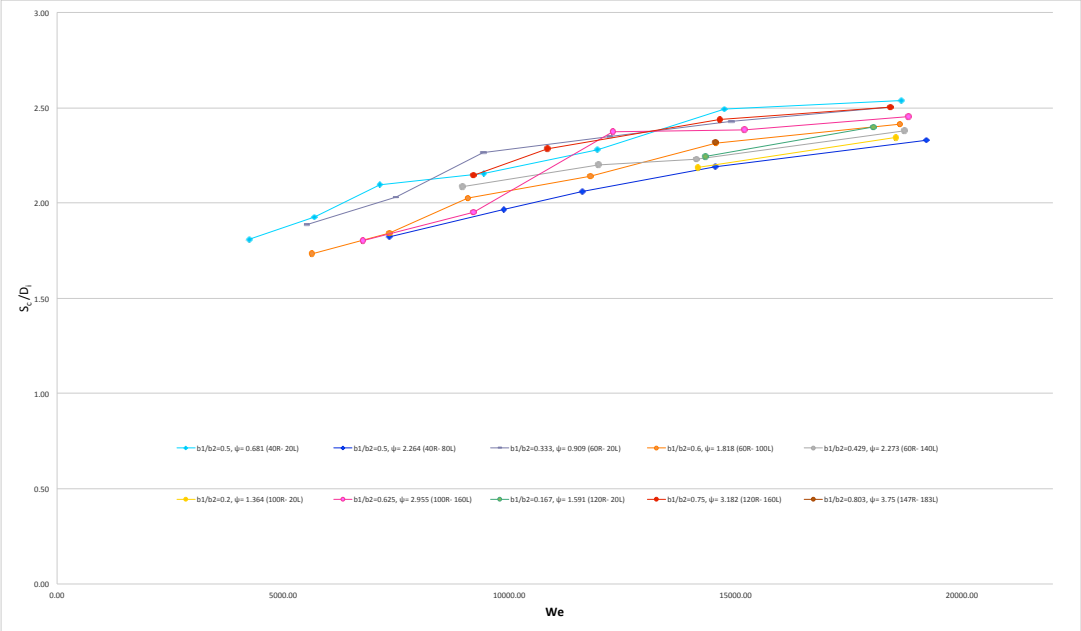

Figure 4.16: Dimensionless Critical Submergence vs Weber Number

Nonlinear regression analysis for dimensionless critical submergence as a function of Froude, Reynolds and Weber numbers and ψ gives us a formula with R^2 value of 0.801 for single intakes as shown in Equation 4.1.

$$\frac{S_c}{D_i} = 2.092\ Fr^{0.427}\ Re^{-0.025}\ We^{0.036}\ \psi^{-0.01} \tag{4.1}$$

When we eliminated We from the general equation, we obtained the formula as in Equation 4.2 with R^2 value of 0.801.

$$\frac{S_c}{D_i} = 2.022\ Fr^{0.471}\ Re^{-0.003}\ \psi^{-0.01} \tag{4.2}$$

Nonlinear regression analysis for dimensionless critical submergence yields Equation 4.3 after eliminating the effect of Re on the value of S_c/D_i with a value of $R^2 = 0.801$.

$$\frac{S_c}{D_i} = 2.1\ Fr^{0.474}\ \psi^{-0.01} \tag{4.3}$$

Figure 4.17 shows that the data of $(S_c/D_i)_{calculated}$ from Equation 4.3 lie within $\pm 10\%$ error lines.

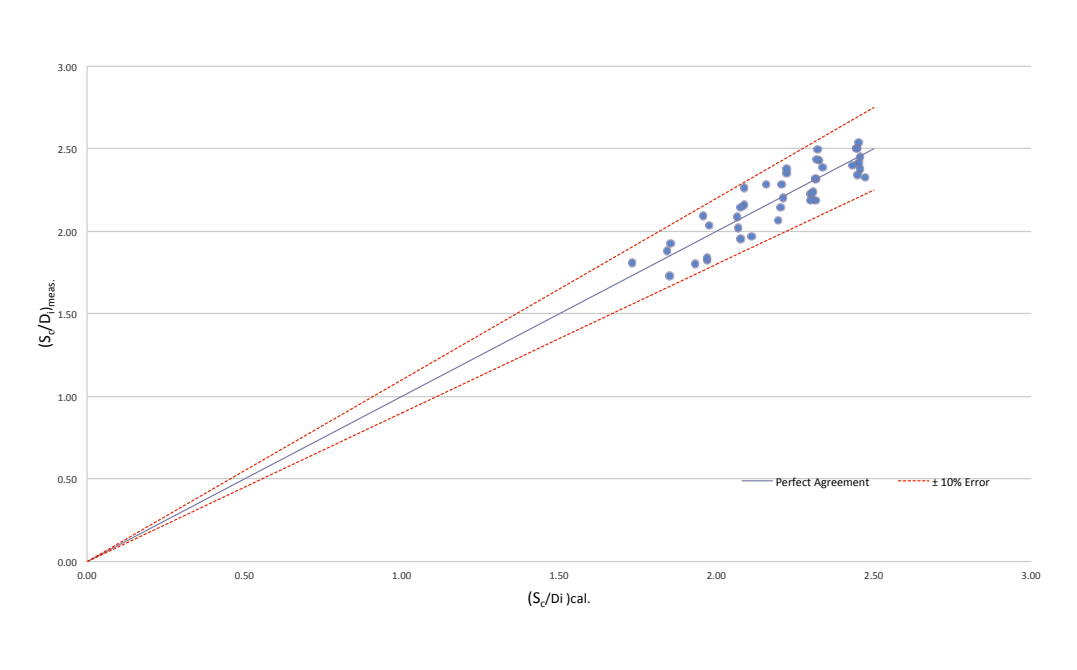

Figure 4.17: Comparison of Measured S_c/D_i Data With Calculated S_c/D_i Data From Equation 4.3

Considering the ease of use of the obtained Equation 4.3, all three constants are rounded up or down to obtain more recognizable mathematical statement. As an outcome Equation 4.4 is determined and it is relationship between the measured S_c/D_i is obtained as could be seen on Figure 4.18. It could be interpreted from Figure 4.18 that there is no significance loss on accuracy between the general equation, Equation 4.3 and rounded general equation,4.4 which also has R^2 value of 0.801 and data points lie between $\pm 10\%$ error lines.

$$\frac{S_c}{D_i} = 2.1\ Fr^{0.5}\ \psi^{-0.01} \tag{4.4}$$

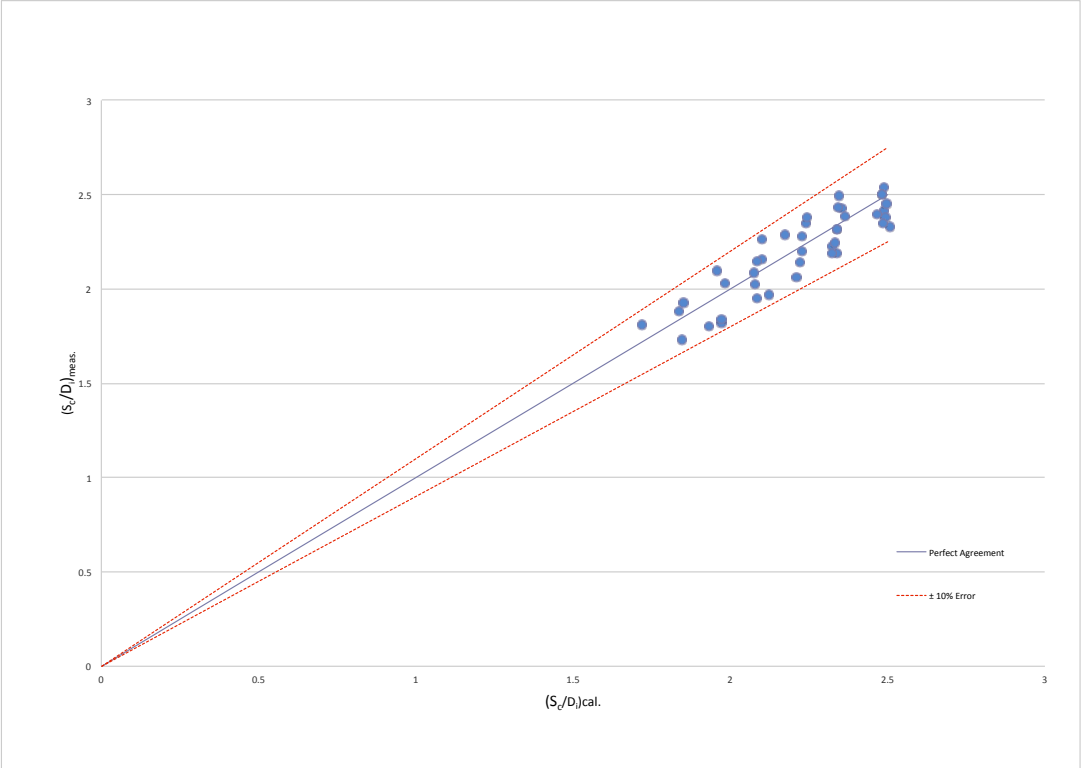

Figure 4.18: Comparison Between the Measured Values of S_c/D_i and the Ones Calculated by Equation 4.4

In order to observe the effect of asymmetrical approach flow condition on the relative critical submergence S_c/D_i, for a given Froude Number, Figure 4.19 was presented from Equation 4.4 for the single intake experiments conducted. This figure clearly shows that S_c/D_i slightly decreases with increasing ψ for a given Fr, and at ψ values larger than about 8, the effect of ψ on the value of S_c/D_i can be assumed to be negligible. Therefore by omitting ψ from the general equation of S_c/D_i, the simplified empirical equation for S_c/D_i, Equation 4.5, is obtained with R^2 value of 0.801. Based on this equation Figure 4.20 shows that all the data points lie between $\pm 10\%$ error lines.

$$\frac{S_c}{D_i} = 2.089\ Fr^{0.467} \tag{4.5}$$

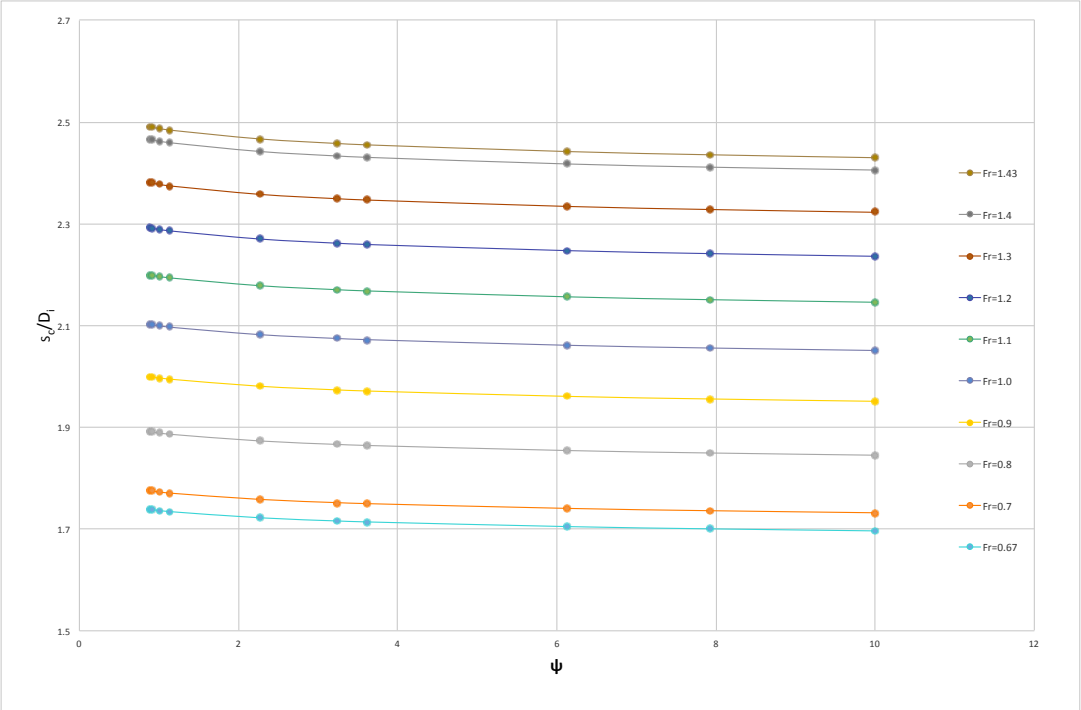

Figure 4.19: Variation of S_c/D_i with ψ as a Function of Fr

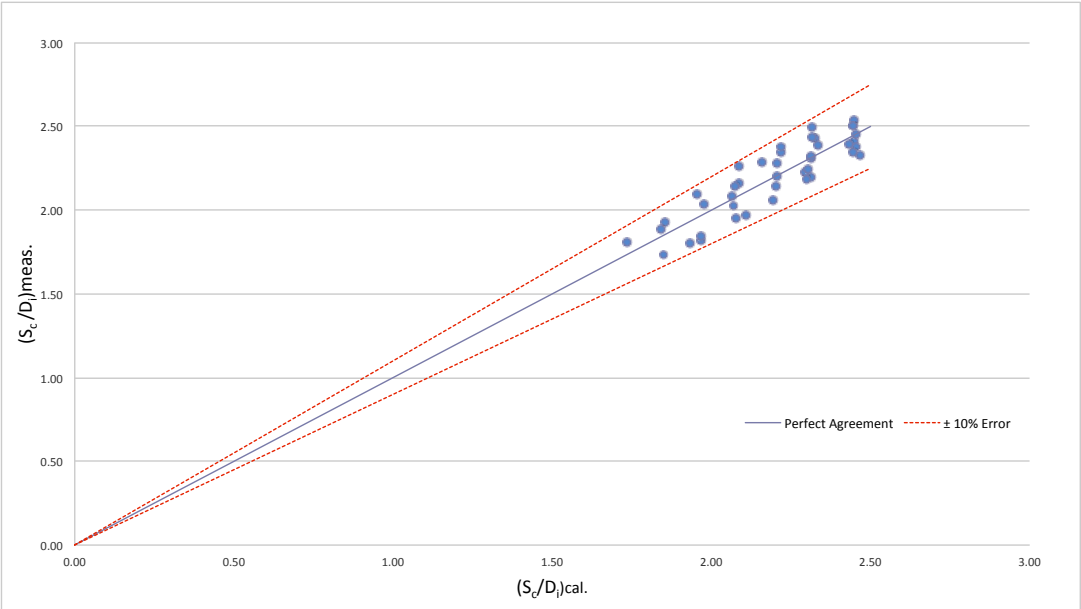

Figure 4.20: Comparison of Measured S_c/D_i Data With Calculated S_c/D_i Data from Equation 4.2

Further simplified form of Equation 4.2 is given as Equation 4.6 after rounding up the related numerical constants. To see the effect of this simplification on the values of S_c/D_i, Figure 4.21 was prepared in which all the data lie again $\pm 10\%$ error lines with R^2 of 0.800. This means that Equation 4.6 can be used with confidence.

$$\frac{S_c}{D_i} = 2.1\ Fr^{0.5} \tag{4.6}$$

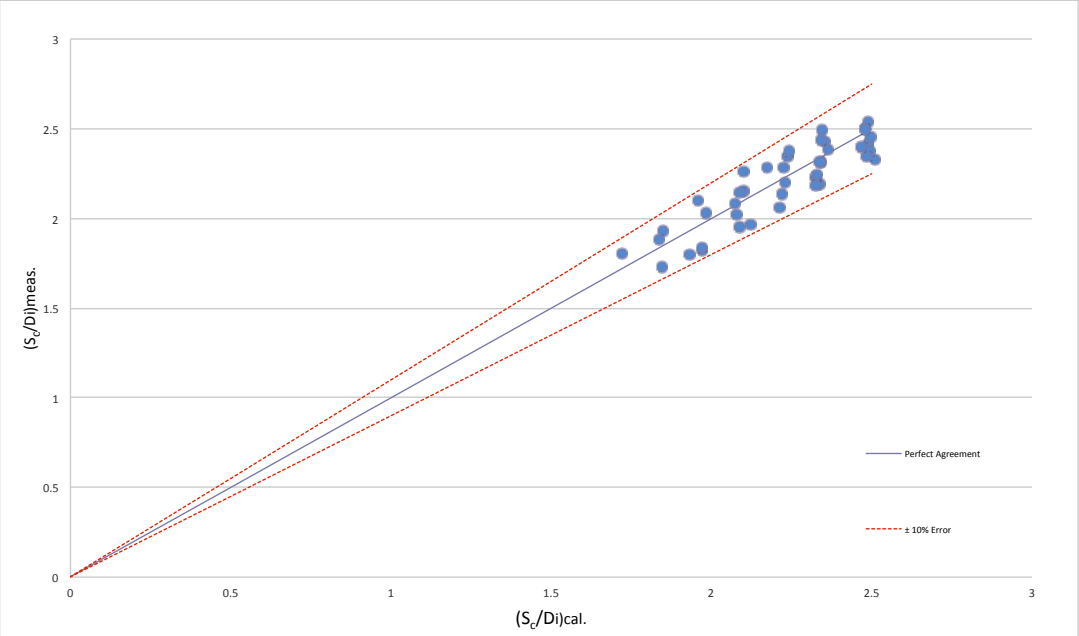

Figure 4.21: Comparison Between the Measured Values of S_c/D_i and the Ones Calculated by Equation 4.6

4.3 Experimental Study on Double Intakes

There were 15 different setups and 77 experiments in double intake study. The middle and third intake pipes were used in the study, different openings were arranged with plexiglass walls. The ranges of parameters tested as a result of the study are shown in Table 4.2, where intermediate values are presented in Appendix B..

Table 4.2: Ranges of the Parameters Tested for Double Intake Case

V_i(m/s)	Fr	Re	We	S_c/D_i	ψ
0.86	0.53	227148.85	4432.69	1.63	4.18
$\sim$	$\sim$	$\sim$	$\sim$	$\sim$	$\sim$
1.78	1.10	471698.11	19115.05	2.41	7.96

Figures 4.22 - 4.24 show the variation of S_c/D_i with Fr, Re and We, respectively. The general trends of all the curves of various ψ values given in those figures are very similar to those explained for the case of single intake.

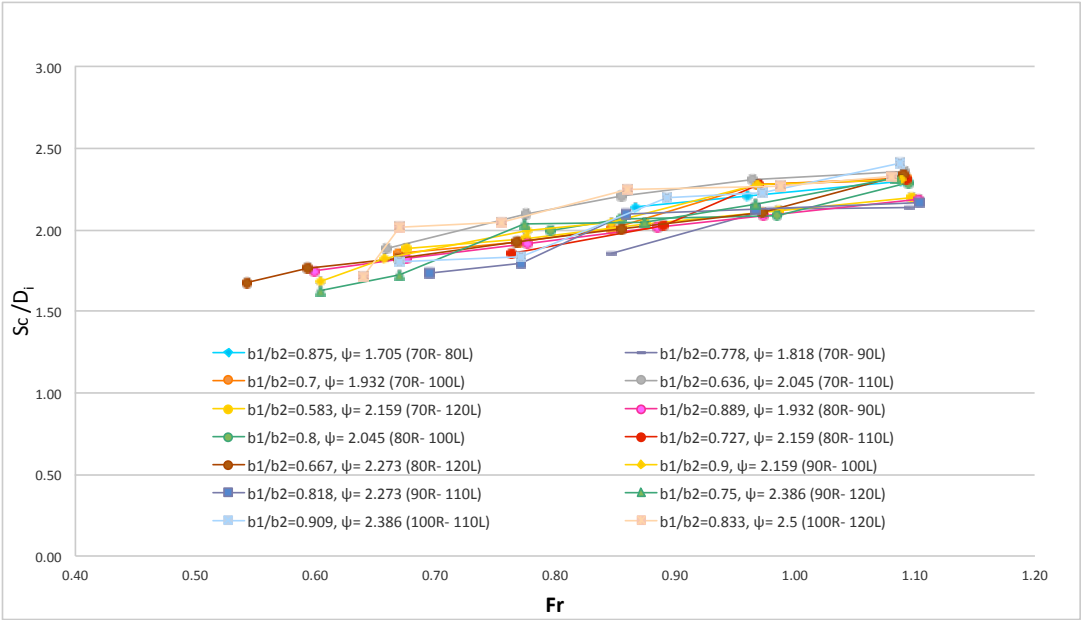

Figure 4.22: Dimensionless Critical Submergence vs Froude Number

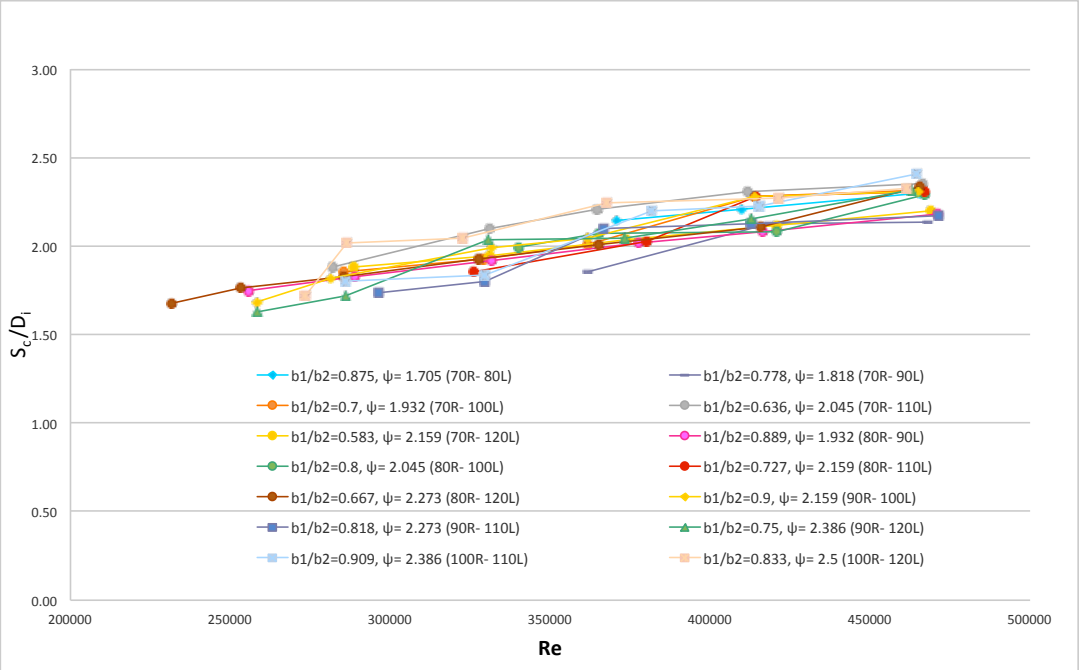

Figure 4.23: Dimensionless Critical Submergence vs Reynolds Number

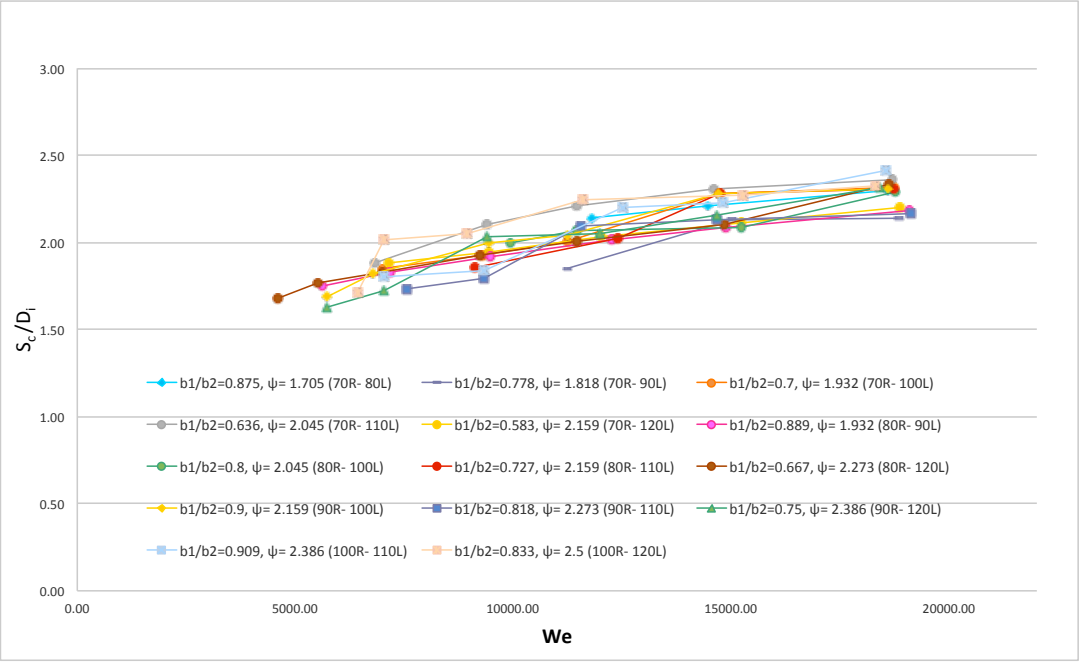

Figure 4.24: Dimensionless Critical Submergence vs Weber Number

Since the predominant variables for the variation of S_c/D_i are Fr, Re, We and ψ, nonlinear regression analysis was applied on the related data set and Equation 4.7 is obtained with R^2 value of 0.812.

$$\frac{S_c}{D_i} = 1.971\ Fr^{0.463}\ Re^{0.0001}\ We^{0.0001}\ \psi^{0.064} \tag{4.7}$$

Ignoring Weber number, Equation 4.8 with R^2 value of 0.812 was obtained:

$$\frac{S_c}{D_i} = 1.973\ Fr^{0.464}\ Re^{0.0001}\ \psi^{0.064} \tag{4.8}$$

Omitting the Reynolds number from the general equation of S_c/D_i, Equation 4.9 with R^2 value of 0.812 was determined.

$$\frac{S_c}{D_i} = 1.975\ Fr^{0.464}\ \psi^{0.064} \tag{4.9}$$

Figure 4.25 gives a comparison of measured S_c/D_i data with calculated data from Equation 4.9. As it is seen from the figure the calculated data lie within $\pm 10\%$ error lines.

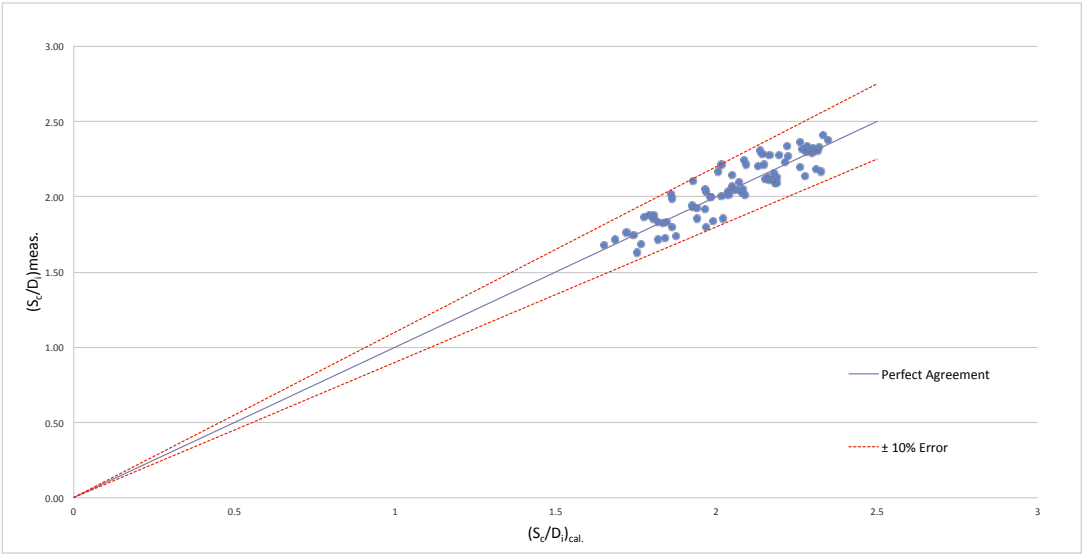

Figure 4.25: Comparison of Measured S_c/D_i Data With Calculated S_c/D_i Data From Equation 4.9

Similar to the process applied for the empirical equations of a single intake case, the simplified form of Equation 4.9 by rounding up the constant empirical numbers is given as shown in Equation 4.10 with R^2 value of 0.811 and the calculated S_c/D_i values from Equation 4.9 are presented in Figure 4.26. This figure reveals that Equation 4.10 is reliable as much as Equation 4.9.

$$\frac{S_c}{D_i} = 2\ Fr^{0.5}\ \psi^{0.06} \tag{4.10}$$

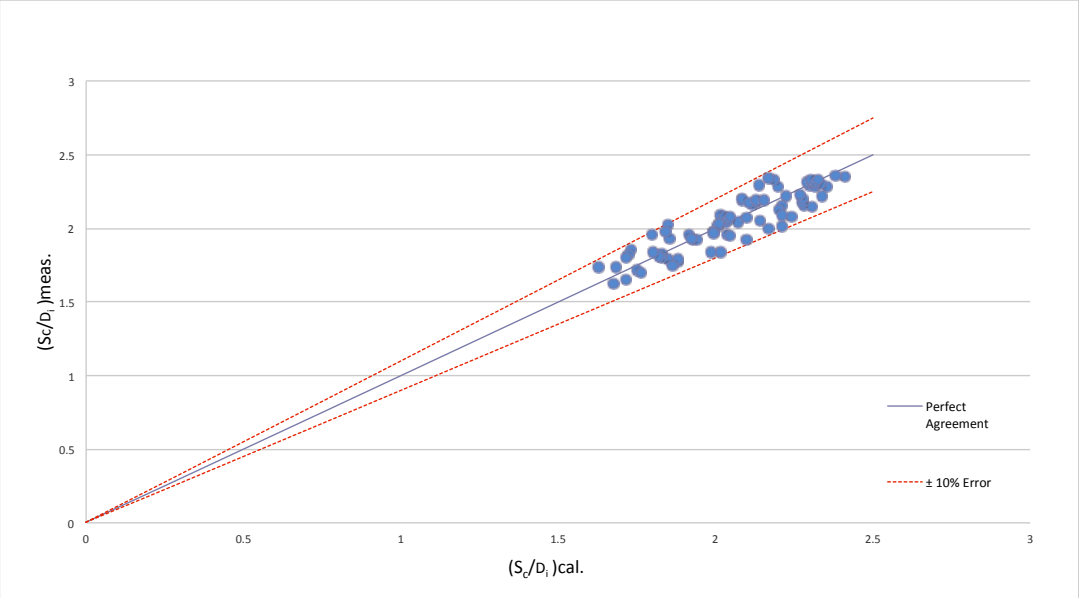

Figure 4.26: Comparison Between the Measured Values of S_c/D_i and the Ones Calculated by Equation 4.10

In order to observe the effect of asymmetrical approach flow condition on the values of relative critical submergence S_c/D_i; the variation of S_c/D_i with ψ for a given Fr was obtained from Equation 4.10 and then plotted as given in Figure 4.27. From this figure one can conclude that S_c/D_i slightly increases with increasing ψ. As done before for single intake case, here also the effect of ψ on S_c/D_i may be neglected and the related empirical equation of S_c/D_i an be given as Equation 4.11.

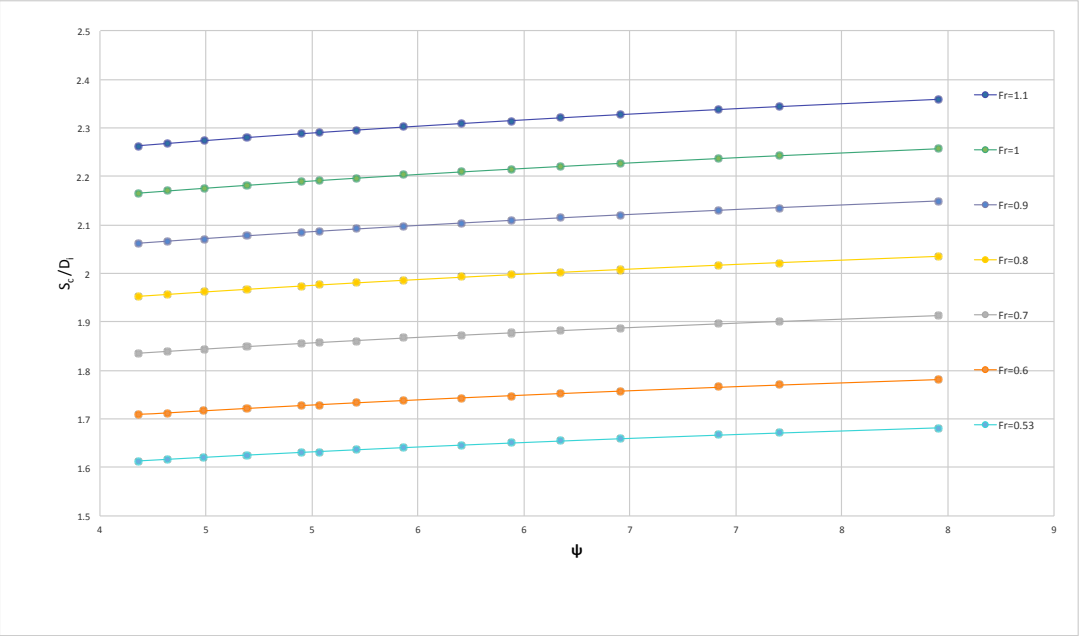

Figure 4.27: Variation of S_c/D_i with ψ as a function of Fr

To make the empirical equation of S_c/D_i more simplified, ψ is omitted from the general relation of S_c/D_i and the following equation Equation 4.11, is obtained for S_c/D_i with R^2 value of 0.798, the calculated data from this equation also lies within $\pm 10\%$ error lines as could be seen in Figure 4.28

$$\frac{S_c}{D_i} = 2.21 Fr^{0.451} \tag{4.11}$$

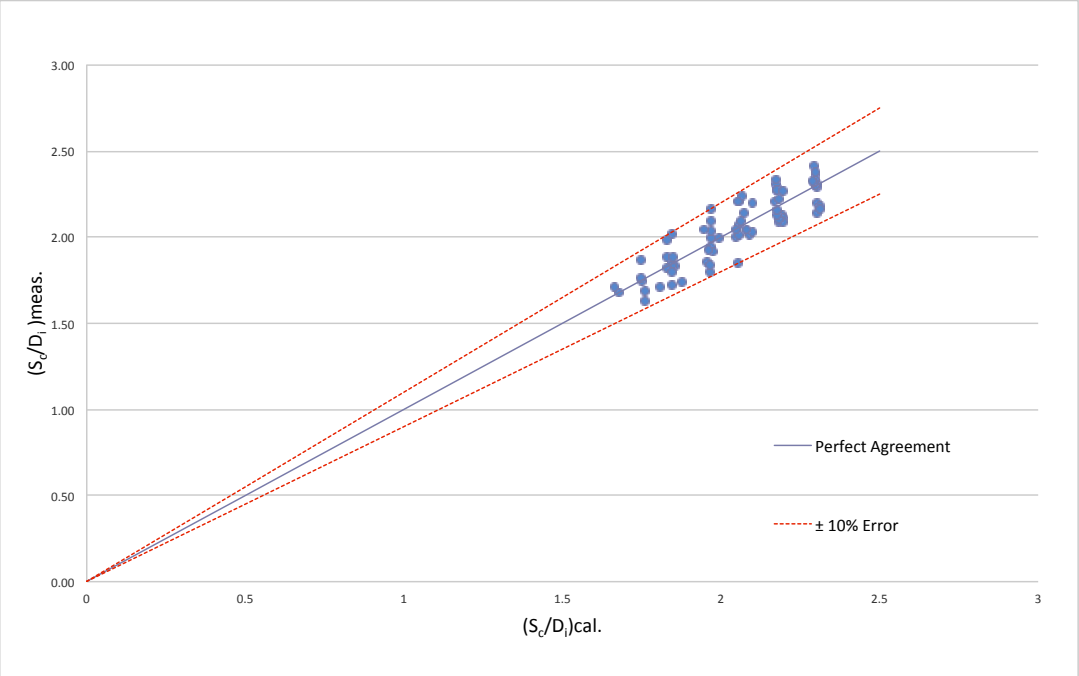

Figure 4.28: Comparison of Measured S_c/D_i Data With Calculated S_c/D_i Data From Equation 4.11

By rounding up the constant numerical values given in Equation 4.11, Equation 4.12 can be written with R^2 value of 0.794 which is pretty close to the corresponding R^2 value of Equation 4.11 (Figure 4.29).

$$\frac{S_c}{D_i} = 2.2\ Fr^{0.5} \tag{4.12}$$

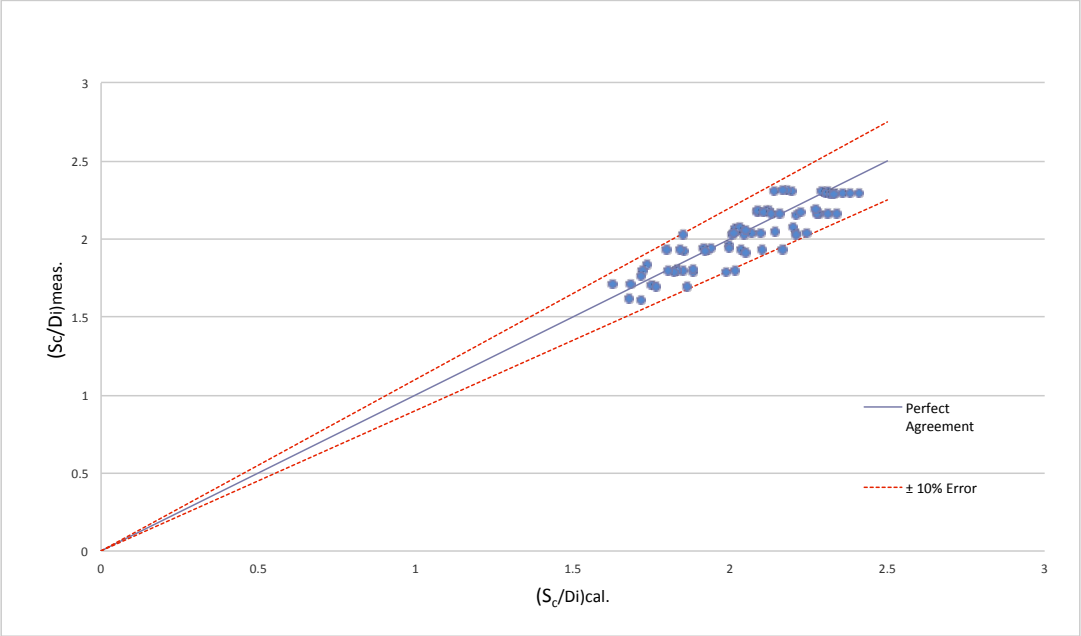

Figure 4.29: Comparison Between the Measured Values of S_c/D_i and the Ones Calculated by Equation 4.12

4.4 Experimental Study on Triple Intakes

There were 5 different setups and 26 experiments in triple intake study. All of the intake pipes were used in the study, different openings were arranged with plexiglass walls. The ranges of parameters tested as a result of the study are shown in Table 4.3, where intermediate values are presented in Appendix C.

Table 4.3: Ranges of the Parameters Tested for Triple Intake Case

V_i (m/s)	Fr	Re	We	S_c/D_i	ψ
0.69	0.43	184486.37	1761.04	1.76	7.92
$\sim$	$\sim$	$\sim$	$\sim$	$\sim$	$\sim$
1.62	1.00	428022.36	9479.23	2.52	10.00

Variation of S_c/D_i with Fr, Re and We are presented in Figures 4.30 - 4.32, respectively. The general trends of all the curves of various ψ values given in those figures are very similar to those of single and double intake cases. Referring to Table 4.3 it could be concluded that Fr is the most important parameter along with ψ on which S_c/D_i depends compared to other parameters of Re and We, similar to the other intake cases described earlier.

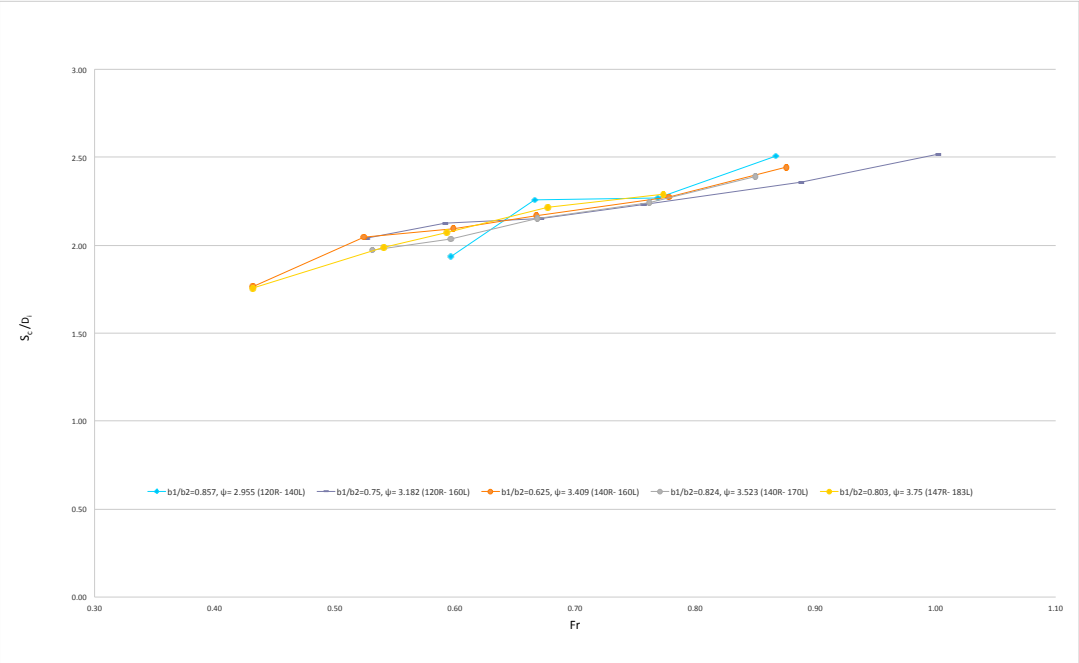

Figure 4.30: Dimensionless Critical Submergence vs Froude Number

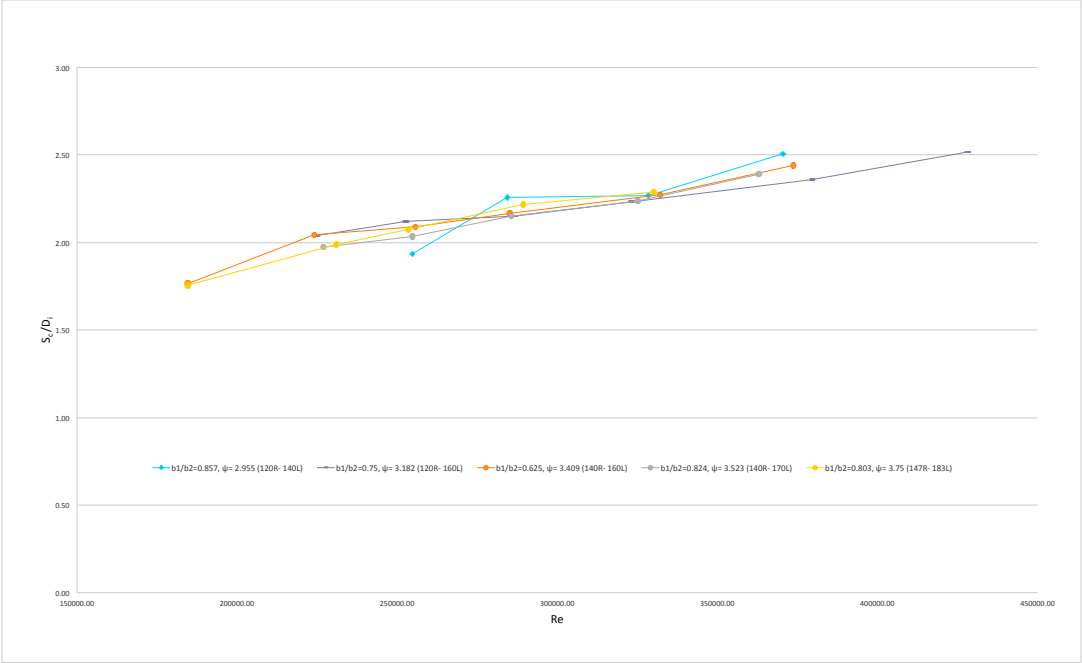

Figure 4.31: Dimensionless Critical Submergence vs Reynolds Number

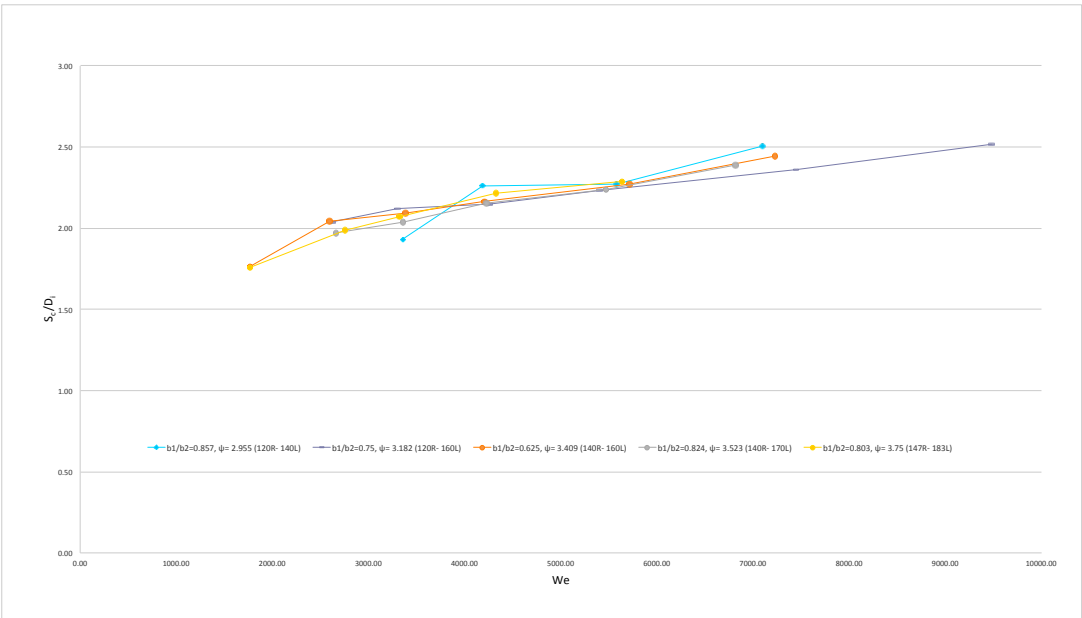

Figure 4.32: Dimensionless Critical Submergence vs Weber Number

Application of nonlinear regression analysis to the data of S_c/D_i versus Fr, Re, We and ψ yields Equation 4.13 with R^2 value of 0.923 for triple intakes.

$$\frac{S_c}{D_i} = 2.47\ Fr^{0.407}\ Re^{0.001}\ We^{0.001}\ \psi^{-0.005} \tag{4.13}$$

Eliminating Weber Number leads Equation 4.14 with R^2 value of 0.923 as:

$$\frac{S_c}{D_i} = 2.545\ Fr^{0.405}\ Re^{0.001}\ \psi^{-0.005} \tag{4.14}$$

Reynolds Number also omitted from the general equation of S_c/D_i leading Equation 4.15 with R^2 value of 0.923 as:

$$\frac{S_c}{D_i} = 2.434\ Fr^{0.387}\ \psi^{0.05} \tag{4.15}$$

Figure 4.33 gives a comparison of measured S_c/D_i data with calculated data from Equation 4.15 and it shows that the calculated data lie within $\pm 10\%$ error lines.

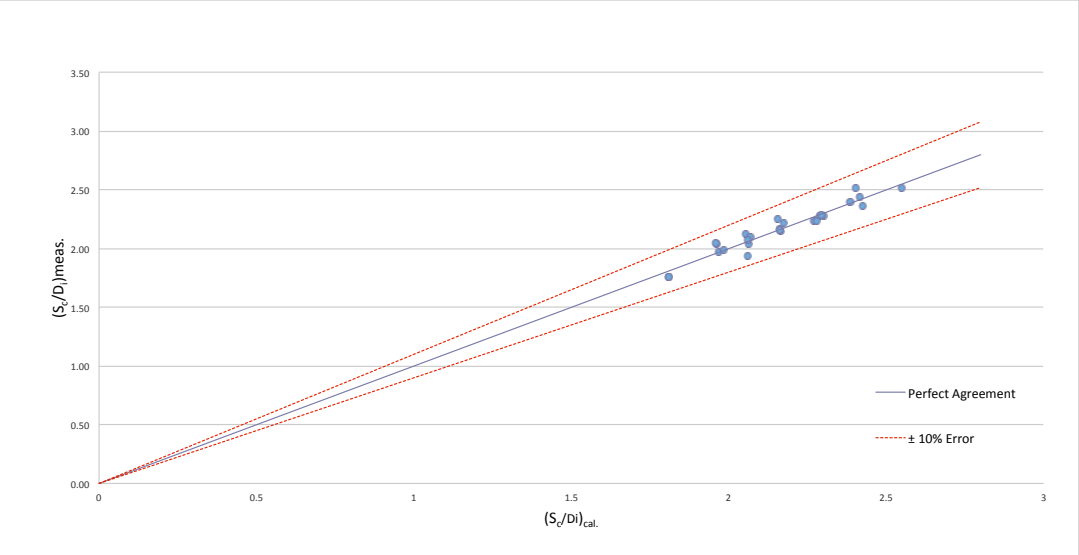

Figure 4.33: Comparison of Measured S_c/D_i Data With Calculated S_c/D_i Data From v Equation 4.15

After rounding up the constant empirical numbers given in Equation 4.15, Equation 4.16 can be obtained with R^2 value of 0.921. Figure 4.34 which shows the comparison of calculated S_c/D_i values based on Equation Equation 4.16 with those of measured ones, reveals that Equation 4.16 can be used instead of Equation 4.15.

$$\frac{S_c}{D_i} = 2.4\ Fr^{0.5}\ \psi^{0.05} \tag{4.16}$$

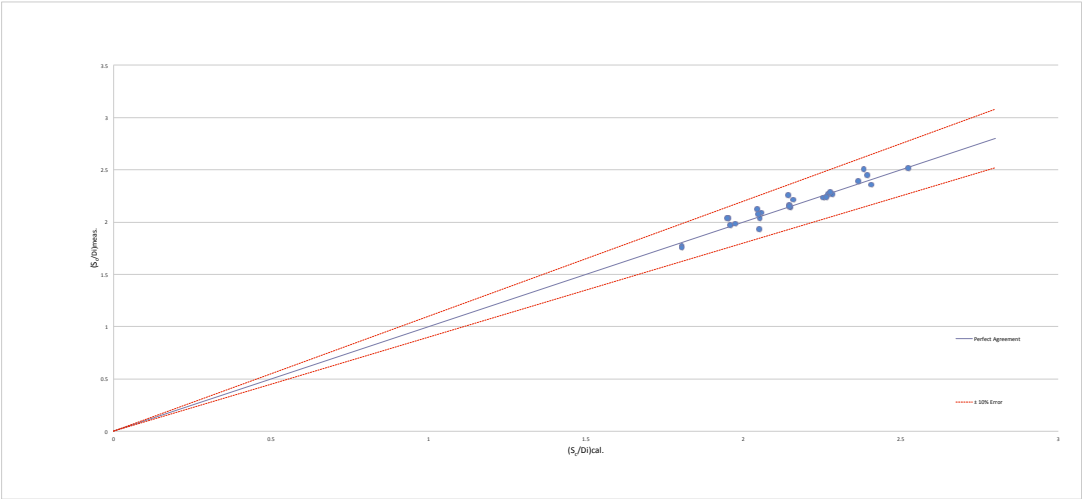

Figure 4.34: Comparison Between the Measured Values of S_c/D_i and the Ones Calculated by Equation 4.16

In order to observe the effect of asymmetrical approach flow condition on the values of relative critical submergence S_c/D_i, the variation of S_c/D_i with ψ for selected constant Froude numbers was obtained from Equation 4.16 and then plotted as given in Figure 4.35. This figure clearly shows that S_c/D_i values are almost constant for a given Fr and not function of ψ. Therefore, one can drop the parameter of ψ from the general equation of S_c/D_i and finally Equation 4.17 can be given with R^2 value of 0.923.

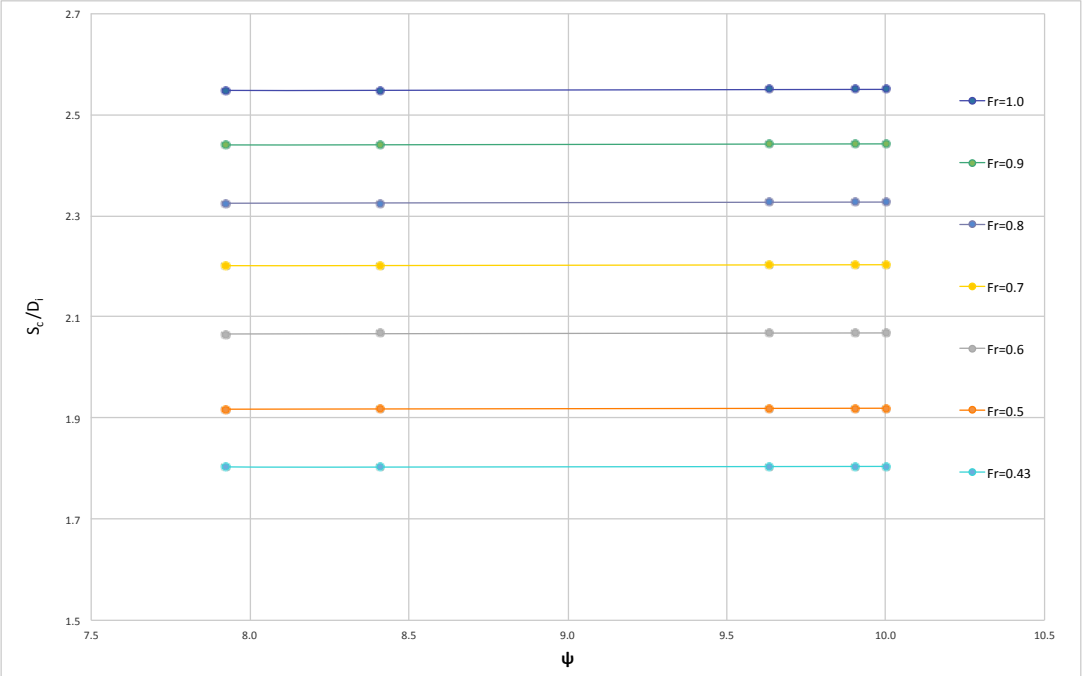

Figure 4.35: Variation of S_c/D_i with ψ as a function of Fr

Based on Equation 4.17, Figure 4.36 shows that the calculated S_c/D_i data fall between error bands of $\pm 10\%$.

$$\frac{S_c}{D_i} = 2.548 Fr^{0.409} \tag{4.17}$$

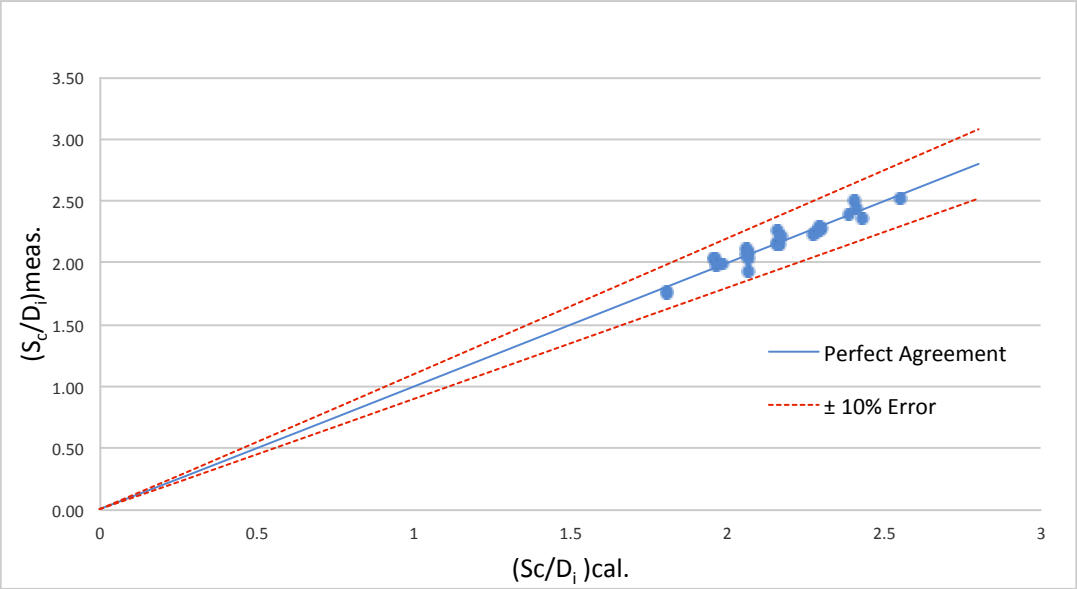

Figure 4.36: Comparison of Measured S_c/D_i Data With Calculated S_c/D_i Data From Equation 4.17

By rounding up he constant numerical values given in Equation 4.17 one can show that Equation 4.18 also predicts the S_c/D_i values as good as Equation 4.17 with R^2 value of 0.922 (Figure 4.37).

$$\frac{S_c}{D_i} = 2.5\ Fr^{0.5} \tag{4.18}$$

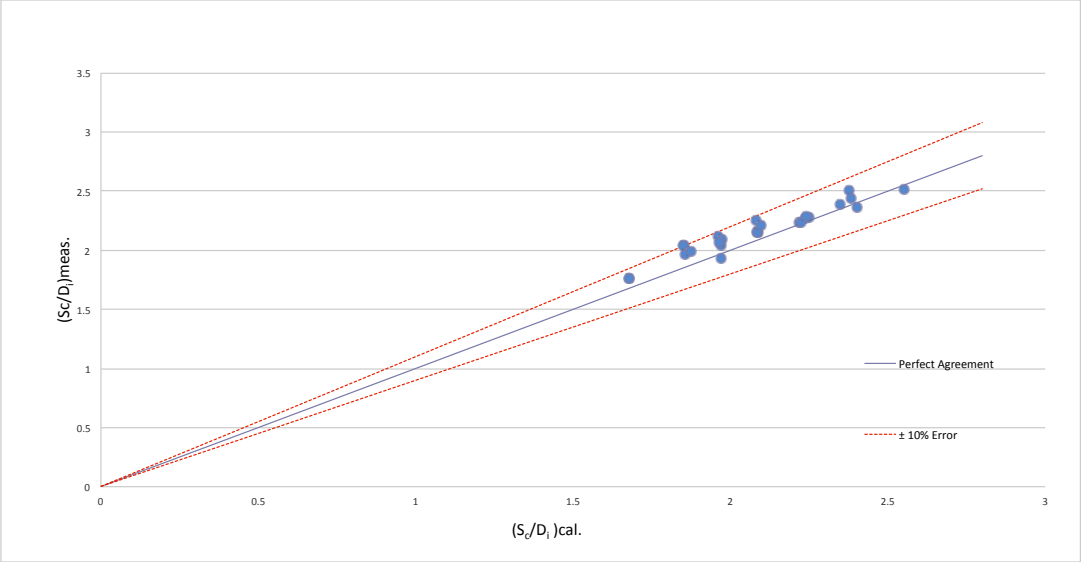

Figure 4.37: Comparison Between the Measured Values of S_c/D_i and the Ones Calculated by Equation Equation 4.18

4.5 Comparison Between the Proposed Equation of Present Study and Related Formulas in The Literature

In this section, firstly the simplified equations of S_c/D_i as a function of Fr obtained within the scope of this study for single, double and triple intakes are compared with each other, considering the ranges of the related parameters tested in this study (Figure 4.38). This figure clearly shows that the general trends of the data points for the intake types tested are very similar; the related curves are almost parallel to each other and S_c/D_i values increase with increasing Fr for a given intake type. For a given Fr the value of the dimensionless critical submergence increases as the number of the intake increases.

The formulas obtained in this study is compared with the well-known equations in the literature as Equation 2.1, Equation 2.2, Equation 2.3, Equation 2.7, Equation 2.10 and Equation2.14 which are more suitable for our case since they are studied in horizontal intakes.

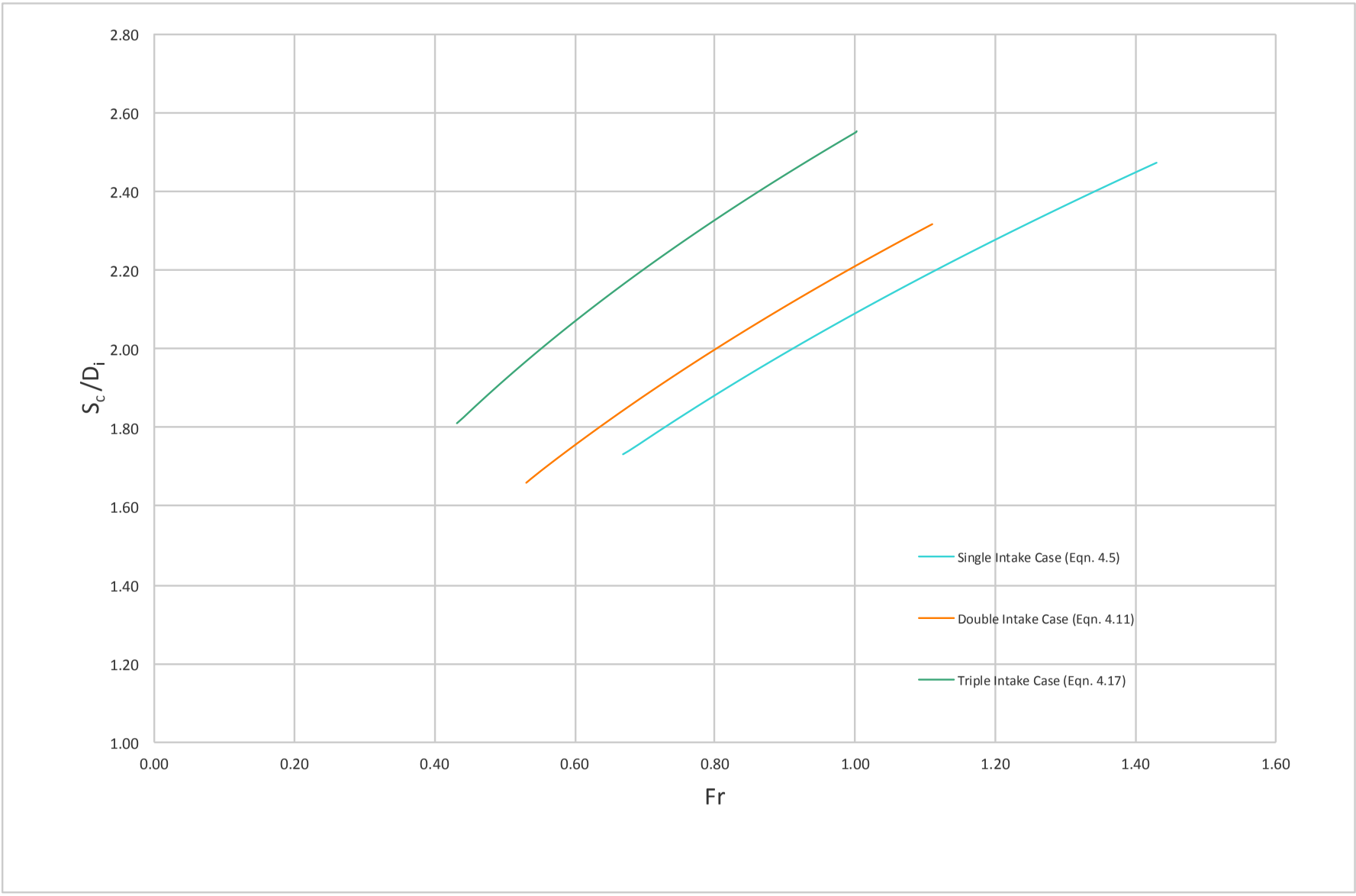

Figure 4.38: Comparison of the Simplified S_c/D_i Equations of Present Study for Single Intake, Double Intake and Triple Intake Structures

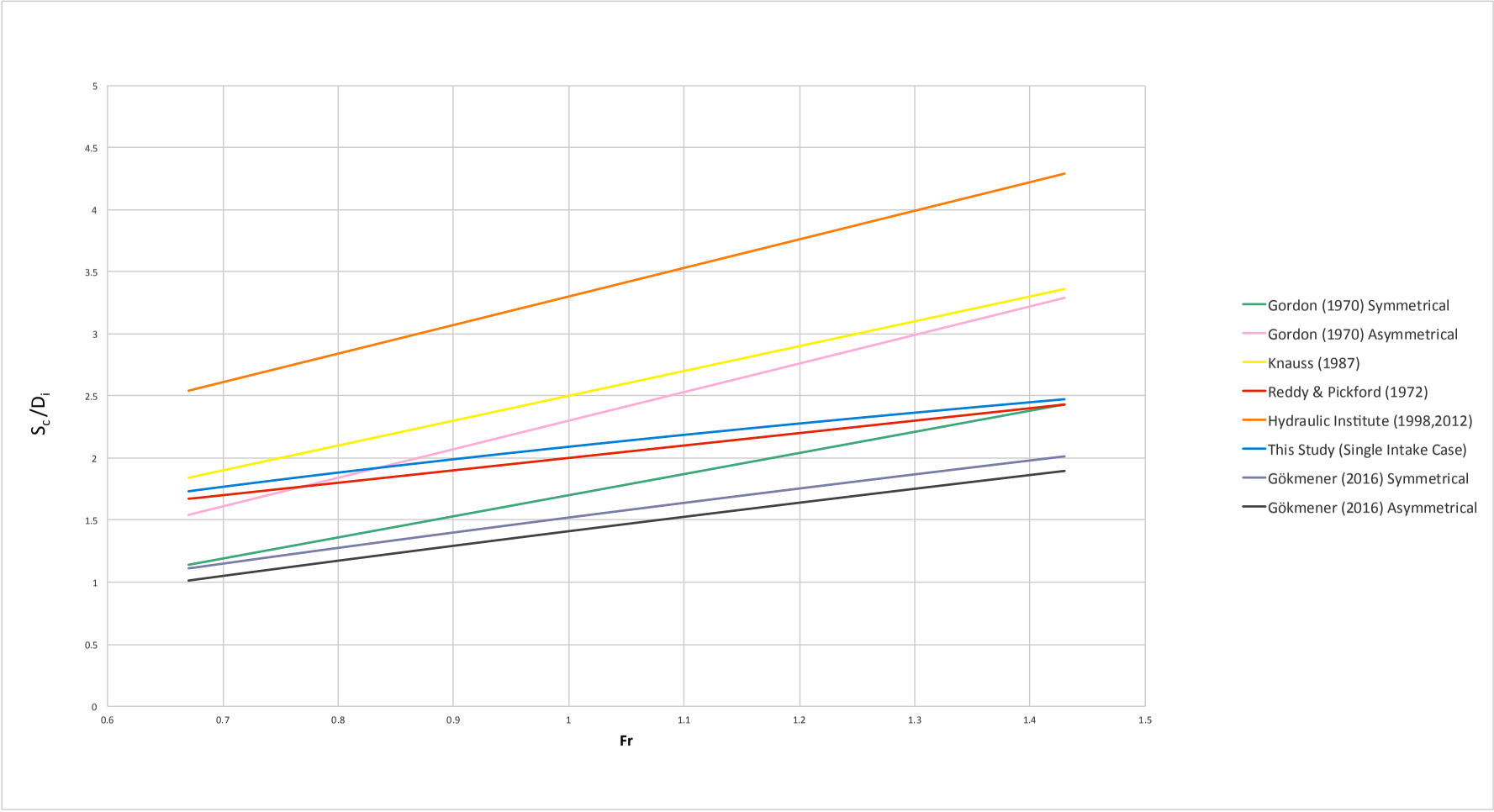

Figure 4.39: Comparison of the Simplified S_c/D_i Equation of Present Study for Single Intake Structure with the Related Ones Presented in Literature

In the literature, there are several equations for S_c/D_i as a function of Fr for horizontal and mostly single intakes under symmetrical approach flow conditions as stated in Section 2.2.1. Since the experimental setups used in the production of the experimental data utilized in the derivation of S_c/D_i equations are different than each other; shapes and locations of the intake structures such as circular, bell-mouth, close to the reservoir bottom or far away from it, it is obvious that one can expect to get similar S_c/D_i values from those equations for a given Fr. Therefore, as it is seen in Figure 4.39 where some of the related S_c/D_i relations were plotted, there is a certain scatter between the curves of various investigators for a given Fr. However, it may be concluded that The Gordon's [1] relationship for asymmetrical approach flow conditions and the one proposed in this study for single intakes are compatible.

CHAPTER 5

NUMERICAL SIMULATION

The development of computational technology has led to approximate Navier Stokes equations with the help of different turbulence models. In order to simulate the experiments commercially available ANSYS Fluent and FLOW-3D programs were preferred which were extensively used in academic researches and also in industry. The aim was to develop a design procedure with validating the CFD program and comparing it with the experimental results. The simulations have been done according to the logic behind the experimental setup with seeking air core vortex to detect the critical submergence. The same geometry with the experimental model was used without scaling, and the same free surface level has been provided in the simulation and then the analysis was made with the same discharges. In order to find the critical submergence air entraining vortex has been searched as in the case of experiments. The vorticity, free surface deformation and streamlines of vortices were successfully obtained. However, despite large deformations of the free surface, no well-defined air entraining vortex has been present.

Both ANSYS Fluent and FLOW-3D use Volume of Fluid (VOF) method in order to simulate the free surface flow. In order to apply VOF method in ANSYS Fluent, two phase flow model should be used in the simulation. However in FLOW-3D VOF approach is different, one fluid flow option of the program solves equations for the fluid, that is water in our case, and void is kept with constant pressure. So the equations are not solved for void, which makes the computational time shorter. The air entrainment model could be applied in order to measure the volume of air entrained via vortex formation, and this model also works in one fluid option. Courant number is adjusted automatically in FLOW-3D in order to provide stability. Time step size is

also adjusted by the program itself and controlled by stability and convergence.

5.1 Numerical Simulation with ANSYS FLUENT

The experimental setup was constructed without scaling for the simulation with ANSYS Fluent software in 3D and maximum opening without walls case in the experiment is tested. The model was created to adjust the different sizes of finite elements of mesh and it is divided into 15 rectangles and 5 trapezoid volumes. Since the vortex formed in the water intake structures were three-dimensional in nature, it is not intended to make the model in two dimensions. Also, since there was no symmetry in the flow, it is not considered to reduce the geometry by using the symmetry condition. As such, solving the geometry as it is, uses the most time possible in terms of calculation time. The mesh planes for mesh construction could be seen in Figure 5.1.

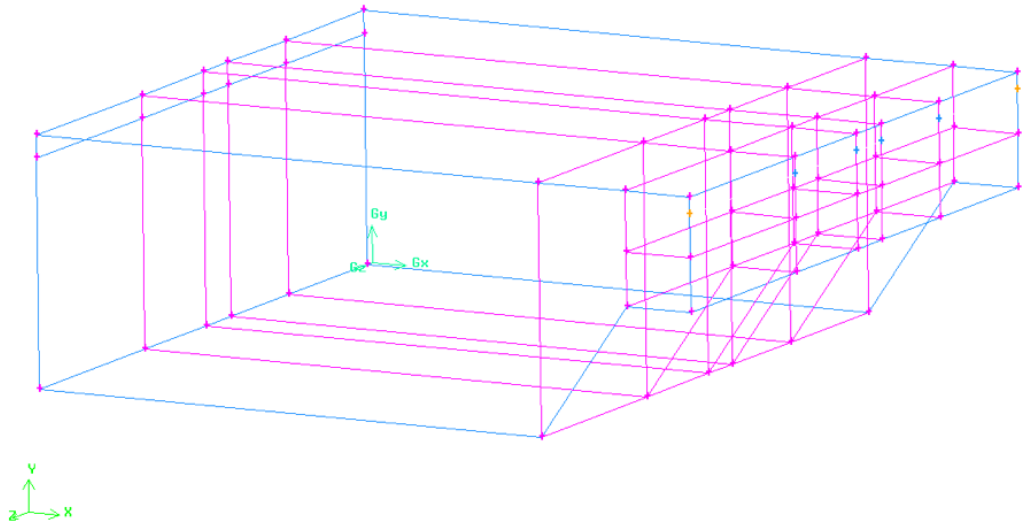

Figure 5.1: Mesh Planes for Fluent Simulation

The mesh constructed could be seen in Figure 5.2 with the boundary conditions used. Fine mesh size is used at the region where vortex formation is expected and coarser mesh size is used at the other parts of the geometry. The finest mesh size is $0.17cm$

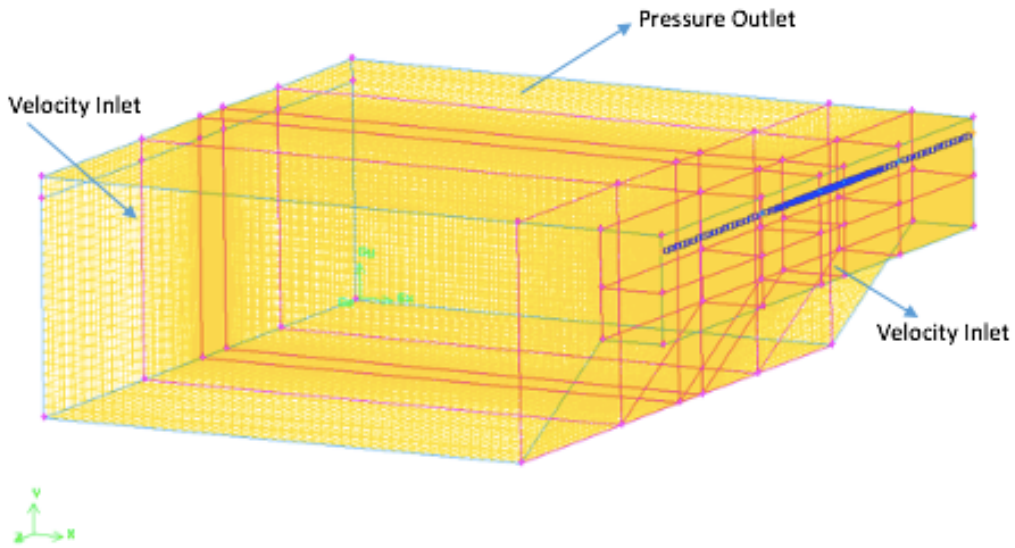

Figure 5.2: General View of Constructed Mesh

where the coarsest is $11.34cm$, constituting a total mesh of $1.556.481$ finite elements. Close view behind the intake could be seen in Figure 5.3

VOF method is used in the simulation in order to represent the two phase flow along with RNG k-$epsilon$ turbulence model. Intake and Outlet boundary conditions are defined as to have the similar discharge in and out, so as to keep the reservoir volume constant as the situation as in the experimental study, so no change is observed in the free surface water level. The water level is defined initially at some level as close to the critical submergence. The simulation has been done for different water levels behind that point for about 100 seconds of simulation time.

In order to observe vortex formation, the volume fraction is defined where there is 50% of air and water in the flow and free surface is represented with that volume fraction as could be seen in Figure 5.4 throughout the reservoir. The disruption of the free surface behind the intake as well as the water bubbles are observed as could be seen in Figure 5.5. The simulations resulted with dimples in the free surface and bubble formation at the intake however a well defined type six vortex with air core could not be observed. Since it takes too much computational time as a week to simulate one case, which is for one opening, one discharge and one water level, it is concluded to move on FLOW-3D software in order to get faster results. It is

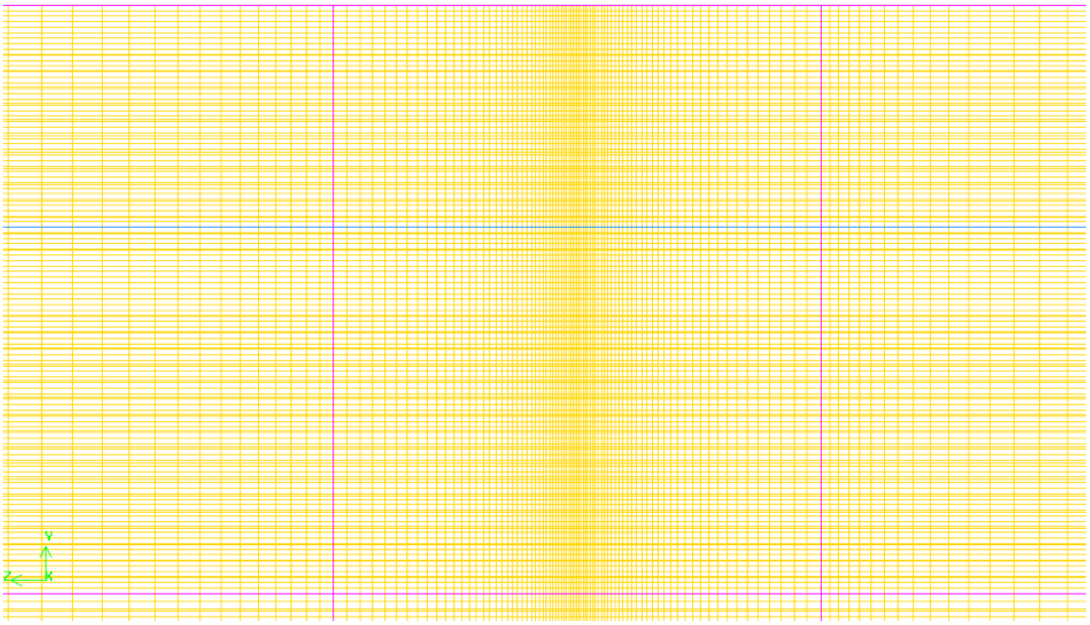

Figure 5.3: Close View of Meshes Behind Intake

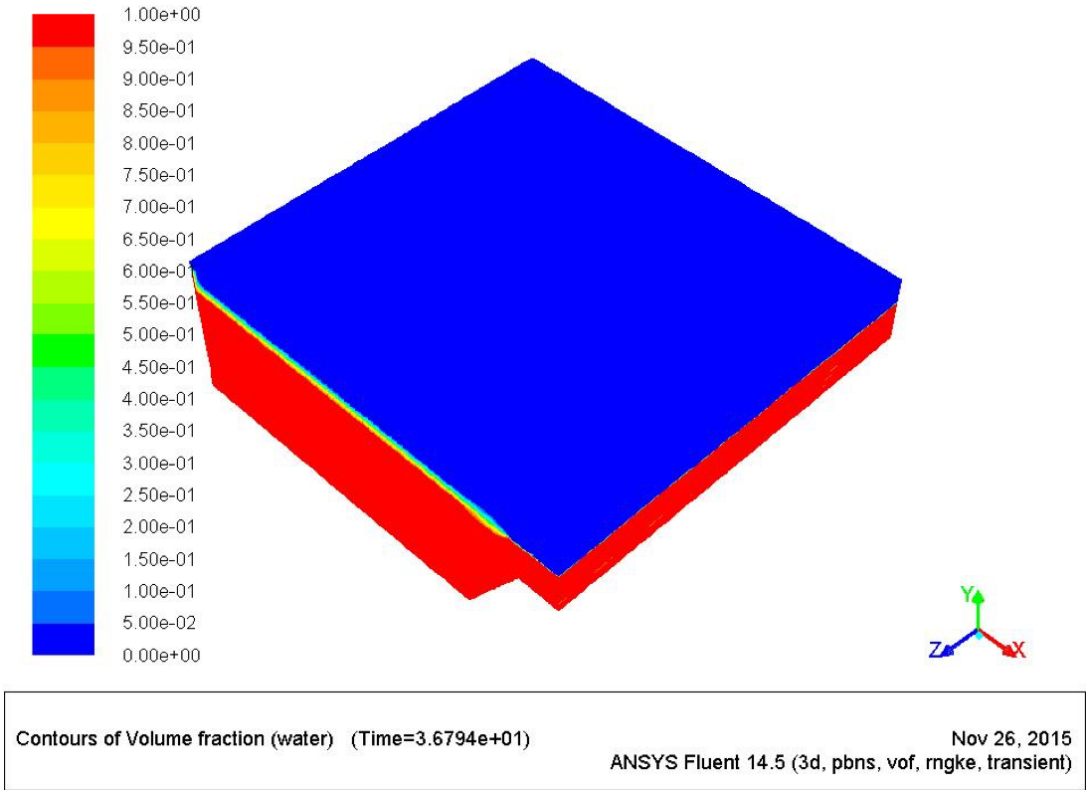

Figure 5.4: Free Surface as Result of the Simulation Represented by Volume Fraction

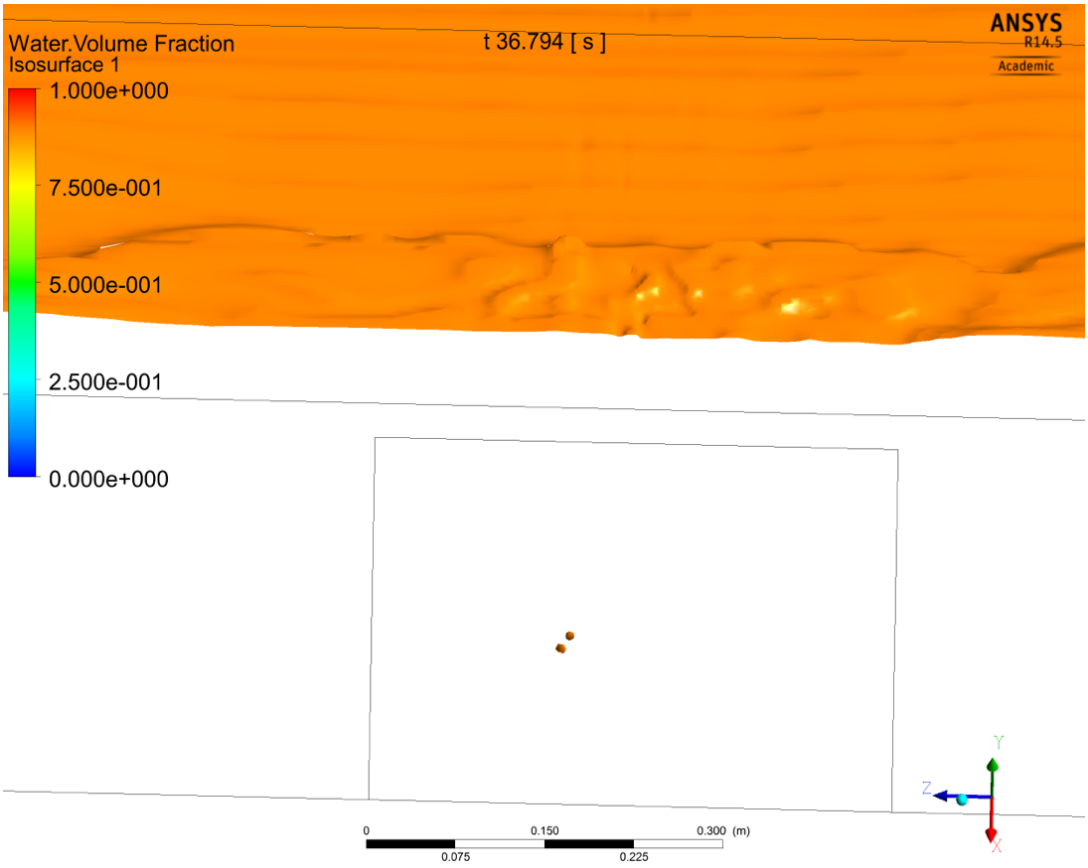

Figure 5.5: Free Surface Behind the Intake and Bubble formation

considered to take the advantage of FLOW-3D's approach to VOF method.

5.2 Numerical Simulation with FLOW-3D

The same geometrical model is also used for FLOW-3D study, it has the same dimensions as the experimental setup. One phase model with VOF option is used in order to decrease computational time.

5.2.1 Large Eddy Simulation (LES)

The aim of large eddy simulation (LES) is to resolve large eddies and model the small eddies by solving large ones, so it is more capable to capture small eddies. Large eddies, also the large scale of motions of turbulent flow are directly computed

In LES whereas solely small scale motions are modelled, resulting in a significant reduction in computational time compared to DNS [25]. Since large ones carry the most of the momentum, mass, energy and other passive scalars, they are effected by the geometry and boundary conditions of the flow while smaller ones are more independent from the geometry and tend to be more isotropic. As a result finding a universal turbulence model for smaller eddies is easier [21]. The capability of LES to simulate vortices is better compared to other turbulence models [2], [3] It has seen that LES better modelled the free surface vortex if the mesh size is fine enough. Large Eddy simulation is applicable to unsteady flows.

5.3 Geometrical Modeling and Computational Mesh

Geometrical modeling of the experimental setup has been done with the help of AUTO CAD software in 3D. The dimensions were kept the same as in the experimental setup, there was no scaling, L40-R80 asymmetrical condition was tested. Geometrical constraints of the setup have been determined and a reservoir volume with an open top surface is created. It is exported to FLOW-3D in STL format. Then the computational mesh has been arranged in FLOW-3D software. In order to capture the air core vortex, the mesh size should be small compared to the reservoir geometry. Dividing all the geometry to small meshes will increase the mesh count and also computational time dramatically. So nested meshes were generated in the places where vortex occurs, they only occur between plates close to the intake in experiments. In order to properly solve the domain, and to be consistent in advective equations the mesh size ratio of nested meshes should not exceed 5. So the computational grid consists of rectangular meshes and 3 different mesh size is used in the geometry, ranging between $0.05\ m, 0.025\ m, 0.005\ m$. The total number of cells has become 4.2 million. Even in some cases another finer mesh is added in order to capture the air entrainment which has a size of 0.0025 m and total cells of 5.6 m itself, with combining other meshes the total number of cells reaches to 9.8 m. L40-R80 case has been chosen at first for the sake of decreasing mesh count since the region between two walls were meshed with finer meshes compared to the rest of the reservoir. The analysis has done with only bigger size mesh is active at first, and after the computation

is stabilized the smaller meshes were activated one by one. This method is used to decrease computational time, which increases dramatically with the decreasing mesh size. The general view of the mesh and the close view of the mesh at the intake area could be seen in Figure 5.6 and Figure 5.7, respectively.

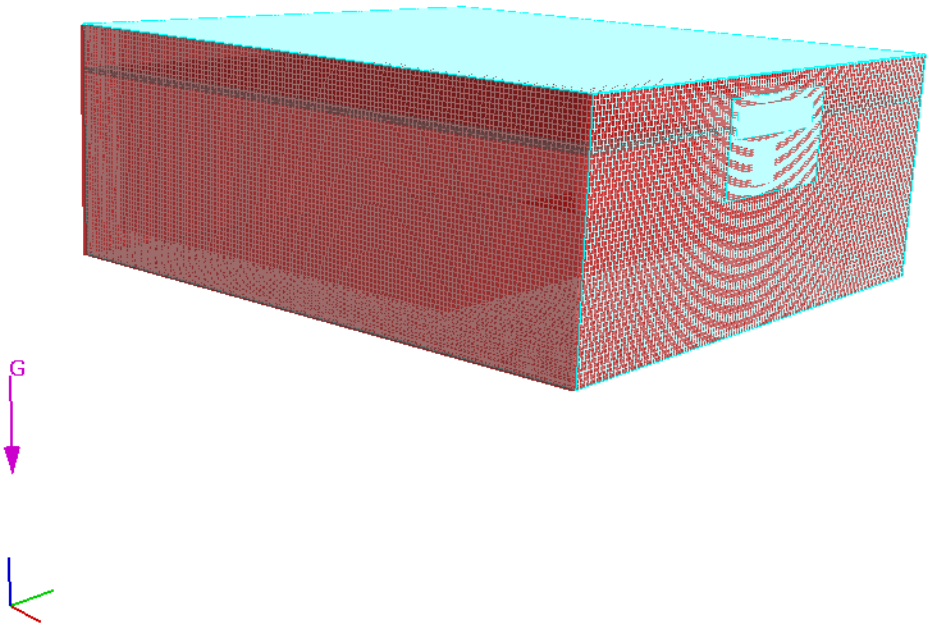

Figure 5.6: General View of Computational Mesh in FLOW-3D

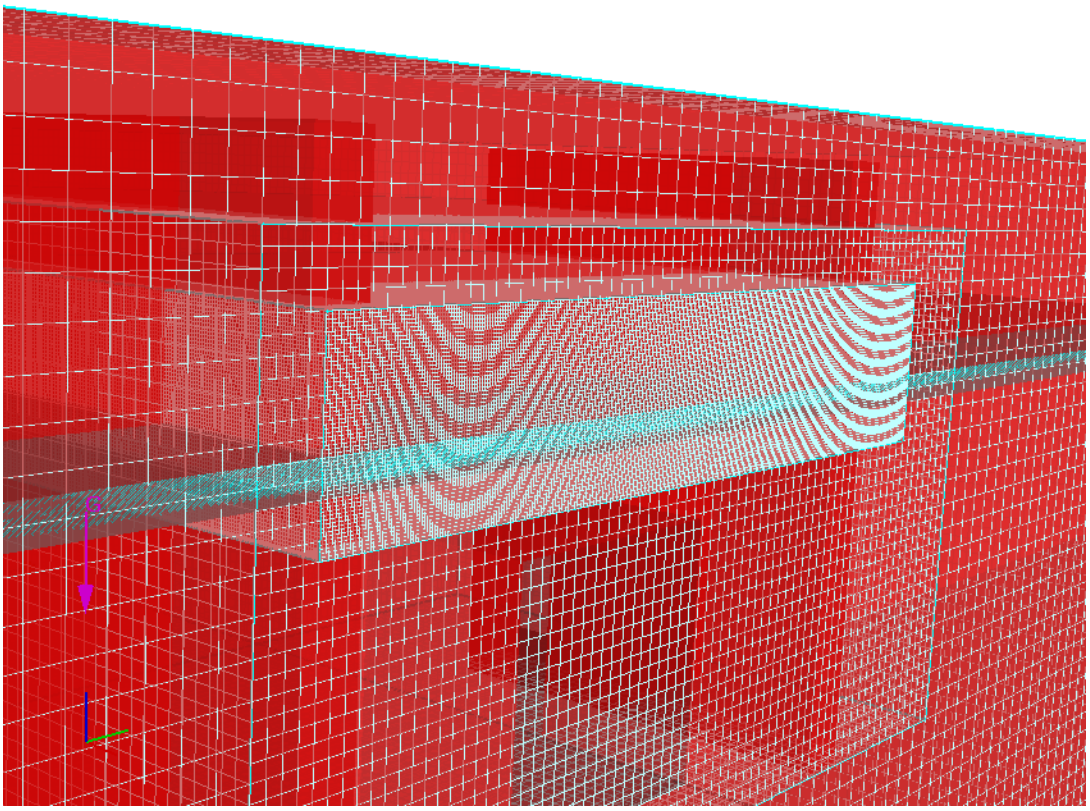

Figure 5.7: Close View of the Mesh in Intake Area

5.4 Numerical Model Development

In this study One fluid option of FLOW-3D is used with incompressible flow mode and free surface or sharp interface in interface tracking option. Large Eddy Simulation is chosen with no-slip wall shear boundary condition. Fluid is specified as water from the programs database with density $1000kg/m^3$ and viscosity $0.001kg/m/s$. Second order Momentum advection is selected for better precision.

5.5 Boundary Conditions

Boundary conditions were set as Volume Flow rate in outlet and volume flow rate is defined as in the experimental case, in order to define the outflow velocity direction is specified. Specified pressure is defined in inlet with constant elevation since the reservoir will be operated in constant elevation in real case and we have a constant height of water in our experiments, the water level is started from 5 cm higher of the critical submergence which we obtain from that specific case in the experiments and it lowered gradually by 1 cm increments. The specified pressure boundary condition is also defined in the top of the reservoir with fluid volume fraction equal to zero, in order to represent the free surface flow which the pressure is equal to the atmospheric pressure. All other parts of the reservoir is defined as walls with a smooth surface and no slip condition, so the bottom and walls of the reservoir have the boundary condition of wall. Nested meshes were defined with symmetrical boundary conditions automatically by the program itself in order to exchange the data between where two meshes meet. The overall boundary conditions could be seen in Figure 5.8 and Figure 5.9 from inlet view and outlet view, respectively, where P is specified pressure, Q is

5.6 Initial Conditions

In order to decrease the computational time, the reservoir is filled with water to some extend initially. This is also the case in experiments. For every critical depth analysis, the water level has been changed initially. So it is aimed to start from a still reservoir, to represent the real operational case in dam reservoirs and also to make it in accordant

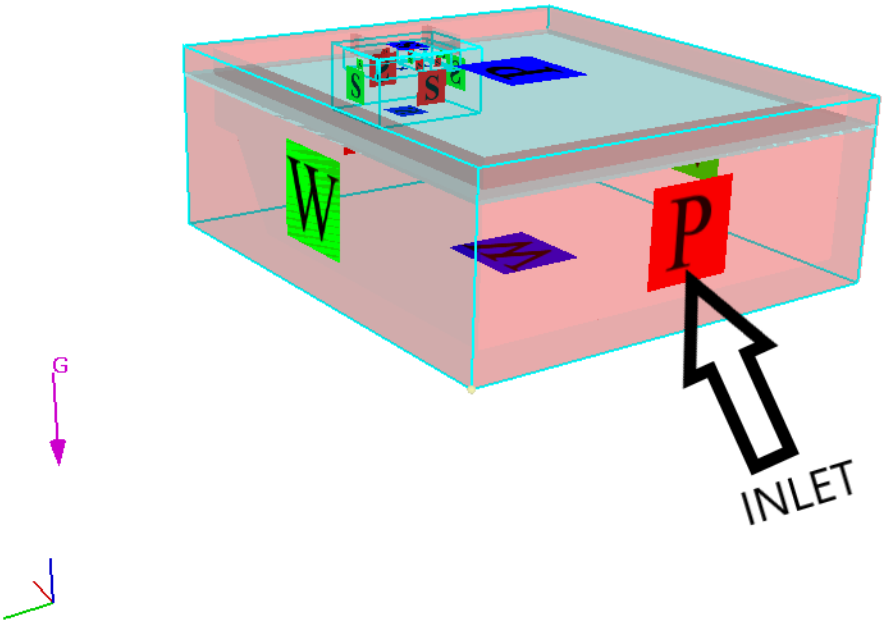

Figure 5.8: View of Boundary Conditions from Inlet

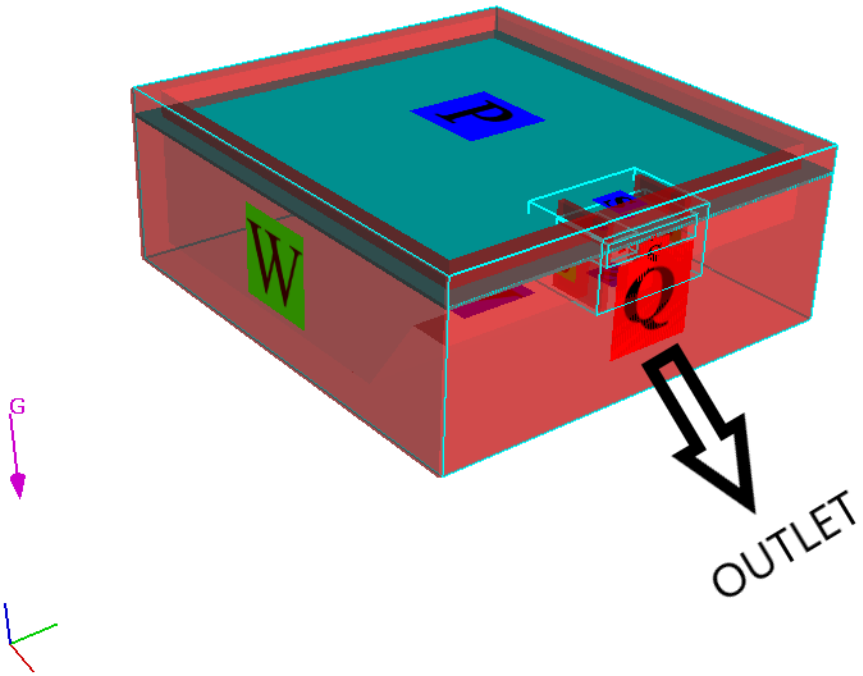

Figure 5.9: View of Boundary Conditions from Outlet

with the experimental study. The starting view of the reservoir can be seen in Figure 5.10

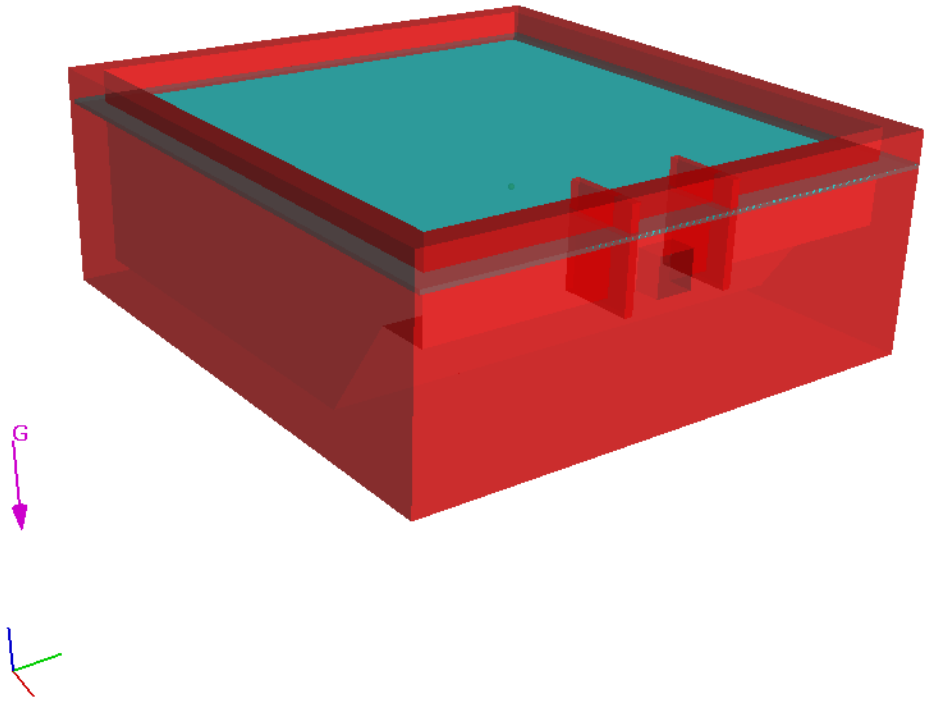

Figure 5.10: Initial Condition of the Reservoir

5.7 Simulation Cases

There have been 20 simulations tried and 11 of them converged while 9 of them failed. The list of the cases that were successful are listed in Table 5.1. One case is tried with k-ϵ model however, the air core vortex could not be represented and LES is chosen to proceed since it is more reliable [2], [3]. Most of the cases were simulated with maximum velocity in the light of experiments, where the most strong and large air core vortex occur at high discharges. Also two cases with lower discharge were simulated. The simulations started at the levels below then the critical submergence aiming to obtain the air core vortex visually, obtaining critical submergence from simulations is the second target after visualizing type 6 vortex. 7 of the cases were simulated without air entrainment model while 4 of them were simulated with air

entrainment model is activated. All of the cases were started with coarse mesh and run for 20 sec simulation time while taking 6 to 10 hours computational time, then the nested meshes were opened one by one. 20 seconds simulation time with second nested mesh is activated took around 24-36 hours in computational time and the same time in simulation with third nested mesh is activated cost 36-48 hours to compute. To summarize one case took about 3 to 5 days in average.

Table 5.1: List of Simulations

Case #	Setup	Discharge (lt/s)	Turbulent Model	Initial Fluid Elevation (cm)	Critical Submergence from Experiment (cm)	Air Entrainment Model
1	40L-80R	126.81	LES	48.5	53	Not activated
2	40L-80R	126.81	LES	50	53	Not activated
3	40L-80R	126.81	LES	47	53	Not activated
4	40L-80R	126.81	LES	36	53	Not activated
5	40L-80R	126.81	k-ϵ	48,5	53	Not activated
6	40L-80R	90.92	LES	38.9	43.4	Not activated
7	40L-80R	78.39	LES	33.5	39.5	Not activated
8	40L-80R	126.81	LES	48.5	53	Activated
9	40L-80R	126.81	LES	43.5	53	Activated
10	40L-80R	126.81	LES	36	53	Activated
11	40L-80R	126.81	LES	34	53	Activated

5.8 Analysing FLOW-3D Simulations

Reservoir steady state is obtained in the simulations, and the free surface level is defined with isosurface of 0.5 which means 50% of air and 50% of water is mixed at the surface. Then the free surface is observed over time for vortex formation, where the results and flow data were captured by 1 sec intervals after 20 sec simulation

time. The general view of the reservoir after simulation and the free surface behind intake at 42.9 sec simulation time could be seen in Figure 5.11 and Figure 5.12, respectively. It could be seen in Figure 5.12 that there are two dimples that originated close to the side walls, which is consistent with the experiments. The location of dimples are coinciding with the vortex formation in the physical model however, no air entraining vortex is observed at the numerical model. Velocity vectors were obtained and coloured with the magnitude and velocity, presented in Figure 5.13. Streamlines, coloured with magnitude of velocity could be seen in Figure 5.14. It could be seen in the figure that vortices at the dimple locations occur, and the strength of the vortex is higher in smaller core diameter dimple. Unfortunately, without air entrainment it could not be said for sure that this is a type 6 vortex. So it could be interpreted that there is vorticity, and vortex locations along with flow parameters such as circulation could be obtained with a numerical simulation that could lead the design process.

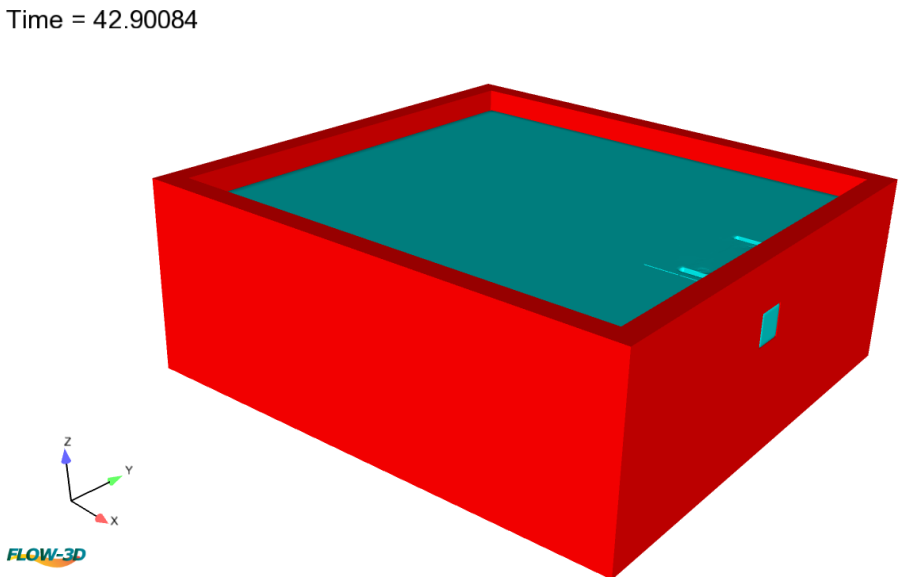

Figure 5.11: Free Surface and View of Reservoir Conditions

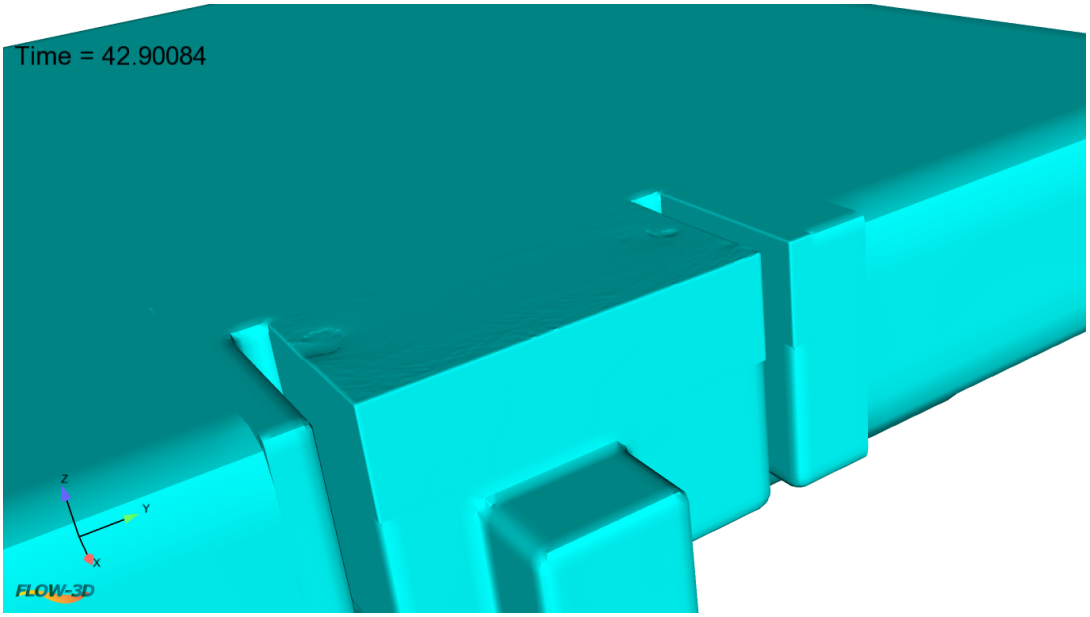

Figure 5.12: Free Surface Behind Intake

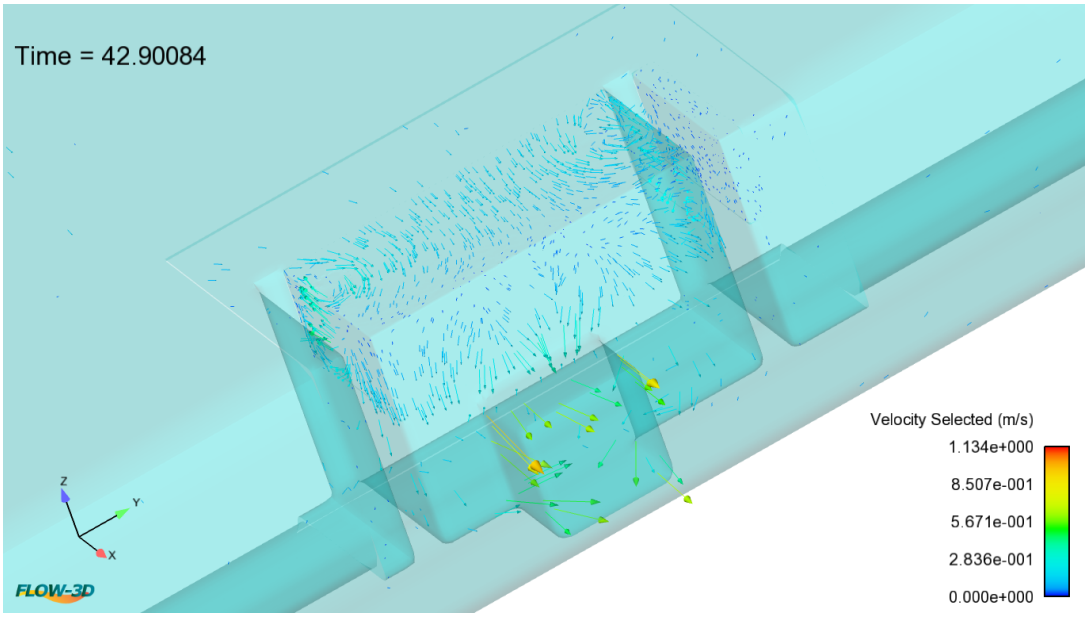

Figure 5.13: Velocity Vectors Coloured by Magnitude of Velocity

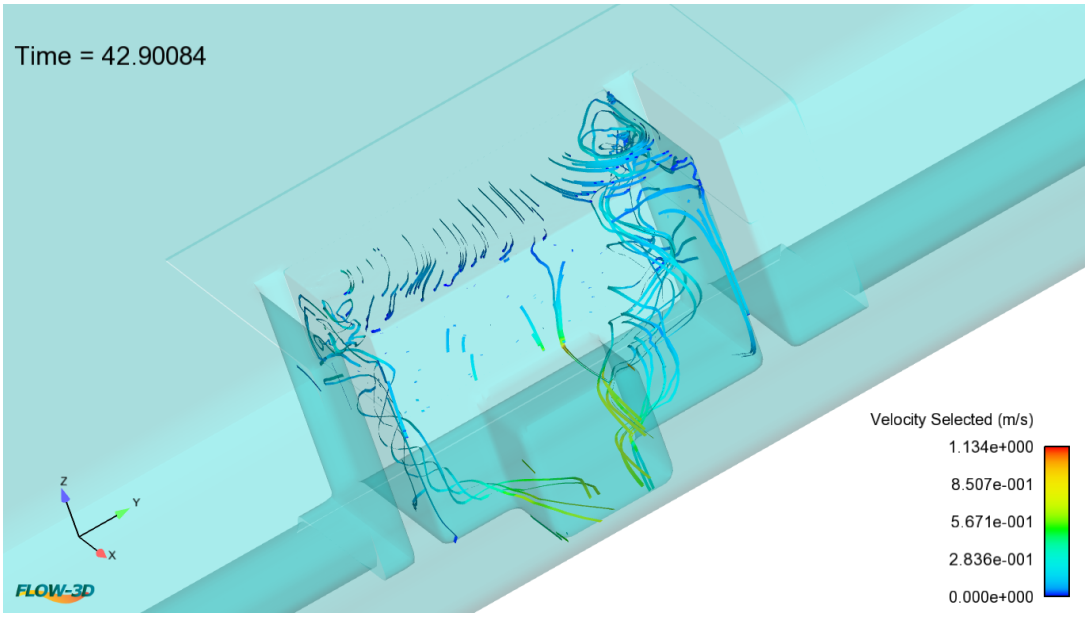

Figure 5.14: Streamlines Coloured by Magnitude of Velocity

CHAPTER 6

CONCLUSION

Asymmetrical approach flow conditions were tested in this study for single, double and triple intakes with different discharges and different wall clearances. Dimensionless critical submergence is determined along with dimensionless numbers as Froude, Weber and Reynolds number. Empirical equations are obtained for dimensionless critical submergence as a function of Fr and ψ, and simplified empirical equations are derived depending only on Fr. The accuracy of these two equations in estimating the value of S_c/D_i is found to be almost the same. It could be concluded that S_c/D_i is increasing with increasing Fr. However, effect of ψ on S_c/D_i for a given Fr is not so clear. As a function of Fr, S_c/D_i value either may increase or decrease with increasing ψ. It could be also achieved that single, double and triple intakes show almost the same trend when they are compared to each other. As the number of intake structures increases, the value of critical dimensionless submergence, S_c/D_i, increases for a given Froude number.

Although there are many studies in the literature, it is not easy to find a suitable match to the prototype of one's interest, when it comes to geometrical parameters as bottom clearance, intake shape as rectangular or circular, approach geometry as symmetrical or asymmetrical, intake location as horizontal, vertical or declined. Also there are other parameters that effect the critical submergence as single intake conditions and multiple intake conditions. So it is not easy to rely on an equation without taking into constraints, since every other hydraulic intake has its own geometrical parameters depending on the geographical conditions of the area. The experimental study gives a chance to model and investigate air entrainment and thus critical submergence, which could be underestimated that may lead to failure of turbines or overestimated resulting

in a decrease of flexibility and efficiency of the power plant.

Numerical models are cheap solutions when compared to physical models and it can be used for design purposes. However one should notice that it needs high investment on the computer source in order to use them reliably and to get an accurate solution. It is not easy to capture air entrainment and free surface dynamics. Nowadays, it is only vortices most of the time that can be captured, not air-entraining vortices. So it could be used successfully to indicate the location and strength of the vortex which is also important in many cases. But for the critical submergence case, it is important to indicate the air entraining vortex which seems not possible in today's conditions with the numerical study, so in order to deeply analyse the intakes for critical submergence physical models should be used.

The numerical techniques will be improved in the future but those techniques are still not as reliable as hydraulic models for predicting either a vortex will occur or not. Although it gives the easiness to model and analyse the prototype in all dimensions and also in the original geometry, numerical model has disadvantages in large geometries in case of fine meshing. Fine meshing is important in order to simulate the vortex occurrence, which corresponds to a small size with respect to the reservoir. But when the mesh gets finer, the simulation times increases accordingly. Even in some cases, as in this case it becomes impossible to catch the tail of vortex even if its mouth can be observed. So CFD tools may be used to determine the location of vortex and circulation amount in horizontal intakes as well as the flow parameters behind the intake, but in order to determine the critical submergence a physical model is needed in most cases. The location of vortex is also important in order to construct anti vortex devices properly. Improvements in computer technology may lead to simulate large geometries with CFD tools in the future also giving a chance to eliminate scale effects in physical models. Further studies may depend on using the circulation parameter to obtain critical submergence.

REFERENCES

[1] J. Knauss, *Swirling Flow Problems at Intakes*. IAHR Design Manual, Taylor & Francis, 1987.

[2] T. E. Tokyay and S. G. Constantinescu, "Investigation of flow physics of pump intake flows using large eddy simulation," no. IIHR Technical Report No. 445, 2005.

[3] T. E. Tokyay and S. G. Constantinescu, "Validation of a large-eddy simulation model to simulate flow in pump intakes of realistic geometry," *Journal of Hydraulic Engineering*, vol. 132, no. 12, pp. 1303–1315, 2006.

[4] S. H. Kleyhans, *Physical Hydraulic Model Investigation of Critical Submergence*. Master's thesis, Stellenbosch University, 2012.

[5] Hydraulic Institude, "Pump Intake Design Standart," tech. rep., 1998.

[6] Hydraulic Institude, "ANSI HI 9.8-2012 Rotodynamic Pumps for Intake Design," tech. rep., 2012.

[7] H. Sarkardeh, A. R. Zarrati, and R. Roshan, "Effect of intake head wall and trash rack on vortices," *Journal of Hydraulic Research*, vol. 48, no. 1, pp. 108–112, 2010.

[8] M. Ansar, T. Nakato, and G. Constantinescu, "Numerical simulations of inviscid three-dimensional flows at single- and dual-pump intakes," *Journal of Hydraulic Research*, vol. July 2002, pp. 461–470, 02 2002.

[9] M. Khanarmuei, H. Rahimzadeh, and H. Sarkardeh, "Effect of dual intake direction on critical submergence and vortex strength," *Journal of Hydraulic Research*, vol. 57, no. 2, pp. 272–279, 2019.

[10] H. O. Anwar, "Vortices in a viscous fluid," *Journal of Hydraulic Research*, vol. 6, no. 1, pp. 1–14, 1968.

[11] L. L. Daggett and G. H. Keulegan, "Similitude conditions in free-surface vortex formations," 1974.

[12] A. Rindels and J. Gulliver, "Experimental study of critical submergence to avoid free-surface vortices at vertical intakes.," *Project Report - University of Minnesota, St. Anthony Falls Hydraulic Laboratory*, no. 224, 1983.

[13] G. Möller, *Vortex-Induced Air Entrainment Rate at Intakes*. PhD thesis, Mitteilungen 220, Versuchsanstalt für Wasserbau, Hydrologie und Glaziologie (VAW), R. M. Boes, Hrsg., ETH Zürich, 2013.

[14] *General Pump Station Design Recommendations Manual*, 2019 (last released December, 2019). available: `https://www.xylem.com/siteassets/brand/flygt/flygt-engineering--expertise/manual_pumpstationdesign_20191209_master_en_lowres.pdf`.

[15] A. Baykara, *Effect of hydraulic parameters on the formation of vortices at intake structures*. Master's thesis, Middle East Technical University, 2013.

[16] S. Gökmener, *Investigation of Critical Submerge Depths at Single and Multiple-Horizontal Intakes Having Air- Entraining Vortices*. Master's thesis, Middle East Technical University, 2016.

[17] D. Werth and C. Frizzell, "Minimum pump submergence to prevent surface vortex formation," *Journal of Hydraulic Research*, vol. 47, no. 1, pp. 142–144, 2009.

[18] N. Yildirim and F. Kocabaş, "Critical submergence for intakes in still-water reservoir," *Journal of Hydraulic Engineering*, vol. 124, no. 1, pp. 103–104, 1998.

[19] P. Pandazis and F. Blömeling, "Investigation of the critical submergence at pump intakes based on multiphase CFD calculations," *WIT Transactions on Engineering Sciences*, vol. 82, pp. 143–152, 07 2014.

[20] P. Pandazis and B. Babcsany, "Numerical and experimental investigation of surface vortex formation in coolant reservoirs of reactor safety systems," *Kerntechnik*, vol. 81, pp. 477–483, 10 2016.

[21] L. Nöid, *CFD computations of hydropower plant intake flow using unsteady RANS*. Master's thesis, KTH, School of Industrial Engineering and Management (ITM), Energy Technology, Heat and Power Technology, 2015.

[22] P. Wu, D. H. Munoz, G. Constantinescu, and Z. Qian, "Two-phase flow des and urans simulations of pump-intake bay vortices," *Journal of Hydraulic Research*, vol. 58, no. 1, pp. 120–132, 2020.

[23] V. P. Rajendran, S. G. Constantinescu, and V. C. Patel, "Experimental validation of numerical model of flow in pump-intake bays," *Journal of Hydraulic Engineering*, vol. 125, no. 11, pp. 1119–1125, 1999.

[24] N. Yildirim and S. C. Jain, "Surface tension effect on profile of a free vortex," in *Journal of the Hydraulics Division, Proceedings of the American Society of Civil Engineers*, vol. 107, 1981.

[25] Y. Zhiyin, "Large-eddy simulation: Past, present and the future," *Chinese Journal of Aeronautics*, vol. 28, no. 1, pp. 11 – 24, 2015.

APPENDIX A

EXPERIMENTAL RESULTS OF THE STUDY FOR SINGLE INTAKES

The data obtained in the experiments are presented according to each setup and each case. Also main parameters calculated such as Velocity, Froude Number, Weber Number and Relative Critical Submergence is presented.

Table A.1: Results for $b_1 = 40\ cm\ and\ b_2 = 20\ cm, \psi = 1.132$

Case	Q (lt/s)	V_i (m/s)	Fr	Re	We	Sc (cm)	Sc/Di
1	125.00	2.27	1.41	600584.69	18663.32	67.25	2.54
2	111.11	2.01	1.25	533853.06	14746.32	66.05	2.49
3	100.00	1.81	1.12	480467.75	11944.52	60.45	2.28
4	88.89	1.61	1.00	427082.45	9437.65	57.15	2.16
5	77.25	1.40	0.87	371161.34	7127.97	55.55	2.10
6	68.94	1.25	0.78	331255.82	5677.63	51.05	1.93
7	59.64	1.08	0.67	286545.63	4248.42	47.95	1.81

Table A.2: Results for $b_1 = 40\ cm\ and\ b_2 = 80\ cm, \psi = 2.264$

Case	Q(lt/s)	V_i (m/s)	Fr	Re	We	Sc	Sc/Di
1	126.81	2.30	1.43	609259.80	19206.37	61.75	2.33
2	110.28	2.00	1.24	529849.16	14525.96	58.05	2.19
3	98.58	1.79	1.11	473661.13	11608.49	54.65	2.06
4	90.92	1.65	1.02	436825.27	9873.15	52.15	1.97
5	78.39	1.42	0.88	376633.33	7339.69	48.25	1.82

Table A.3: Results for $b_1 = 60\ cm\ and\ b_2 = 20\ cm, \psi = 1.006$

Case	Q(lt/s)	V_i (m/s)	Fr	Re	We	Sc	Sc/Di
1	124.17	124.17	1.40	596580.79	18415.30	66.35	2.50
2	111.69	2.03	1.26	536655.79	14901.57	64.35	2.43
3	101.14	1.83	1.14	485939.75	12218.14	62.25	2.35
4	88.81	1.61	1.00	426682.06	9419.96	59.95	2.26
5	79.17	1.44	0.89	380370.30	7486.06	53.85	2.03
6	67.94	1.23	0.76	326451.15	5514.13	49.95	1.88

Table A.4: Results for $b_1 = 60\ cm\ and\ b_2 = 100\ cm, \psi = 3.623$

Case	Q(lt/s)	V_i (m/s)	Fr	Re	We	Sc	Sc/Di
1	124.86	2.26	1.40	599917.37	18621.87	63.95	2.41
2	110.42	2.00	1.24	530516.48	14562.57	61.35	2.32
3	99.31	1.80	1.12	477131.17	11779.20	56.75	2.14
4	87.14	1.58	0.98	418674.26	9069.70	53.65	2.02
5	78.39	1.42	0.88	376633.33	7339.69	48.75	1.84
6	68.67	1.24	0.77	329921.19	5631.98	45.85	1.73

Table A.5: Results for $b_1 = 60\ cm\ and\ b_2 = 140\ cm, \psi = 3.235$

Case	Q(lt/s)	V_i (m/s)	Fr	Re	We	Sc	Sc/Di
1	125.22	2.27	1.41	601652.40	18729.73	63.05	2.38
2	108.75	1.97	1.22	522508.68	14126.26	59.05	2.23
3	100.08	1.81	1.13	480868.14	11964.44	58.35	2.20
4	86.61	1.57	0.97	416138.46	8960.17	55.25	2.08

Table A.6: Results for $b_1 = 100\ cm\ and\ b_2 = 20\ cm, \psi = 0.906$

Case	Q(lt/s)	V_i (m/s)	Fr	Re	We	Sc	Sc/Di
1	124.53	2.26	1.40	598315.82	18522.57	62.15	2.35
2	108.89	1.97	1.22	523176.00	14162.37	57.95	2.19

Table A.7: Results for $b_1 = 100\ cm\ and\ b_2 = 160\ cm, \psi = 6.132$

Case	Q(lt/s)	V_i (m/s)	Fr	Re	We	Sc	Sc/Di
1	125.50	2.28	1.41	602987.03	18812.92	64.95	2.45
2	112.75	2.04	1.27	541727.39	15184.55	63.15	2.38
3	101.42	1.84	1.14	487274.38	12285.35	62.95	2.38
4	87.81	1.59	0.99	421877.38	9209.01	51.75	1.95
5	75.22	1.36	0.85	361418.52	6758.67	47.75	1.80

Table A.8: Results for $b_1 = 120\ cm\ and\ b_2 = 20\ cm, \psi = 0.881$

Case	Q(lt/s)	V_i (m/s)	Fr	Re	We	Sc	Sc/Di
1	122.83	2.23	1.38	590174.56	18021.93	63.55	2.40
2	109.50	1.99	1.23	526112.19	14321.78	59.45	2.24

Table A.9: Results for $b_1 = 120\ cm\ and\ b_2 = 160\ cm, \psi = 7.925$

Case	Q(lt/s)	V_i (m/s)	Fr	Re	We	Sc	Sc/Di
1	124.17	2.25	1.40	596580.79	18415.30	66.35	2.50
2	110.72	2.01	1.25	531984.57	14643.28	64.55	2.44
3	95.22	1.73	1.07	457512.07	10830.42	60.55	2.28
4	87.75	1.59	0.99	421610.45	9197.36	56.85	2.15

Table A.10: Results for $b_1 = 147\ cm\ and\ b_2 = 183\ cm, \psi = 10.003$

Case	Q(lt/s)	V_i (m/s)	Fr	Re	We	Sc	Sc/Di
1	110.28	2.00	1.24	529849.16	14525.96	61.45	2.32

APPENDIX B

EXPERIMENTAL RESULTS OF THE STUDY FOR DOUBLE INTAKES

Table B.1: Results for $b_1 = 70\ cm\ and\ b_2 = 80\ cm, \psi = 4.953$

Case	Q(lt/s)	V_i (m/s)	Fr	Re	We	Sc	Sc/Di
1	123.29	1.76	1.09	465251.57	18596.14	60.95	2.30
2	108.61	1.55	0.96	409853.25	14431.25	58.55	2.21
3	98.19	1.40	0.87	370545.07	11795.85	56.75	2.14

Table B.2: Results for $b_1 = 70\ cm\ and\ b_2 = 90\ cm, \psi = 4.696$

Case	Q(lt/s)	V_i (m/s)	Fr	Re	We	Sc	Sc/Di
1	124.01	1.77	1.10	467976.94	18814.64	56.65	2.14
2	110.83	1.58	0.98	418238.99	15027.83	56.35	2.13
3	95.90	1.37	0.85	361897.27	11251.69	49.05	1.85

Table B.3: Results for $b_1 = 70\ cm\ and\ b_2 = 100\ cm, \psi = 4.491$

Case	Q(lt/s)	V_i (m/s)	Fr	Re	We	Sc	Sc/Di
1	123.67	1.76	1.09	466666.67	18709.44	61.35	2.32
2	109.68	1.56	0.97	413888.89	14716.84	60.45	2.28
3	95.83	1.36	0.85	361635.22	11235.40	53.15	2.01
4	87.22	1.24	0.77	329140.46	9307.00	51.15	1.93
5	75.69	1.08	0.67	285639.41	7009.44	49.05	1.85

Table B.4: Results for $b_1 = 70\ cm\ and\ b_2 = 110\ cm, \psi = 4.322$

Case	Q(lt/s)	V_i (m/s)	Fr	Re	We	Sc	Sc/Di
1	123.60	1.76	1.09	466404.61	18688.43	62.45	2.36
2	109.19	1.55	0.96	412054.51	14586.68	61.15	2.31
3	96.69	1.38	0.85	364884.70	11438.22	58.55	2.21
4	87.72	1.25	0.78	331027.25	9414.01	55.65	2.10
5	74.67	1.06	0.66	281761.01	6820.39	49.85	1.88

Table B.5: Results for $b_1 = 70\ cm\ and\ b_2 = 120\ cm, \psi = 4.182$

Case	Q(lt/s)	V_i (m/s)	Fr	Re	We	Sc	Sc/Di
1	124.22	1.77	1.10	468763.10	18877.91	58.25	2.20
2	111.57	1.59	0.99	421016.77	15228.11	56.05	2.12
3	99.07	1.41	0.88	373846.96	12007.01	53.85	2.03
4	87.79	1.25	0.78	331289.31	9428.92	51.45	1.94
5	76.43	1.09	0.68	288417.19	7146.43	49.85	1.88

Table B.6: Results for $b_1 = 80\ cm\ and\ b_2 = 90\ cm, \psi = 5.702$

Case	Q(lt/s)	V_i (m/s)	Fr	Re	We	Sc	Sc/Di
1	124.86	1.78	1.10	471174.00	19072.59	57.85	2.18
2	110.28	1.57	0.97	416142.56	14877.55	55.25	2.08
3	100.14	1.43	0.88	377882.60	12267.64	53.35	2.01
4	87.92	1.25	0.78	331761.01	9455.79	50.75	1.92
5	76.53	1.09	0.68	288784.07	7164.63	48.45	1.83
6	67.78	0.97	0.60	255765.20	5619.92	46.35	1.75

Table B.7: Results for $b_1 = 80\ cm\ and\ b_2 = 100\ cm, \psi = 5.434$

Case	Q(lt/s)	V_i (m/s)	Fr	Re	We	Sc	Sc/Di
1	123.79	1.76	1.09	467138.36	18747.28	60.65	2.29
2	111.51	1.59	0.99	420807.13	15212.94	55.25	2.08
3	96.76	1.38	0.85	365146.75	11454.65	54.85	2.07
4	90.10	1.28	0.80	339989.52	9930.66	52.85	1.99

Table B.8: Results for $b_1 = 80\ cm\ and\ b_2 = 110\ cm, \psi = 5.214$

Case	Q(lt/s)	V_i (m/s)	Fr	Re	We	Sc	Sc/Di
1	123.76	1.76	1.09	467033.54	18738.86	61.15	2.31
2	109.79	1.56	0.97	414308.18	14746.68	60.35	2.28
3	100.74	1.43	0.89	380136.27	12414.40	53.75	2.03
4	86.35	1.23	0.76	325838.57	9121.20	49.15	1.85

Table B.9: Results for $b_1 = 80\ cm\ and\ b_2 = 120\ cm, \psi = 5.031$

Case	Q(lt/s)	V_i (m/s)	Fr	Re	We	Sc	Sc/Di
1	123.38	1.76	1.09	465566.04	18621.29	61.85	2.33
2	110.14	1.57	0.97	415618.45	14840.10	55.85	2.11
3	96.71	1.38	0.85	364937.11	11441.51	53.25	2.01
4	86.78	1.24	0.77	327463.31	9212.39	50.95	1.92
5	75.68	1.08	0.67	285587.00	7006.87	48.45	1.83
6	67.15	0.96	0.59	253406.71	5516.75	46.75	1.76
7	61.39	0.87	0.54	231656.18	4610.36	44.45	1.68

Table B.10: Results for $b_1 = 90\ cm\ and\ b_2 = 100\ cm, \psi = 6.453$

Case	Q(lt/s)	V_i (m/s)	Fr	Re	We	Sc	Sc/Di
1	123.22	1.75	1.09	464989.52	18575.20	61.05	2.30
2	109.65	1.56	0.97	413784.07	14709.39	60.35	2.28
3	95.81	1.36	0.85	361530.40	11228.89	54.15	2.04
4	87.89	1.25	0.78	331656.18	9449.82	52.85	1.99
5	74.51	1.06	0.66	281184.49	6792.50	48.25	1.82
6	68.40	0.97	0.60	258123.69	5724.04	44.65	1.68

Table B.11: Results for $b_1 = 90\ cm\ and\ b_2 = 110\ cm, \psi = 6.175$

Case	Q(lt/s)	V_i (m/s)	Fr	Re	We	Sc	Sc/Di
1	125.00	1.78	1.10	471698.11	19115.05	57.45	2.17
2	109.44	1.56	0.97	412997.90	14653.55	56.45	2.13
3	97.22	1.38	0.86	366876.31	11563.42	55.55	2.10
4	87.36	1.24	0.77	329664.57	9336.66	47.65	1.80
5	78.61	1.12	0.69	296645.70	7560.03	45.95	1.73

Table B.12: Results for $b_1 = 90\ cm\ and\ b_2 = 120\ cm, \psi = 5.943$

Case	Q(lt/s)	V_i (m/s)	Fr	Re	We	Sc	Sc/Di
1	122.69	1.75	1.08	462997.90	18416.42	61.45	2.32
2	109.44	1.56	0.97	412997.90	14653.55	57.15	2.16
3	98.89	1.41	0.87	373165.62	11963.28	54.25	2.05
4	87.63	1.25	0.77	330660.38	9393.15	53.95	2.04
5	75.83	1.08	0.67	286163.52	7035.19	45.65	1.72
6	68.47	0.98	0.60	258385.74	5735.67	43.15	1.63

Table B.13: Results for $b_1 = 100\ cm\ and\ b_2 = 110\ cm, \psi = 7.204$

Case	Q(lt/s)	V_i (m/s)	Fr	Re	We	Sc	Sc/Di
1	123.08	1.75	1.09	464465.41	18533.35	63.85	2.41
2	110.03	1.57	0.97	415199.16	14810.17	58.95	2.22
3	101.13	1.44	0.89	381603.77	12510.44	58.35	2.20
4	87.38	1.24	0.77	329716.98	9339.63	48.75	1.84
5	75.79	1.08	0.67	286006.29	7027.46	47.75	1.80

Table B.14: Results for $b_1 = 100\ cm\ and\ b_2 = 120\ cm, \psi = 6.918$

Case	Q(lt/s)	V_i (m/s)	Fr	Re	We	Sc	Sc/Di
1	122.26	1.74	1.08	461373.17	18287.39	61.65	2.33
2	111.71	1.59	0.99	421540.88	15266.04	60.15	2.27
3	97.38	1.39	0.86	367452.83	11599.79	59.45	2.24
4	85.49	1.22	0.76	322589.10	8940.18	54.25	2.05
5	75.86	1.08	0.67	286268.34	7040.34	53.45	2.02
6	72.49	1.03	0.64	273532.49	6427.84	45.45	1.72

Table B.15: Results for $b_1 = 110\ cm\ and\ b_2 = 120\ cm, \psi = 7.956$

Case	Q(lt/s)	V_i (m/s)	Fr	Re	We	Sc	Sc/Di
1	123.31	1.76	1.09	465303.98	18600.33	63.05	2.38
2	109.17	1.55	0.96	411949.69	14579.26	61.95	2.34
3	95.94	1.37	0.85	362054.51	11261.47	58.55	2.21
4	87.69	1.25	0.77	330922.43	9408.05	57.45	2.17
5	74.72	1.06	0.66	281970.65	6830.54	52.65	1.99
6	67.29	0.96	0.59	253930.82	5539.59	49.35	1.86
7	60.19	0.86	0.53	227148.85	4432.70	45.45	1.72

APPENDIX C

EXPERIMENTAL RESULTS OF THE STUDY FOR TRIPLE INTAKES

Table C.1: Results for $b_1 = 120\ cm\ and\ b_2 = 140\ cm, \psi = 8.410$

Case	Q(lt/s)	V_i (m/s)	Fr	Re	We	Sc	Sc/Di
1	98.15	1.40	0.87	370370.37	7097.62	66.45	2.51
2	87.03	1.24	0.77	328406.71	5580.39	60.15	2.27
3	75.37	1.07	0.67	284416.49	4185.52	59.85	2.26
4	67.50	0.96	0.60	254716.98	3357.04	51.25	1.93

Table C.2: Results for $b_1 = 120\ cm\ and\ b_2 = 160\ cm, \psi = 7.925$

Case	Q(lt/s)	V_i (m/s)	Fr	Re	We	Sc	Sc/Di
1	113.43	1.62	1.00	428022.36	9479.23	66.65	2.52
2	100.56	1.43	0.89	379454.93	7450.08	62.55	2.36
3	85.65	1.22	0.76	323200.56	5404.86	59.15	2.23
4	76.02	1.08	0.67	286862.33	4257.82	56.95	2.15
5	66.94	0.95	0.59	252620.55	3302.00	56.25	2.12
6	59.63	0.85	0.53	225017.47	2619.83	54.05	2.04

Table C.3: Results for $b_1 = 140\ cm\ and\ b_2 = 160\ cm, \psi = 9.906$

Case	Q(lt/s)	V_i (m/s)	Fr	Re	We	Sc	Sc/Di
1	99.07	1.41	0.88	373864.43	7232.17	64.75	2.44
2	88.02	1.25	0.78	332145.35	5708.17	60.25	2.27
3	75.57	1.08	0.67	285185.19	4208.18	57.45	2.17
4	67.78	0.97	0.60	255765.20	3384.72	55.45	2.09
5	59.35	0.85	0.52	223969.25	2595.48	54.15	2.04
6	48.89	0.70	0.43	184486.37	1761.04	46.75	1.76

Table C.4: Results for $b_1 = 140\ cm\ and\ b_2 = 170\ cm, \psi = 9.634$

Case	Q(lt/s)	V_i (m/s)	Fr	Re	We	Sc	Sc/Di
1	96.20	1.37	0.85	363032.84	6819.18	63.35	2.39
2	86.18	1.23	0.76	325192.17	5471.68	59.35	2.24
3	75.69	1.08	0.67	285604.47	4220.56	57.05	2.15
4	67.49	0.96	0.60	254682.04	3356.12	53.95	2.04
5	60.08	0.86	0.53	226729.56	2659.85	52.25	1.97

Table C.5: Results for $b_1 = 147\ cm\ and\ b_2 = 183\ cm, \psi = 10.003$

Case	Q(lt/s)	V_i (m/s)	Fr	Re	We	Sc	Sc/Di
1	87.49	1.25	0.77	330153.74	5639.92	60.65	2.29
2	76.65	1.09	0.68	289238.29	4328.64	58.75	2.22
3	67.15	0.96	0.59	253389.24	3322.13	54.95	2.07
4	61.19	0.87	0.54	230922.43	2759.13	52.65	1.99
5	48.92	0.70	0.43	184591.19	1763.04	46.55	1.76

CURRICULUM VITAE

PERSONAL INFORMATION

Surname, Name: Yıldırım, Tuğçe
Nationality: Turkish (TC)
Date and Place of Birth: 04.01.1985, Ankara
Marital Status: Married
Phone: 0 533 5200863
E-mail tugcey@gmail.com

EDUCATION

Degree	Institution	Year of Graduation
M.S.	METU, Civil Engineering	2010
B.S.	METU, Civil Engineering	2007
High School	Süleyman Demirel Anadolu Lisesi	2002

PROFESSIONAL EXPERIENCE

Year	Place	Enrollment
2018-Recent	Hidro Dizayn Consultancy Inc.	Project Control Proposals Eng.
2008-2018	METU, Civil Engineering Department	Research Assistant

PUBLICATIONS

International Conference Publications

Yıldırım, T. and Altınbilek H.D., Southeastern Anatolia Project (GAP) as a Case Study of a Regional Sustainable Development Project, XVIth World Water Congress, Cancun Mexico, 23 May - 3 June 2017

Yıldırım, T. and Tiğrek, Ş., Numerical Modeling of Draft Tube, Surge Tank and Tailwater Tunnel, ACE 2016, the 12th International Congress on Advances Civil Engineering, Istanbul TURKEY, September 2016

Yıldırım, T. and Tiğrek, Ş., Numerical Simulation of Spillway Aerators; A case Study, 6th International Perspectives on Water Resources and the Environment Conference (IPWE 2013), ASCE-EWRI, January 7-9, 2013, İzmir, Turkey

Tigrek, S., Sahin, A.N., and Yildirim, T. Su Yapılarında Fluent Uygulamaları, 4. Su Yapıları Sempozyumu, Civil Engineering Chamber, Antalya TURKEY. November 2015

Peer Reviewed Articles

Yildirim, T., and Altinbilek, D., Rehabilitation of urban estuary: Turkey (Golden Horn, Istanbul), World Water Council / Government of Korea (2012): Water and green growth: thematic publication, Report edition 1 March 2012

Altinbilek, D.,Yildirim, T., Participatory irrigation management: Turkey, World Water Council / Government of Korea (2012): Water and green growth: thematic publication, Report edition 1 March 2012